AWARD NUMBER: W81XWH-14-1-0423

TITLE: Deciphering the role of alternative non-homologous end joining (Alt-NHEJ) DNA repair in Breast cancer

PRINCIPAL INVESTIGATOR: Pedro A. Mateos-Gomez

CONTRACTING ORGANIZATION: New York University School Of Medicine

REPORT DATE: December 2017

TYPE OF REPORT: Final report

PREPARED FOR: U.S. Army Medical Research and Materiel Command
Fort Detrick, Maryland 21702-5012

REPORT DOCUMENTATION PAGE

Form Approved
OMB No. 0704-0188

1. REPORT DATE	2. REPORT TYPE	3. DATES COVERED
December 2017	Final	15Sept2014 - 14Sept2017

4. TITLE AND SUBTITLE

Deciphering the role of alternative non-homologous end joining (Alt-NHEJ) DNA repair in Breast cancer

5a. CONTRACT NUMBER

5b. GRANT NUMBER
W81XWH-14-1-0423

5c. PROGRAM ELEMENT NUMBER

6. AUTHOR(S)
Pedro A. Mateos-Gomez

E-Mail: pedro.mateosgomez@med.nyu.edu

5d. PROJECT NUMBER

5e. TASK NUMBER

5f. WORK UNIT NUMBER

7. PERFORMING ORGANIZATION NAME(S) AND ADDRESS(ES)
New York University School of Medicine
540 1st Avenue
New York, NY 10016-6402

8. PERFORMING ORGANIZATION REPORT NUMBER

9. SPONSORING / MONITORING AGENCY NAME(S) AND ADDRESS(ES)

U.S. Army Medical Research and Materiel Command
Fort Detrick, Maryland 21702-5012

10. SPONSOR/MONITOR'S ACRONYM(S)

11. SPONSOR/MONITOR'S REPORT NUMBER(S)

12. DISTRIBUTION / AVAILABILITY STATEMENT

Approved for Public Release; Distribution Unlimited

13. SUPPLEMENTARY NOTES

14. ABSTRACT
The alternative non-homologous end-joining (NHEJ) machinery facilitates several genomic rearrangements, some of which can lead to cellular transformation. This error-prone repair pathway is triggered upon telomere de-protection to promote the formation chromosome end-to-end fusions. We showed that Polq inhibition suppresses alternative NHEJ at dysfunctional telomeres, and hinders chromosomal translocations at non-telomeric loci. In addition, we found that loss of Polq results in increased rates of homology-directed repair (HR), evident by recombination of dysfunctional telomeres and accumulation of RAD51 at double-stranded breaks. Lastly, we showed that depletion of PolQ had a synergistic effect on cell survival in the absence of BRCA genes, suggesting that the inhibition of this mutagenic polymerase represents a valid therapeutic avenue for tumors carrying mutations in homology-directed repair genes. Here we report that PolQ inhibition can be used to increase the efficiency of CRISPR targeting. Function-Structure analysis of PolQ indicated that the helicase and polymerase domains are relevant for its activity, having an impact in translocation frequency, RAD51 foci formation or survival of BRCA1 depleted cells. Finally, PolQ though its helicase domain and RPA interplay at DSB to promote A-NHEJ or HR respectively.

15. SUBJECT TERMS
DNA double strand break. Alternative non-homologous end-joining. Homologous recombination. Breast cancer associated genes 1 and 2.

16. SECURITY CLASSIFICATION OF:			17. LIMITATION OF ABSTRACT	18. NUMBER OF PAGES	19a. NAME OF RESPONSIBLE PERSON
a. REPORT	b. ABSTRACT	c. THIS PAGE			USAMRMC
Unclassified	Unclassified	Unclassified	UU	84	19b. TELEPHONE NUMBER *(include area code)*

Table of Contents

Page

1. Introduction:

DNA damage and particularly double strand breaks (DSB) are highly dangerous for cells, improper repair of those lesions contributes to the accumulation of mutations and genomic instability, which can lead to cellular transformation and cancer progression. DSBs are repaired by three different mechanisms, the Homologous Recombination (HR; error-freee), the Classical Non-Homologous end-joining (C-NHEJ; minimally error-prone) and the Alternative-NHEJ (A-NHEJ; highly error-prone). In contrast to the former two the last one is poorly studied, only few factors involved in the A-NHEJ are already known. In recent years, a number of evidences for its implication on generating genomic instability in tumor cells have been found, including HR deficient tumors of the breast. Interestingly, it has been shown that tumors deficient in HR are sensitive to PARP1 inhibition, a factor required for the A-NHEJ. The mechanism under this sensitivity is not fully understood and resistance to these inhibitors has been reported. My hypothesis is that HR deficient tumors are dependent on the A-NHEJ DNA repair pathway for its survival. Therefore, cell death due to PARP1 inhibition is at least in part due to blocking of the A-NHEJ, what would drive the accumulation of improperly or unrepaired breaks. Inhibition of other relevant factors for the A-NHEJ could have the same impact on the survival of breast tumors that relies on this mechanism. Altogether, understanding the underlying basis of A-NHEJ and its impact of breast cancer progression should provide new insights that can be translated into the clinic. To that end, I will pursue the following three aims: 1- establish the function of the A-NHEJ in inherited and sporadic breast cancers; 2- elucidate the function of PolQ in the A-NHEJ and in breast cancer progression; 3- define the molecular mechanism of alt-NHEJ.

2. Keywords:

- DNA double strand break, DSB.
- Alternative non-homologous end-joining, A-NHEJ.
- Classical non-homologous end-joining, C-NHEJ.
- Homologous Recombination, HR.
- DNA Polymerase theta, PolQ.
- Breast cancer.
- Breast cancer associated gene 1 and 2, BRCA1 and BRCA2.
- Telomeres.
- Poly-ADP-ribose polymerase 1, PARP1.
- Chromosomal translocation.
- Chromosomal aberrancies.
- Chromosomal fusions.
- CRISPR: Clustered Regularly Interspaced Short Palindromic Repeats.
- DNA ligase 3 and 4
- Ku80

- Mouse embryonic fibroblast, MEF.
- Mouse embryonic stem cells, mESC.

3. Accomplishments:

Major goals of the project:

1- Characterize alt-NHEJ in cell lines and patient samples.
Completion percentage: 10%

2- Elucidate the function of PolQ in A-NHEJ and its relevance to breast cancer progression.
Completion percentage: 100%

3- Define the molecular mechanism of alt-NHEJ. Screen for factors involved in the A-NHEJ.
Completion percentage: 15%

Accomplished under these goals:

1- Characterize alt-NHEJ in cell lines and patient samples:

Subtask 1: The first part of this aim was to determine whether several breast cancer cell lines significantly use the A-NHEJ repair pathway. We have already shown (last year report and Mateos-Gomez et al. Nature 2015) the relevance of the A-NHEJ for the proliferation of two breast cancer cell lines, MCF-7 (HR proficient) and HCC1937 (BRCA1 and HR deficient). Our results indicated that the absence of HR was the reason for this cell line to require A-NHEJ, but it was not clear why an HR proficient cell line (MCF-7) was sensitive to PolQ depletion.

2- Elucidate the function of PolQ in A-NHEJ and its relevance to breast cancer progression:

Subtask 2.1: Determine the mechanism of PolQ recruitment to sites of breaks

I used a chromosomal translocation assay to analyze the role of PolQ in A-NHEJ. This method involves the simultaneous cleavage of two different chromosomes (6 and 11) by the Cas9 nuclease. Then, by a nested-PCR one can quantify the formation of chromosomal translocations. Sequencing of identified translocations also allows

the analysis of the corresponding junctions. To introduce the cleavages, I expressed the CRISPR Cas9 nuclease and two different guide RNAs in PolQ proficient and PolQ deficient mouse embryonic stem cells (mESC).
I reported as preliminary data a reduction in the frequency of translocations in PolQ deficient cells. Further analysis also revealed that there were not sequence insertions at the junctions and the presence of micro-homology at these was significantly reduced. These results indicated that PolQ it is not only required to include the sequence insertions at the junctions, PolQ is actually promoting the end joining between the two DNA ends.

	Total number of translocations	Average nucleotide deletions/translocation	% junctions with insertions	% junctions with microhomology
Polq$^{+/+}$	185	23	24%	75%
Polq$^{-/-}$	51	28	0%	47%

Table 1. Signature of translocations in *PolQ*$^{-/-}$ and *PolQ*$^{+/+}$ cells. Table records the total number of translocation events identified following CRISPR-Cas9 induced-cleavage. On average, the same number of nucleotides was deleted at the fusion junction in *PolQ*$^{-/-}$ and *PolQ*$^{+/+}$ cells. No nucleotide insertions were found in the absence of *PolQ*. Lastly, the percentage of junctions exhibiting microhomology was significantly reduced in cells lacking *PolQ*.

To study the recruitment of PolQ to DSBs, first I obtained a plasmid for the expression of PolQ with a myc-tag that will allow its detection with an anti-myc antibody. This plasmid was transfected into HeLa cells to perform laser micro-irradiation and into the DSB reporter cell line U2OS-263. Myc-PolQ transfected HeLa cells were laser irradiated and then stained for gH2AX (DNA damage marker) and Myc. The co-localization of both indicated the recruitment of PolQ to the site of damage. The usage of different inhibitors and siRNA allowed us to identify PARP1 as the signaling molecule required for PolQ recruitment. Laser micro-irradiation has the caveat of inducing different types of DNA damage and not only DSBs, not letting us to rule out the possibility of being recruited to other types of DNA damage. Using the second approach with U2OS-263, bona fide DSBs reported cell line, we obtained similar results confirming that PolQ was recruited when only DSB were introduced and that PARP1 was required for its recruitment to DSBs.

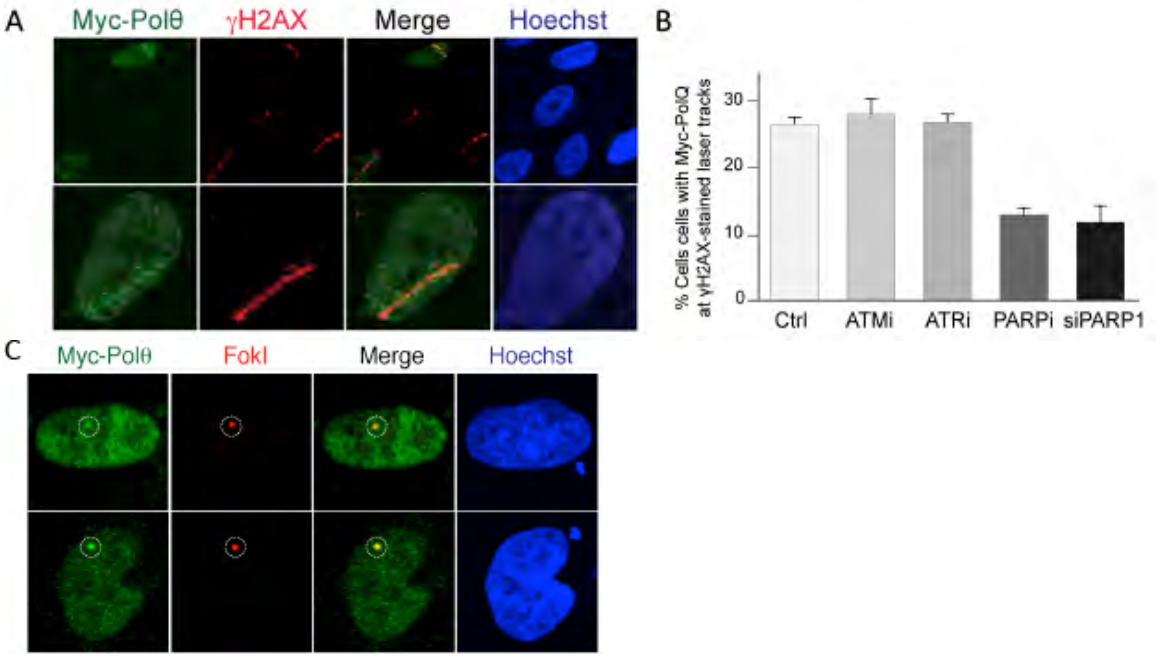

Figure 1. Polθ is recruited to DSBs by PARP1. **A)** Myc-PolQ localization to DNA damage was monitored after laser micro-irradiation of HeLa cells. Cells were fixed and stained for γH2AX and Myc, one hour after damage induction. **B)** Quantification of PolQ accumulation at sites of laser damage in the presence different inhibitor or siRNA (Mean ± s.e.m, n=2). **C)** Results from immunofluorescence performed at 4 hours after induction (Shield1 ligand, Clontech 631037; 0.5 μM 4-OH tamoxifen) of DSBs by mCherry-LacI-FokI in the U2OS-DSB reporter cells transfected with the Myc-PolQ and treated with PARP inhibitor (KU58948). The mCherry signal is used to identify the area of damage and to assess the recruitment of Myc-PolQ to cleaved LacO repeats.

Subtask 2.2: Assess the impact of PolQ inhibition on survival of HDR defective breast cancer.

First I decided to study the interplay between the A-NHEJ and the Homologous Recombination. It has been previously described that A-NHEJ and HR are both maximally active during the S-G2 phases of the cell cycle, we decided to analyze the impact of PolQ in HR activity. To this end I used the TRF1/2$^{F/F}$ p53$^{-/-}$ Lig4$^{-/-}$ mouse embryonic fibroblast (MEFs), where in the spread of metaphasic chromosomes from individual cells we can observe fusions of chromosomes due to the A-NHEJ, and exchanges of sequence between telomere sister chromatids (T-SCE) due to the HR. I depleted two components of the A-NHEJ by shRNA, PolQ and DNA ligase 3 (that would act downstream of PolQ), and quantify the chromosome fusions and the T-SCEs on the metaphase spreads. In both cases, we observed the expected decrease in the number of chromosome fusions (A-NHEJ), in contrast we only observed an increase in the number of T-SCEs (HR) when PolQ was depleted. These results indicate that PolQ promotes the A-NHEJ while is counteracting the HR. In order to

confirm these results, I monitored HR by quantifying the formation of Rad51 foci after inducing DSBs by gamma irradiation in PolQ proficient and PolQ deficient MEFs. Rad51 is a single stranded DNA binding protein essential for HR. I found a significant increase in the number of Rad51 foci in the absence of PolQ, confirming that PolQ activity counteracts the HR.

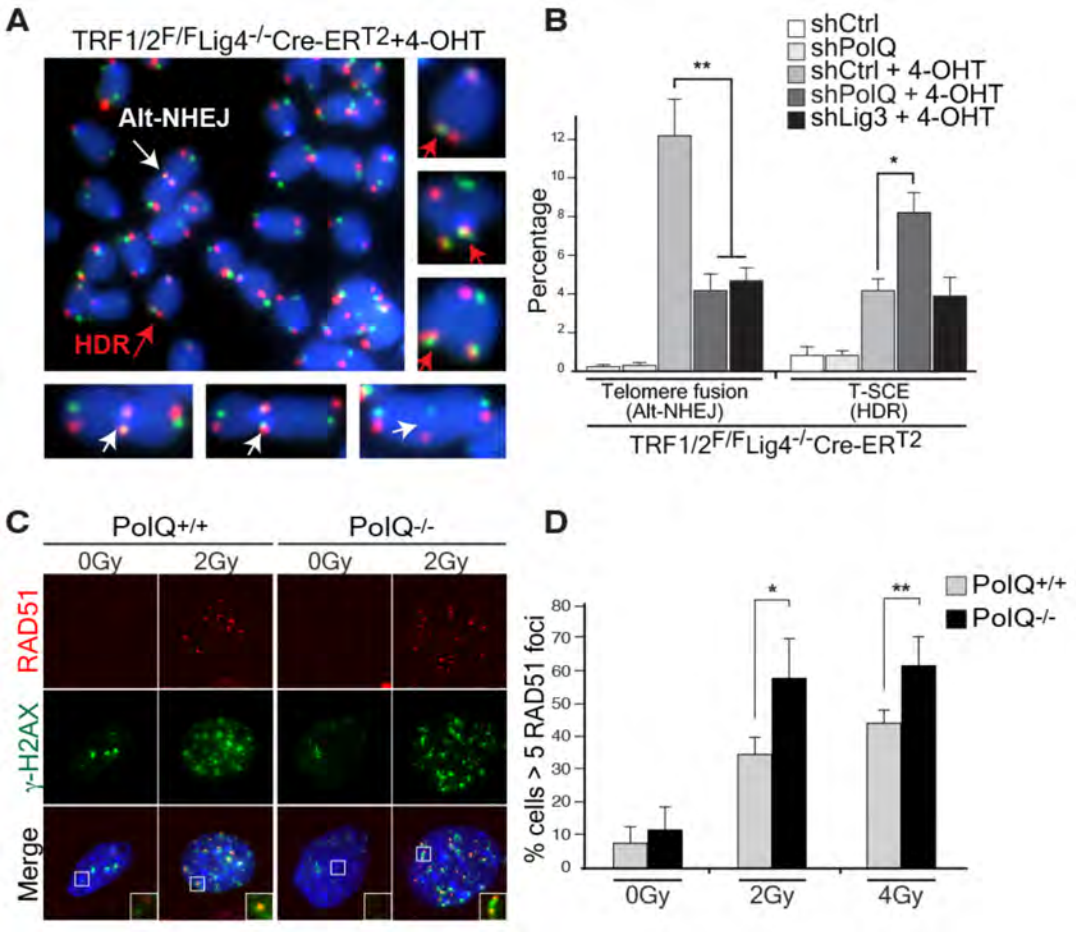

Figure 2. PolQ promotes A-NHEJ while counteracting HR. **A)** To test if PolQ represses recombination at telomeres, we depleted the polymerase in TRF1/2$^{F/F}$ p53$^{-/-}$ Lig4$^{-/-}$ MEFs, and both repair pathways were monitored using CO-FISH. White arrows indicate alt-NHEJ events, red arrows highlight HDR-mediated T-SCEs. **B)** Quantification of telomere fusion (alt-NHEJ) and T-SCE (HDR) in cells transduced with *PolQ*, *Lig3,* or control shRNA. **C)** Immunofluorescence for Rad51 and γH2AX in the indicated MEFs 3 hours post-irradiation. **D)** Graph representing quantification of IR-induced RAD51 foci. (Mean ± SD, n=3, *p<0.05, **p<0.01;two-tailed student's *t*-test).

Second I decided to analysis what would happens to chromosomes in cells with blocked HR and A-NHEJ.

In this experiment I also performed spreads of metaphasic chromosomes, without specific staining of the telomeres, I analyzed whole chromosomes looking for breaks, sequence gaps and fusions of more than one chromatid to the same DNA end (radial chromosomes). In order to block both pathways at the same time, I depleted

PolQ (A-NHEJ) by shRNA in BRCA1$^{F/F}$Cre-ER^{T2} and BRCA2$^{F/F}$Cre-ER^{T2} MEFs. In these cell lines BRCA1 and BRCA2 genes (HR) can be deleted by the addition of 4-OH-tamoxifen that activates the Cre recombinase. Inhibition of both repair pathways led to a significant increase in the presence of chromosomal aberrancies: non-repair breaks, gaps and radial chromosomes typical of the repair by the C-NHEJ outside of the G1 phase of the cell cycle. To confirm the results I also depleted BRCA1 or BRCA2 in PolQ proficient and PolQ deficient MEFs.

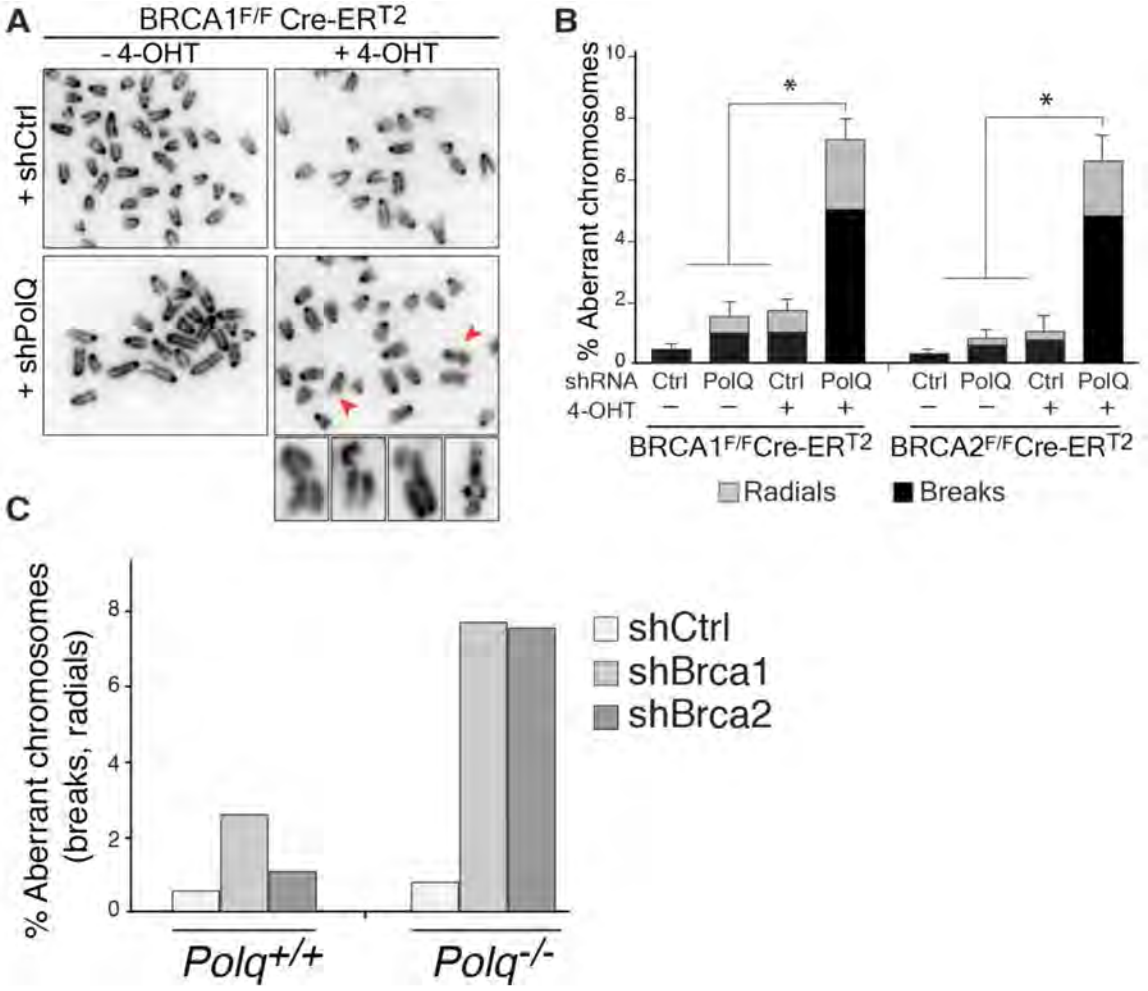

Figure 3. Lack of PolQ in combination with BRCA1 or BRCA2 increase chromosomal aberrancies. **A)** Analysis of genomic instability in metaphase spreads from *BRCA1$^{F/F}$*Cre-ER^{T2} MEFs treated with shRNA against *PolQ* or vector control. **B)** Quantification of breaks (chromatid and chromosome) and radials in *BRCA1$^{F/F}$*Cre-ER^{T2} *and BRCA2$^{F/F}$*Cre-ER^{T2} MEFs with the indicated treatment. **C)** Analysis of genomic instability in metaphase spreads from PolQ$^{+/+}$ or PolQ$^{-/-}$ MEFs treated with shRNA against BRCA1, BRCA2 or vector control.

To analyze the ability to proliferate of cells with blocked HR and A-NHEJ I performed colony formation assays. For this assay I depleted PolQ by shRNA in BRCA1$^{F/F}$Cre-ER^{T2} where BRCA1 can be deleted by the addition of tamoxifen. I

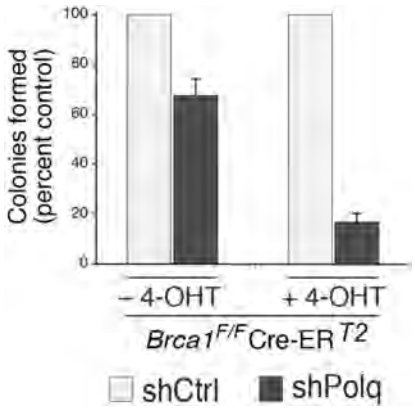

quantified the number of colonies in each condition after plating the same number of cells and waiting time enough to see colonies in the plates. The results showed that depletion of PolQ in the absence of BRCA1 significantly reduced the survival of the cells compare to those expressing BRCA1. Therefore PolQ inhibition in HR deficient cells compromises its survival.

Figure 4. Quantitative analysis of colony formation in *BRCA1*$^{F/F}$Cre-ER^{T2} cells. 4OH-Tamoxifen was added to delete BRCA1. *PolQ* depletion by shRNA indicated. The number of colonies in control shRNA- treated cells was set to 100%.

Since PolQ depletion clearly reduce survival of BRCA1 deficient MEFs, we decided to study what would be the effect of depleting PolQ in breast cancer cell lines and in non-tumorigenic cell line. We performed colony formation assay with HCC1937 cells (BRCA1 deficient), MCF-7 (BRCA1 proficient) and BJ-hTERT (non-tumor human fibroblast immortalized by the expression of telomerase and BRCA1 proficient). The colony formation capability of the normal cells (BJ-hTERT) was not affected by PolQ depletion. In contrast, we observed a reduction on the number of colonies for the breast cancer cells lines, being almost lethal for the BRCA1 deficient HCC1937 cells. To confirm that the reduction in the survival was due the inhibition of the repair by the A-NHEJ, I perform the same assay, using the same cell lines, but depleting the DNA ligase 3. In this case the survival of all cell lines was reduced due to the requirement of ligase 3 at the mitochondria. Interestingly, the number of colonies in the HCC1937 and MCF-7 compared the normal cell lines was equivalent to what we observed with PolQ depletion. All together, we can conclude that PolQ depletion sensitized these two breast cancer cell lines, particularly the BRCA1 deficient HCC1937, and that this effect was due to the inhibition of the A-NHEJ.

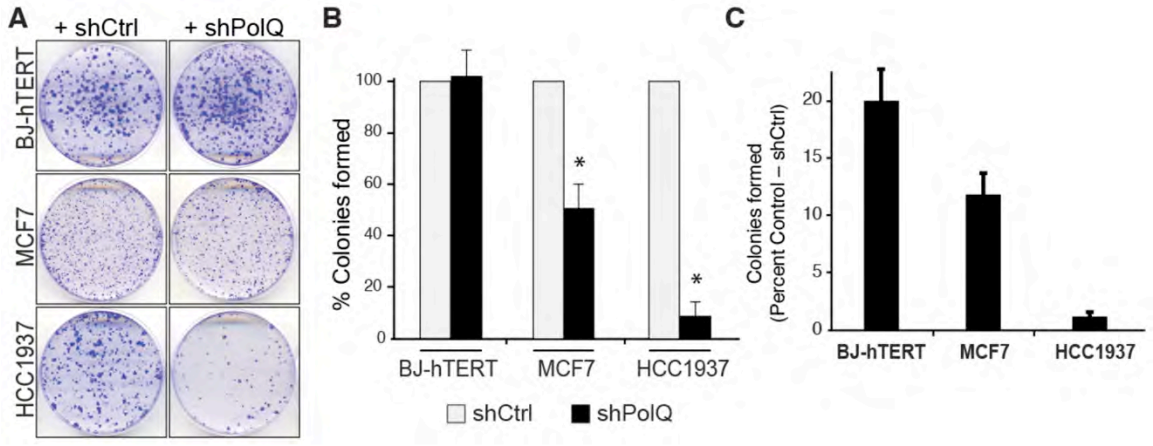

Figure 5. Clonogenic survival following *PolQ* depletion. **A)** Crystal violet staining of BJ-hTERT, MCF7, and HCC1937 cells treated with shRNA against *PolQ* or vector control. **B)** Quantitative analyses of colony formation assay shown in A. **C)** Quantitative analyses of colony formation assay after Ligase 3 depletion. Colonies in each control shRNA cell line were set to 100%. Colonies in sh*PolQ* expressing cells normalized to sh*Ctrl* (Mean ± SD, n=3' *p<0.05' **p<0.01;two-tailed student's *t*-test).

Subtask 2.3: since in subtask 2.2 we showed that HR deficient tumor cell lines are extremely dependent on PolQ for its survival, and that even when they are not treated with DNA damaging agents in combination with PolQ depletion, I decided to explore more deeply the mechanism by which PolQ acts.

In subtask 2.2 I showed that PolQ promotes A-NHEJ while suppresses HR and I have analyzed the impact of PolQ on CRISPR targeting when HR is required to introduce the desired modification. The method I used was to fused a T2A-ZsGreen cassette to the end of two different genes, Sox2 (Fig. 6) and Hsp90 (Fig. 7). After targeting of the loci, HR is required to use the provided template to copy in frame the T2A-ZsGreen. This strategy allows to quantify the efficiency of targeting through by flow cytometry, since the new mRNA transcribed from these genes now leads to the production of two proteins, the corresponding one (Sox2 or Hsp90) and ZsGreen.

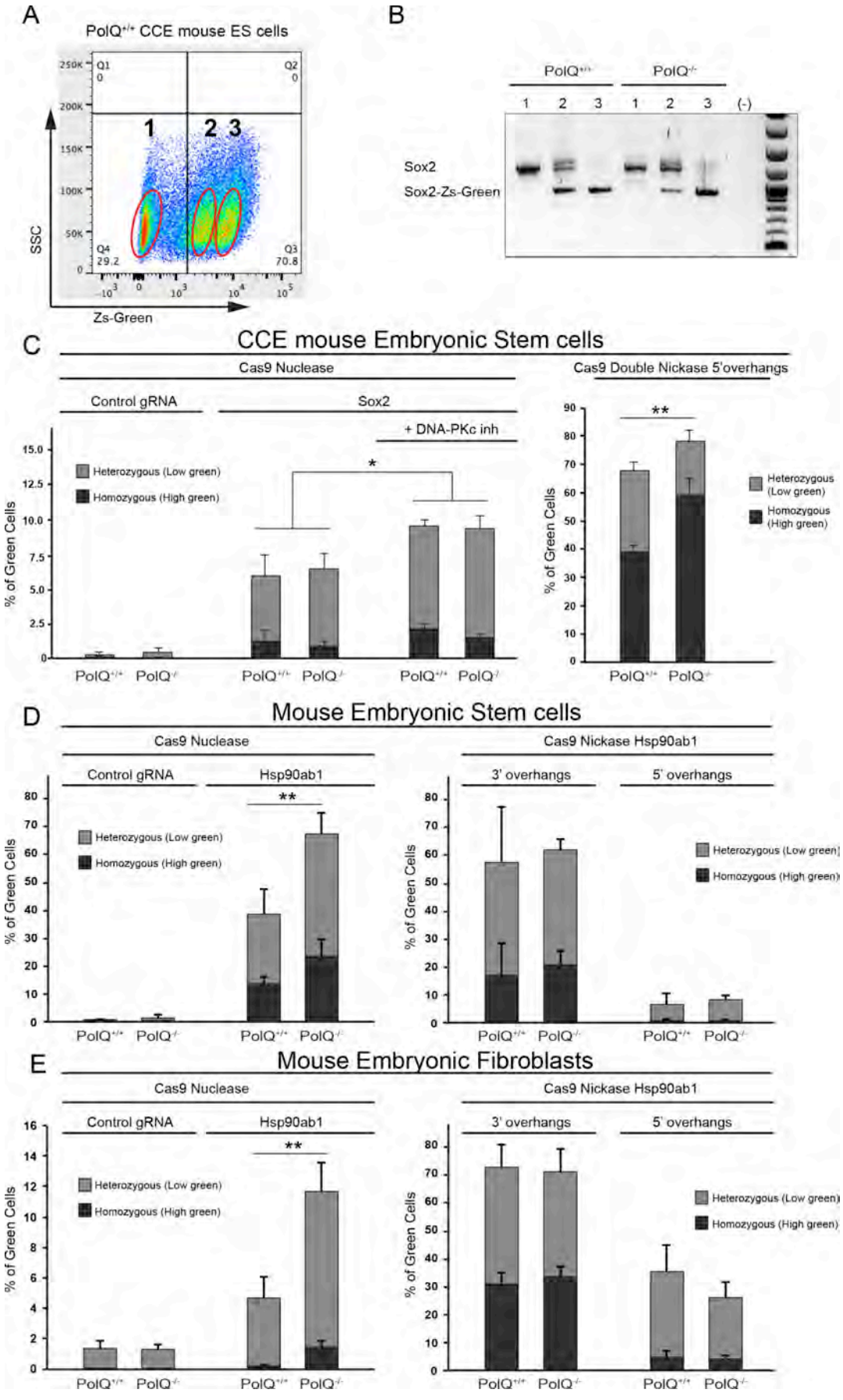
A
PolQ+/+ CCE mouse ES cells
Q1
0
Q2
0
Q4
29.2
Q3
70.8
1
2 3
SSC
Zs-Green
B
PolQ+/+
PolQ-/-
1 2 3 1 2 3 (-)
Sox2
Sox2-Zs-Green
C
CCE mouse Embryonic Stem cells
Cas9 Nuclease
Cas9 Double Nickase 5'overhangs
Control gRNA
Sox2
+ DNA-PKc inh
Heterozygous (Low green)
Homozygous (High green)
% of Green Cells
PolQ+/+ PolQ-/-
D
Mouse Embryonic Stem cells
Cas9 Nuclease
Cas9 Nickase Hsp90ab1
Control gRNA
Hsp90ab1
3' overhangs
5' overhangs
E
Mouse Embryonic Fibroblasts

Figure 6. CRISPR targeting is enhanced with PolQ absence in the Sox2 locus. **A)** Flow cytometry analysis to quantify ZsGreen expression in mouse CCE embryonic stem cells (mESc) (CCE a mES cell line derived from 129/Sv mouse strain; Robertson E, Bradley A, Kuehn M, Evans M, Nature. 1986 Oct 2-8; 323(6087):445-8. Keller G, Kennedy M, Papayannopoulou T, Wiles MV, Mol Cell Biol. 1993 Jan; 13(1):473-86. Numbers represent the percentage of cells in each quadrant. Three independent populations of CCE mES cells, with distinct ZsGreen intensity were isolated (highlighted in 1, 2 and 3 circles). **B)** Genotyping PCR for Sox2 on DNA extracted from the three highlighted groups of cells (1A) in POLQ proficient (POLQ+/+ ,WT) and PolQ deficient (PolQ-/-, Null) CCE mES cells. Group 1 depicts non-targeted cells, Group 2 represents cells carrying heterozygous Sox2 cells and in group 3 both alleles of Sox 2 were targeted. **C)** Left, graph depicting results of FACS analysis for ZsGreen positive CCE mES cells (POLQ+/+ and PolQ-/-) treated with the indicated Cas9 nuclease plasmid (also encoding for a gRNA targeting the Sox2 gene) and a donor plasmid with the sequence to be inserted at the end of the gene. DNA-PK inhibitor was used to block repair by classical NHEJ (Non-Homologous End-Joining). Right, cells treated with Cas9-nickase containing plasmid that also encodes for two Sox2 gRNAs. Three independent experiments, each performed in duplicate. The control gRNAs were designed to target two independent loci in the cells (H3F3B and Rosa26) to which, the donor plasmid has no homology. **D)** Left, depicts results of FACS analysis for ZsGreen positive mES cells (POLQ WT and null, derived from B6.Cg-*Polq*^{tm1Jcs}/J mouse) treated with the indicated Cas9 nuclease and the donor plasmid. The Cas9 plasmid also encodes the gRNA that targets Hsp90ab1. Right, cells treated with a Cas9-nickase containing plasmid that encodes for two Hsp90ab1 gRNAs. This experiment was performed with two different Cas9-nickase plasmids, one encoding two gRNAs that generates 3' overhangs after cleavage and other that generates 5' overhangs). Three independent experiments, each performed in duplicate. **E)** Depicts results of FACS analysis for ZsGreen positive MEFs cells (POLQ WT and null, derived from B6.Cg-*Polq*^{tm1Jcs}/J mouse) treated with the indicated Cas9 as in Figure 1D. Three independent experiments, each performed in duplicate.

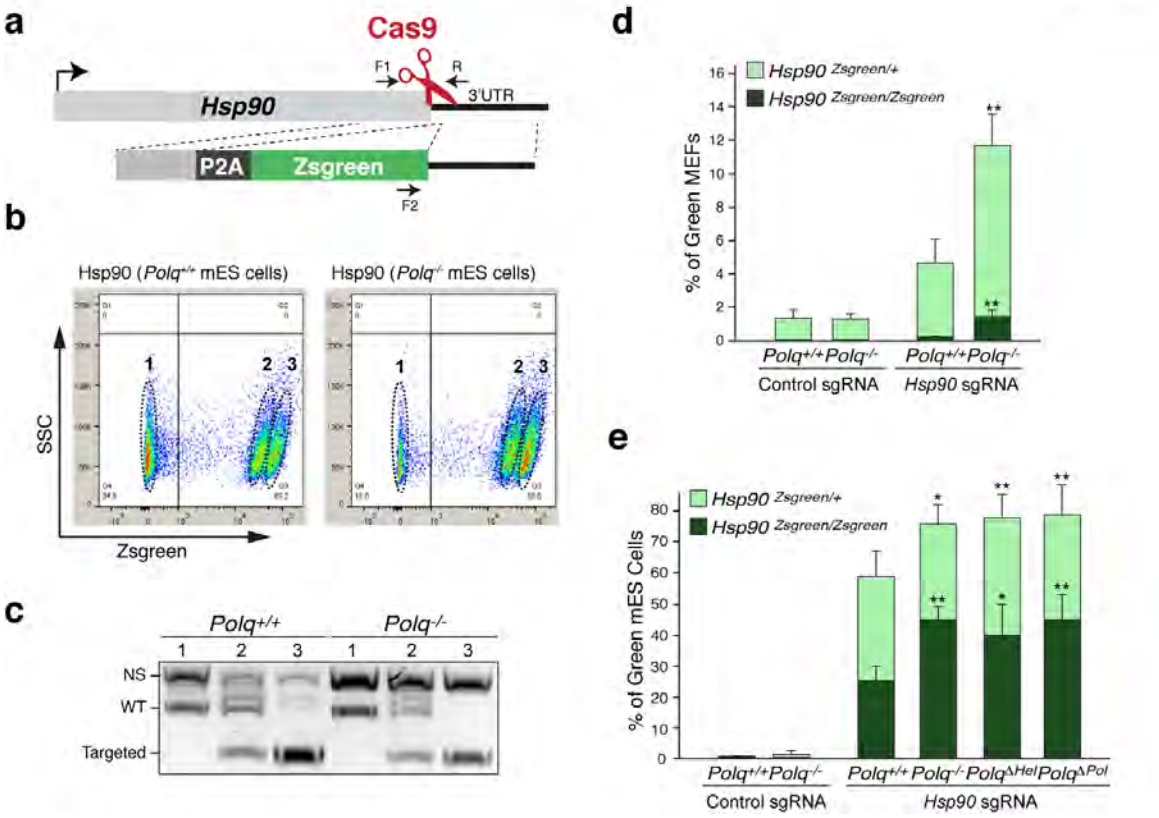

Figure 7. CRISPR targeting is enhanced with PolQ absence in the Hsp90 locus. **A)** Scheme depicting gene targeting assay at the Hsp90 locus. The donor plasmid contains a Zsgreen coding sequence and 600 base pairs of homology arms. **B)** (FACS) analysis to determine the percentage of ZsGreen positive cells. Three distinct populations were isolated (highlighted as 1, 2 and 3). **C)** Genotyping PCR for *Hsp90* on DNA corresponding to the three highlighted populations of cells (indicated in (B)). **D)** Gene-targeting efficiency at the *Hsp90* locus in *Polq-/-* and *Polq+/+* MEFs. Bars represent mean ± S.D. (n = 3). **E)** Gene-targeting efficiency at the *Hsp90* locus in mES cells with the indicated genotype. Bars represent mean ± S.D. (n = 3). **p<0.01; two-tailed Student's t-test.

In order to understand better how PolQ works I decided to use CRISPR to mutate the different motives of the protein that has been already identified:

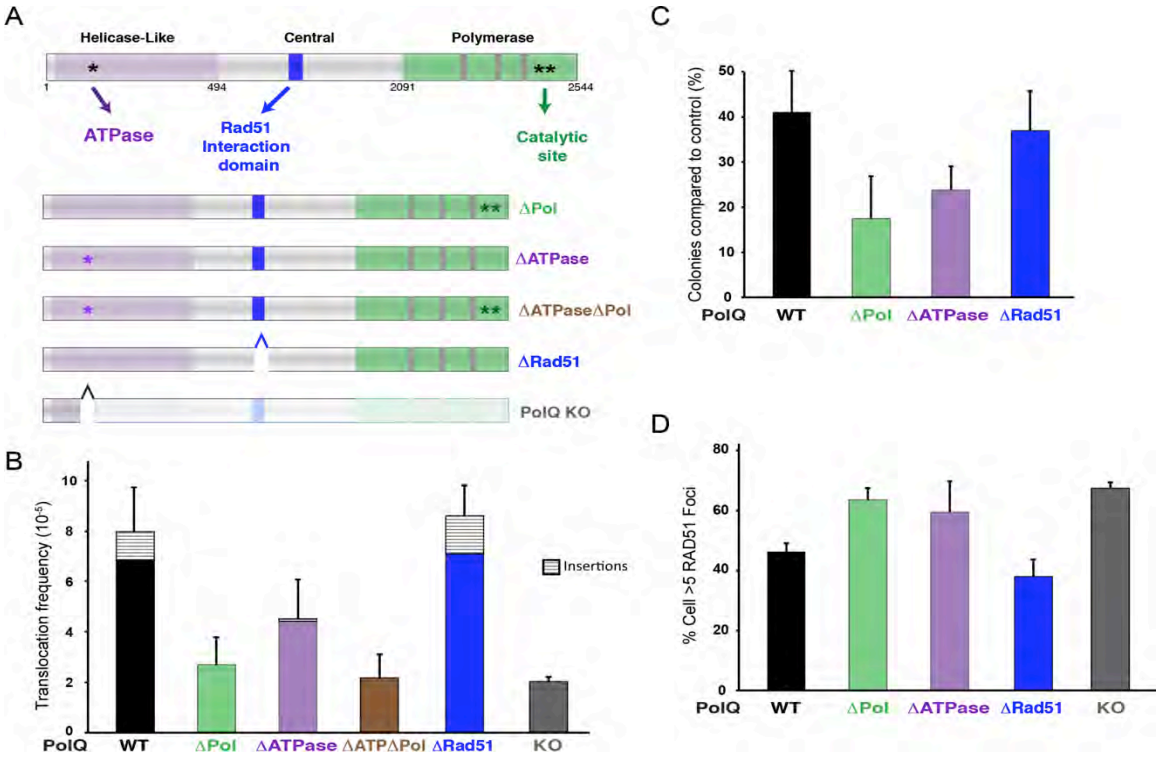

Figure 8. PolQ lacking polymerase activity (ΔPol) or ATPase activity (ΔATPase) does not promote A-NHEJ, favors HR and reduce the viability in the absence of BRCA1. **A)** Scheme depicting Polθ domains. CRISPR/Cas9 gene targeting was employed to create ΔPol (two aminoacids substitutions at D2494G and E2495S), ΔATPase (one aminoacid substitution K120GS), ΔRad51 (deletion of aminoacids D844-M890) and KO (deletion of the exon 3 that introduces a STOP codon after exon 2). Two independently clonal cell lines for each mutant were analyzed. **B)** Frequency of chromosomal translocations (Der-6). Bars represent mean of four independent experiments ± SD (two experiments per clonal cell line). ** represents p=0.006 (two-tailed student's t test). PCR products were sequenced to confirm translocation and identify possible insertions. **C)** Quantitative analyses of colony formation in embryonic stem cells carrying the indicated mutations after BRCA1 depletion. The number of colonies in control shRNA-treated cells was set to 100%. The knockdown efficiency for BRCA1 was 80%. Bars represent mean of two independent experiments ± s.e.m. **D)** Graph representing Rad51 accumulation following IR treatment (2Gy). Cell were fixed 3 hours after irradiation. Bars represent mean of two independent experiments ± s.e.m.

In our previous studies I characterized the interplay between the A-NHEJ and the Homologous Recombination. I used the TRF1/2$^{F/F}$ p53$^{-/-}$ Lig4$^{-/-}$ mouse embryonic fibroblast (MEFs), where in the spread of metaphasic chromosomes from individual cells we can observe fusions of chromosomes due to the A-NHEJ, and exchanges of sequence between telomere sister chromatids (T-SCE) due to the HR. I showed that depletion by shRNA of two components of the A-NHEJ, PolQ and DNA ligase 3 (that would act downstream of PolQ), led to a reduction of the number of chromosome fusions (A-NHEJ), and that only PolQ depletion increased the number of T-SCEs (HR). These results indicate that PolQ promotes the A-NHEJ while is counteracting the HR. It has been described that RPA1, a single stranded DNA binding protein that is involved in HR, counteracts annealing of resected DNA ends and promotes further resection. It is also known that PolQ binds short over hangs. In order to explore a possible role of RPA in counteracting the A-NHEJ I analyzed metaphasic chromosomes from TRF1/2$^{F/F}$ p53$^{-/-}$ Lig4$^{-/-}$ MEFs after RPA1 depletion.

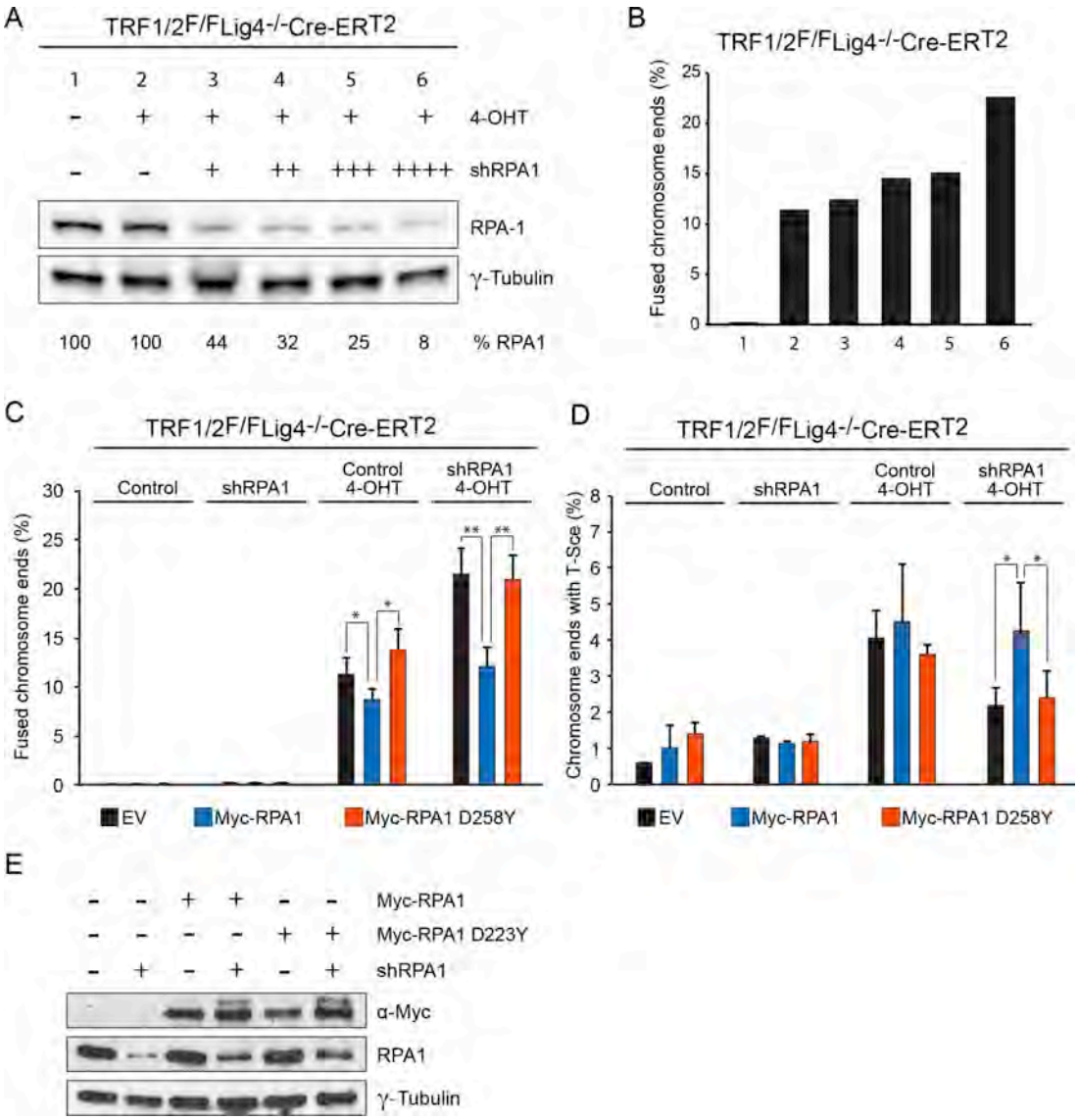

Figure 9. RPA1 counteracts A-NHEJ. **A)** To test if RPA1 represses A-NHEJ at telomeres, I depleted RPA1 in TRF1/2$^{F/F}$ p53$^{-/-}$ Lig4$^{-/-}$ MEFs and monitored the fusion of telomeres. Western blot showing RPA1 levels after shRNA treatment. **B)** Quantification of telomere fusion (alt-NHEJ) by FISH. **C)** and **D)** Quantification of telomere fusion (alt-NHEJ) and T-SCE (HDR), C and D respectively, using CO-FISF in cells transduced with *RPA1*, or control shRNA. Cells were previously transduced with empty vetor (EV), Myc-RPA1 and Myc-RPA-D258Y (that has reduced DNA binding activity). Myc-RPA1 versions were resistant to the shRNA. Mean ± SD, n=3, *p<0.05, **p<0.01;two-tailed student's *t*-test. **E)** Representative western blot for what shown in C) and D).

Finally, I examined the effect of Polq–helicase on the accumulation of RPA at DSBs *in vivo*. It was recently noted that Fok1-induced telomere breaks were not processed by C-NHEJ, but fixed by HR and alt-NHEJ. The expression of TRF1-FokI fusion protein in U2OS cells lead to significant co-localization of Myc-RPA1 at damaged telomeres (Figure 9A). Interestingly, we observed a small, but significant reduction in the accumulation of RPA1 at telomere breaks in cells expressing Polq–helicase. Importantly, expression of a helicase-defective Polθ allele (K121M) did not impact the formation of RPA1 foci at telomere breaks. These results highlight a role for Polq–helicase in displacing RPA from ssDNA while catalyzing overhang annealing, thereby facilitating alt-NHEJ at the expense of HR.

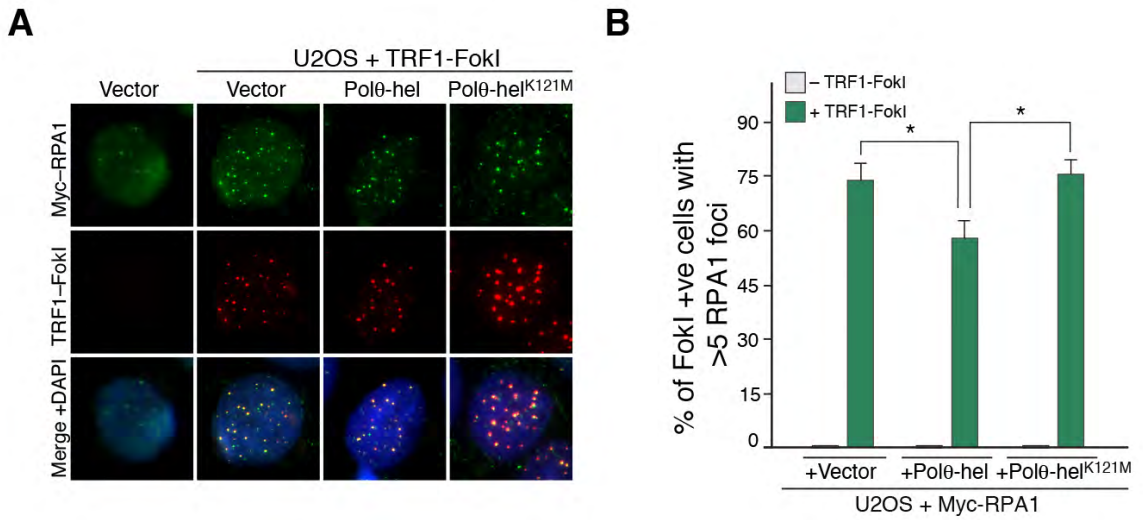

Figure 9. PolQ helicase counteracts the accumulation of RPA1 at DSBs. **A)** Immunofluorescence for Myc-RPA1 and TRF1-FokI-mCherry in U2OS cells expressing the indicated alleles. TRF1-Fok1-mCherry expression was induced upon treatment with doxycycline, shield-1, and 4-OHT. **B)** Graph representing the quantification of Myc-RPA1 accumulation in cells expressing TRF1-FokI (as in c). Bars represent mean ± S.D. from three independent experiments. *P < 0.05 and **P < 0.01; two-tailed Student's t-test.

3- Screen for factors involved in the A-NHEJ:

Subtask 1: Validation of the clonal cell line obtained to perform the screen.

On the preliminary data of the application I showed that in order to achieve reversible, complete, and rapid TRF1/2 depletion, I implemented the auxin-inducible degron (AID) system. AID-tagged proteins are rapidly degraded from auxin treated mammalian cells expressing TIR1 protein. Protein degradation is reversible, and previous protein levels are re-instated after Auxin withdrawal. I adapted this robust system by expressing AID-tagged TRF1/2 as well as TIR1 in $TRF1^{F/F}TRF2^{F/F}Ku80^{-/-}p53^{-/-}$ MEFs from which the endogenous TRF1/2 were deleted with Cre. The screen is based on the transient de-protection of telomeres (AID-TRF1/2 degradation) by the addition of auxin, what activates the DNA damage signaling and allows chromosome fusion by the A-NHEJ to happen. Removal of the auxin should quench the DNA damage signaling but maintain the covalent fusions of telomeres, reducing the cellular proliferation due to the presence of fusions. If siRNAs in the screen target the A-NHEJ, the fusions would be blocked and cellular proliferation would be higher after auxin withdrawal.

In the 2015 annual report, I showed that the system worked efficiently for the transient degradation of AID-TRF1/2, but also that AID-TRF1/2 did not fully replace the function of endogenous TRF1/2 reducing the proliferation of the clonal cell lines. I conclude that this cell lines were not suitable for the purpose of the screen.

Then I started the generation of a cell line with endogenous TRF1 and TRF2 tagged with HA-AID and Myc-AID minimal versions in mESC, using CRISPR genome editing tool. I did not obtain a clone that properly expressed the tagged TRF1 and TRF2 with the TIR1.

Opportunities for training and professional development that the project has provided:

- One to one weekly meeting with my mentor Agnel Sfeir.
- Weekly lab meeting or journal club.
- I have presented my work twice per year in the lab meeting.
- Poster presentation at the annual retreat of the Skirball Institute of Biomolecular Medicine. October 2014.
- **Oral presentation**: Keystone Symposia on Molecular and Cellular Biology. Genomic Instability and DNA Repair. Whistler Conference Centre, Whistler, British Columbia Canada. March 1-6th, 2015. "Mammalian Polymerase Theta Promotes Alternative-NHEJ and Suppresses Recombination". Pedro A. Mateos-Gómez, Gong F, Nair N, Miller KM, Lazzerini-Denchi E, Sfeir A. Department of Cellular Biology. NYU School of Medicine, New York, USA.
- **Oral presentation**. Department weekly meeting. May 2015.
- Poster presentation for the Genome Integrity discussion group at the New York Academy of Sciences. June 2015.
- **Oral presentation**: Cold Spring Harbor Meetings. Telomeres and Telomerase. Cold Spring Harbor, NY 11724-2213, USA. April 28-May 2, 2015.

"Functional analysis of mammalian Polθ reveals its role in double-strand break repair". Pedro A. Mateos-Gómez, Gong F, Nair N, Miller KM, Lazzerini-Denchi E, Sfeir A. Department of Cellular Biology. NYU School of Medicine, New York, USA.

- **Oral presentation, invited speaker**: 3rd Annual Re-writing Genomes Symposium, A one-day symposium hosted by QB3 Berkeley and the Innovative Genomics Initiative. August 24, 2015 University of California, Berkeley. "How Does Polθ Regulate DNA DSB Repair?". Pedro A. Mateos-Gómez and A. Sfeir.
- Poster presentation at the annual retreat of the Skirball Institute of Biomolecular Medicine. October 2015.
- Poster presentation for the Genome Integrity discussion group at the New York Academy of Sciences. June 2016.
- Poster Presenter at the Gordon Research Seminar on Mutagenesis (GRS) held 06/04/2016 - 06/05/2016 at PGA Catalunya Business and Convention Centre in Gerona, Spain. Presented poster titled: Investigating the Interplay between Polymerase theta and RPA1 during DNA double-strand break repair.
- Poster Presenter at the Gordon Research Conference on Mutagenesis held 06/05/2016 - 06/10/2016 at PGA Catalunya Business and Convention Centre in Gerona, Spain. Presented poster titled: Investigating the Interplay between Polymerase theta and RPA1 during DNA double-strand break repair.

Dissemination of result to communities of interest:

Nothing to report.

Plan to do during the next reporting period to accomplish the goals:

Nothing to report.

4. Impact:

Impact on the development of the principal discipline of the project:

Our findings about the relevance of the A-NHEJ repair pathway, and particularly PolQ, for the survival of breast cancer cell lines is opening a new avenue for the treatment of this kind of tumors, and some others where the A-NHEJ or PolQ could also have a relevant role. Our data indicate that PolQ mediated A-NHEJ repair is not simply a backup pathway with a minor role, only being activated when other pathways are blocked, but is instead a constitutive part of the DNA damage response with a significant importance for the cancer cells survival and tumor progression.

Impact on other disciplines:

Nothing to report.

Impact on technology transfer:

Nothing to report.

Impact on society beyond science and technology:

Nothing to report.

5. Changes/Problems:

Nothing to report.

6. Products:

Journal publications: attached as appendices.

Mateos-Gomez PA, Gong F, Nair N, Miller KM, Lazzerini-Denchi E, Sfeir A. (2015). Mammalian polymerase θ promotes alternative NHEJ and suppresses recombination. Nature; 518(7538): 254-7. 2015, Feb 12. Published.
Federal support was acknowledged.

Pedro A. Mateos-Gomez, Tatiana Kent, Ekaterina Kashkina, Richard T Pomerantz, and Agnel Sfeir (2017). The helicase domain of Polθ counteracts RPA to promote alt-NHEJ. Nat Struct Mol Biol. Under revision.
Federal support is being acknowledged.

7. Participants & other collaborating organizations:

Individuals that have worked on the project:

No change.

Changes in the active or other support of the PI or senior/key personnel since last reporting period:

Nothing to report.

Other organizations that were involved as partners:

Nothing to report.

8. Special reporting requirements:

Not applicable.

9. Appendices:

LETTER

doi:10.1038/nature14157

Mammalian polymerase θ promotes alternative NHEJ and suppresses recombination

Pedro A. Mateos-Gomez[1], Fade Gong[2], Nidhi Nair[3], Kyle M. Miller[2], Eros Lazzerini-Denchi[3] & Agnel Sfeir[1]

The alternative non-homologous end-joining (NHEJ) machinery facilitates several genomic rearrangements, some of which can lead to cellular transformation. This error-prone repair pathway is triggered upon telomere de-protection to promote the formation of deleterious chromosome end-to-end fusions[1–3]. Using next-generation sequencing technology, here we show that repair by alternative NHEJ yields non-TTAGGG nucleotide insertions at fusion breakpoints of dysfunctional telomeres. Investigating the enzymatic activity responsible for the random insertions enabled us to identify polymerase theta (Polθ; encoded by *Polq* in mice) as a crucial alternative NHEJ factor in mammalian cells. *Polq* inhibition suppresses alternative NHEJ at dysfunctional telomeres, and hinders chromosomal translocations at non-telomeric loci. In addition, we found that loss of *Polq* in mice results in increased rates of homology-directed repair, evident by recombination of dysfunctional telomeres and accumulation of RAD51 at double-stranded breaks. Lastly, we show that depletion of Polθ has a synergistic effect on cell survival in the absence of *BRCA* genes, suggesting that the inhibition of this mutagenic polymerase represents a valid therapeutic avenue for tumours carrying mutations in homology-directed repair genes.

Chromosome end-to-end fusions are inhibited by shelterin; a multisubunit complex anchored to telomeric DNA by two Myb-containing proteins—TRF1 and TRF2 (ref. 4). Telomere fusions are executed by two independent end-joining pathways. Classical non-homologous end-joining (C-NHEJ), mediated by LIG4 and the Ku70/80 heterodimer, is primarily blocked by TRF2 (ref. 5). Conversely, alternative NHEJ (alt-NHEJ), which is dependent on LIG3 (ref. 6) and PARP1 (ref. 7), is repressed in a redundant manner[2,3]. Alt-NHEJ is fully unleashed after the simultaneous deletion of TRF1 and TRF2, and the creation of shelterin-free telomeres in cells deficient for *Ku70* and *Ku80* (also known as *Xrcc6* and *Xrcc5*, respectively)[2]. This error-prone end-joining pathway mediates fusion of naturally eroded telomeres[1], joining of switch regions during class-switch recombination[8], and formation of chromosomal translocations in mouse cells[9,10].

To characterize the differences between C-NHEJ and alt-NHEJ at dysfunctional telomeres, we determined whether the sequence of the junction between two fused telomeres differed depending on the type of repair pathway used. Telomere fusions by C-NHEJ were triggered by Cre-mediated depletion of TRF2 using previously described mouse embryonic fibroblasts (MEFs) (*Trf2*$^{F/F}$Cre-ER^{T2})[11] (Extended Data Fig. 1a). To induce robust fusions by the alt-NHEJ pathway, we depleted the entire shelterin complex by deleting *Trf1* and *Trf2* from *Trf1*$^{F/F}$ *Trf2*$^{F/F}$ *Ku80*$^{-/-}$ Cre-ER^{T2} MEFs[2] (Extended Data Fig. 1a). DNA was subjected to next-generation sequencing, and reads corresponding to telomeres were identified on the basis of the presence of at least three consecutive TTAGGG repeats. To detect rare reads containing fusion junctions, we exploited the novel sequence arrangement created by the ligation of the 3′ G-rich strand (TTAGGG-3′) to the 5′ C-rich strand (5′-CCCTAA) (Fig. 1a), and filtered reads that started with at least three G-rich repeats and ended with two or more C-rich repeats. We confirmed that this approach could successfully identify telomere fusions by comparing reads derived from *Trf2*-proficient and *Trf2*-deficient cells. Starting with a similar number of telomere-repeat containing reads, we identified >90 fusogenic events in *Trf2*-knockout MEFs, compared to only three events in wild-type

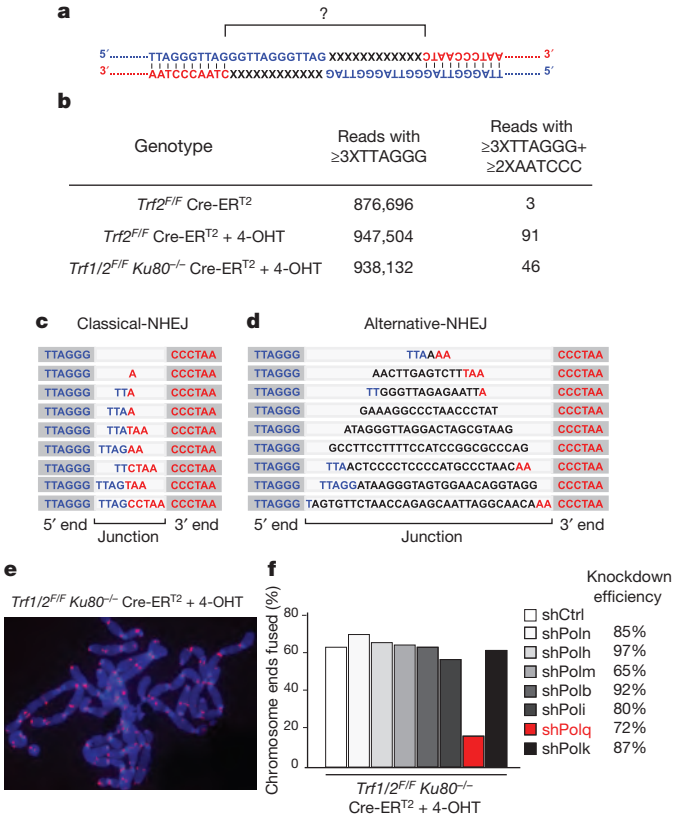

Figure 1 | Random nucleotide insertions at the junction of telomeres fused by alt-NHEJ. **a**, Schematic of the junction of a telomere fusion. The 3′ end of the telomeric G-rich strand of a chromosome (blue) is fused to the 5′ end of the C-rich strand of a different chromosome (red). **b**, Illumina sequencing to analyse telomere fusion junctions. Reads ≥3XTTAGGG consecutively were scored as derived from telomere fragments. Those with ≥3XTTAGGG on the 5′ end and ≥2XCCCTAA at the 3′ end were scored as telomere fusion junctions (see Supplementary Information). **c**, Examples of telomere fusions generated by C-NHEJ of TRF2-depleted telomeres. Light grey highlights fusion junctions, dark grey marks the flanking telomere repeats. **d**, Examples of insertions in shelterin-free *Ku80*-null MEFs. **e**, Telomere fusions in metaphase spreads from *Trf1*$^{F/F}$ *Trf2*$^{F/F}$ *Ku80*$^{-/-}$ Cre-ER^{T2} MEFs. Telomeres in red (peptide nucleic acid (PNA) probe) and chromosomes in blue (4′,6-diamidino-2-phenylindole; DAPI). **f**, Frequency of telomere fusions after the depletion of candidate polymerases. 4-OHT, 4-hydroxytamoxifen; shCtrl, control shRNA. Bars represent mean of $n > 1{,}000$ chromosome ends derived from one experiment.

[1]Skirball Institute of Biomolecular Medicine, Department of Cell Biology, NYU School of Medicine, New York, New York 10016, USA. [2]Department of Molecular Biosciences, Institute for Cellular and Molecular Biology, University of Texas at Austin. 2506 Speedway Stop A5000, Austin, Texas 78712, USA. [3]Department of Molecular and Experimental Medicine, The Scripps Research Institute, La Jolla, California 92037, USA.

cells (Fig. 1b). Sequence analysis of the junctions highlighted different permutations of TTAGGG/AATCCC sequences. Notably, the spectrum of the fusion junctions was different in shelterin-free settings, in which frequent non-telomeric nucleotide insertions (9 out of 46 events) were identified at fusion breakpoints (Fig. 1b–d and Supplementary Information).

To identify the enzyme that incorporated nucleotides at dysfunctional telomeres, we depleted known low-fidelity DNA polymerases in shelterin-free cells lacking *Ku80*, and analysed chromosome-end fusions on metaphase spreads. Notably, we observed a reduction in the frequency of telomere fusions in cells with reduced levels of polymerase theta (Polθ, encoded by *Polq* in mice) (Fig. 1e, f and Extended Data Fig. 1b). The activity of Polθ is specific to alt-NHEJ as its inhibition in *Trf2*-knockout cells did not affect the frequency of C-NHEJ (Fig. 2a, b and Extended Data Fig. 2a–c).

Polθ is an A-family DNA polymerase that exhibits low fidelity on templated DNA[12], and also displays a terminal transferase-like activity that catalyses nucleotide addition in a template-independent manner[13]. The relevance of these activities *in vivo* was highlighted in *Drosophila melanogaster*, in which Polθ was shown to stimulate nucleotide insertions during double-stranded break (DSB) repair by alt-NHEJ[14]. More recently, Polθ was shown to promote end-joining of replication-associated DSBs in *Caenorhabditis elegans*[15], preventing large deletions around G-rich DNA[16]. The exact function of Polθ during DSB repair in mammalian cells remains elusive.

The crucial role for Polθ at dysfunctional telomeres prompted us to test whether it is required for DSB repair at non-telomeric loci. To this end, we tested whether the depletion of Polθ affects chromosomal translocations in the context of mouse pluripotent cells, reported to be mediated by alt-NHEJ[10] in a LIG3-dependent manner[9]. To model chromosomal translocations, we induced DSBs in the Rosa26 and H3f3B mouse loci using the CRISPR/Cas9 system (Fig. 2c). When introduced into $Polq^{+/+}$ and $Polq^{-/-}$ cells[17], the Cas9-gRNA(Rosa26;H3f3b) expression plasmid induced simultaneous cleavage of both loci with comparable efficiencies (Extended Data Fig. 2d, e). Consistent with previous reports, 24% of translocation events in $Polq^{+/+}$ cells were scarred by random insertions. Interestingly, the overall frequency of translocations in cells lacking *Polq* was significantly reduced (Fig. 2d). Sequence analysis of residual translocations in $Polq^{-/-}$ cells highlighted the absence of insertions, and a concomitant decrease in micro-homology at junctions (Fig. 2d and Extended Data Figs 2–5). Notably, we observed similar results when assessing translocation frequency in cells expressing a catalytically inactive form of Polθ (Extended Data Fig. 2g–k). Altogether, our data indicate that the promiscuous activity of Polθ during DSB repair contributes to the increased mutagenicity of alt-NHEJ. Importantly, our results indicate that mammalian Polθ plays a critical part by stimulating the end-joining reaction.

We next investigated the upstream signalling event(s) required for the recruitment of Polθ to DNA damage sites, induced after micro-irradiation of HeLa cells expressing Myc-tagged Polθ. Accumulation of Polθ at laser-induced DNA breaks, discerned by its co-localization with the phosphorylated histone H2AX (γ-H2AX), occurred in ~25% of cells that stained positive for Myc (Fig. 3a, b), and was independent of either ATM or ATR signalling (Extended Data Fig. 6). Instead,

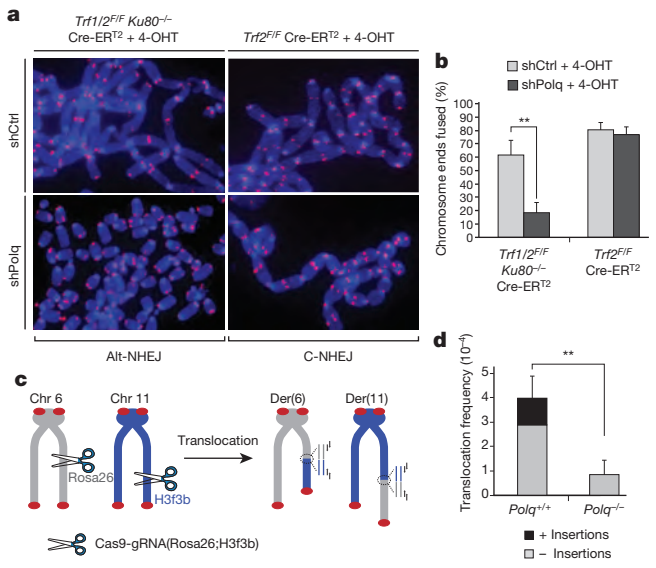

Figure 2 | Polθ is required for alt-NHEJ-dependent DSB repair in mammalian cells. **a**, Metaphases from TRF2-depleted ($Trf2^{F/F}$ Cre-ER^{T2} + 4-OHT) and shelterin-free ($Trf1^{F/F}$ $Trf2^{F/F}$ $Ku80^{-/-}$ Cre-ER^{T2} + 4-OHT) MEFs infected with the indicated short hairpin RNA (shRNA). **b**, Quantification of telomere fusions in MEFs with the indicated treatment (mean values ± s.d. derived from six independent experiments. $^{**}P = 0.003$; two-tailed Student's *t*-test). **c**, Design of the translocation assay in which DSBs are induced by Cas9-gRNA(Rosa26;H3f3b). Joining of DNA ends generates der(6) and der(11), detected by nested PCR[9]. **d**, Translocation frequency in $Polq^{+/+}$ and $Polq^{-/-}$ cells 60 h after Cas9-gRNA(Rosa26;H3f3b) expression. Mean values ± s.d. derived from three independent experiments. $^{**}P = 0.009$; two-tailed Student's *t*-test.

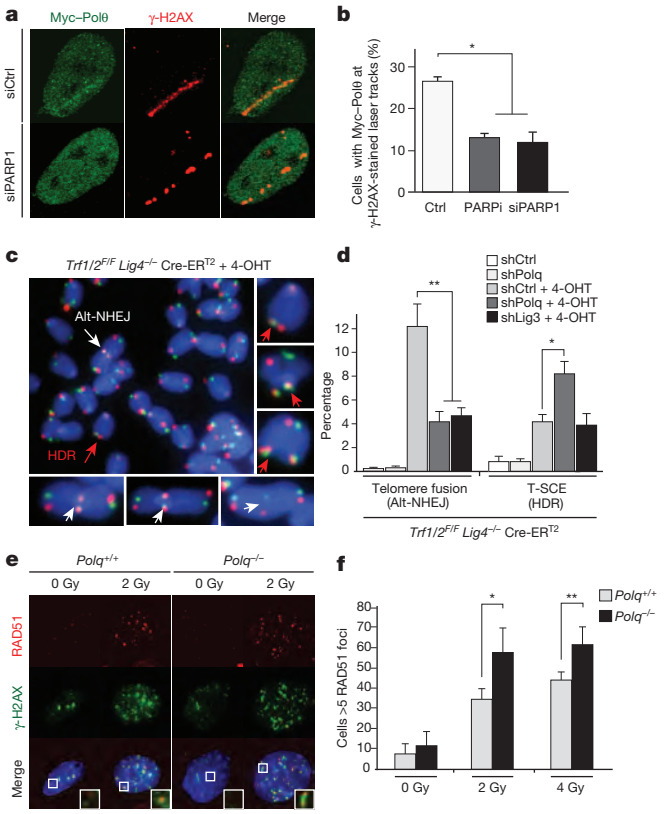

Figure 3 | Polθ is recruited by PARP1 to promote alt-NHEJ at the expense of HDR. **a**, Myc–Polθ localization to DNA damage was monitored after laser micro-irradiation of HeLa cells. Cells were fixed and stained for γ-H2AX and Myc, 1 h after damage induction. **b**, Quantification of Polθ accumulation at sites of laser damage (mean values ± s.e.m. derived from two independent experiments). **c**, To test whether Polθ represses recombination at telomeres, we depleted the polymerase in shelterin-free and *Lig4*-deficient MEFs[2], and both repair pathways were monitored using CO-FISH. White arrows indicate alt-NHEJ events, red arrows highlight HDR-mediated T-SCEs. **d**, Quantification of telomere fusion (alt-NHEJ) and T-SCE (HDR) in cells transduced with shRNAs against *Polq*, *Lig3* or control shRNA. Error bars denote ± s.d. from three independent experiments. **e**, Immunofluorescence for RAD51 and γ-H2AX in the indicated MEFs 3 h after irradiation. **f**, Graph representing quantification of ionizing-radiation-induced RAD51 foci. Mean values ± s.d. derived from three independent experiments. $^{*}P < 0.05$, $^{**}P < 0.01$; two-tailed Student's *t*-test.

co-localization of Polθ with γ-H2AX was reduced after depletion of PARP1 with short interfering RNAs (siRNAs), or after the inhibition of PARP1 activity (using KU58948) (Fig. 3a, b). In a parallel experiment that used a recently developed U2OS-DSB reporter cell line[18], we were able to ascertain the localization of Myc–Polθ to bona fide DSBs, induced after FOK1 cleavage of a LacO-tagged genomic locus (Extended Data Fig. 7). In conclusion, our data suggest that PARP1, previously known to be required for alt-NHEJ[7,19], facilitates the recruitment of Polθ to DSBs.

Homology-directed repair (HDR) is prevalent during the S/G2 phase of the cell cycle, which coincides with the peak of alt-NHEJ activity, and these pathways also share the initial resection step mediated by MRE11 and CtIP[20]. To test whether inhibiting alt-NHEJ could potentially result in increased HDR, we depleted shelterin in *Lig4*-deficient MEFs, a genetic setting that is conducive to the activity of alt-NHEJ as well as HDR[2]. To investigate the relative contribution of the two repair pathways, we used a chromosome-orientation fluorescence *in situ* hybridization (CO-FISH) assay[21], and monitored the exchange of telomeres between sister chromatids by HDR (telomere sister chromatid exchange, T-SCE), and, at the same time, measured the frequency of chromosome end–end fusion by end-joining (Fig. 3c). After depletion of shelterin from *Trf1*$^{F/F}$ *Trf2*$^{F/F}$ *Lig4*$^{-/-}$ Cre-ER^{T2} MEFs, ~10% of the telomeres were processed by alt-NHEJ, whereas ~5% of chromosome ends showed T-SCEs[2] (Fig. 3c, d and Extended Data Fig. 8a–c). As expected, we observed a substantial reduction in the frequency of alt-NHEJ at shelterin-free telomeres in *Lig4*$^{-/-}$ cells that lack *Polq* or *Lig3* (Fig. 3d and Extended Data Fig. 8a–e). Remarkably, *Polq*-depleted cells exhibited a concomitant increase in T-SCE, which was not evident in cells lacking *Lig3* (Fig. 3d), thereby highlighting a unique role for Polθ in counteracting HDR. To gain insight into this novel Polθ function, we show that the promiscuous polymerase is not required for end-resection of DSBs (Extended Data Fig. 8f, g). Instead, its activity counteracts the accumulation of RAD51 foci (Fig. 3e, f and Extended Data Fig. 8h). To corroborate these findings, we used the traffic light reporter (TLR) system, designed to generate a flow-cytometric readout for HDR and end-joining at a site-specific DNA break induced by I-Sce1 (ref. 22). We observed that after knocking down *Polq* in *Lig4*$^{-/-}$ cells, resolution of the I-Sce1-induced DNA break by HDR is increased, in conjunction with a significant reduction in the frequency of alt-NHEJ (Extended Data Fig. 9).

Alt-NHEJ is often considered as a back-up choice for DSB repair, operating at the expense of genomic stability. Circumstantial evidence suggests that this pathway could be enhanced when HDR is impaired[23,24]. We therefore postulated that this error-prone mode of repair has an essential role in cells with compromised HDR activity. We tested this hypothesis by inhibiting *Polq* in cells lacking the breast cancer susceptibility genes—*Brca1* and *Brca2*. Chromosome analysis revealed a four-fold increase in chromosomal aberrancies after *Polq* depletion in MEFs lacking either *Brca1* or *Brca2*. Such aberrancies included chromatid and chromosome breaks, in addition to radial chromosome structures characteristic of *Lig4*-mediated processing of chromatid breaks via the C-NHEJ pathway (Fig. 4a, b and Extended Data Fig. 10a, b). Ultimately, the increased genomic instability in cells co-depleted for *Polq* and *Brca* genes compromised cellular survival. We observed that *BRCA1*-mutated human cells (Fig. 4c, d), and mouse cells lacking *Brca1* (Extended Data Fig. 10c–f), displayed significantly reduced colony-forming capabilities after *Polq* impairment. Although we cannot exclude that Polθ performs additional activities required for the survival of *Brca*-deficient cells[25], our data suggest that Polθ-mediated alt-NHEJ promotes the survival of cells with a compromised HDR pathway. In the absence of a safer means to repair breaks, alt-NHEJ may therefore prevent genomic havoc by resolving unrepaired lesions.

Here we provide direct evidence linking Polθ to alt-NHEJ repair in mammalian cells (Fig. 4e). We also show that while Polθ hinders error-free repair by HDR, its activity is essential for the survival of HDR-deficient cells (Fig. 4e). The question remains as to how this promiscuous polymerase orchestrates DSB repair. After DSB formation in the S/G2 phase

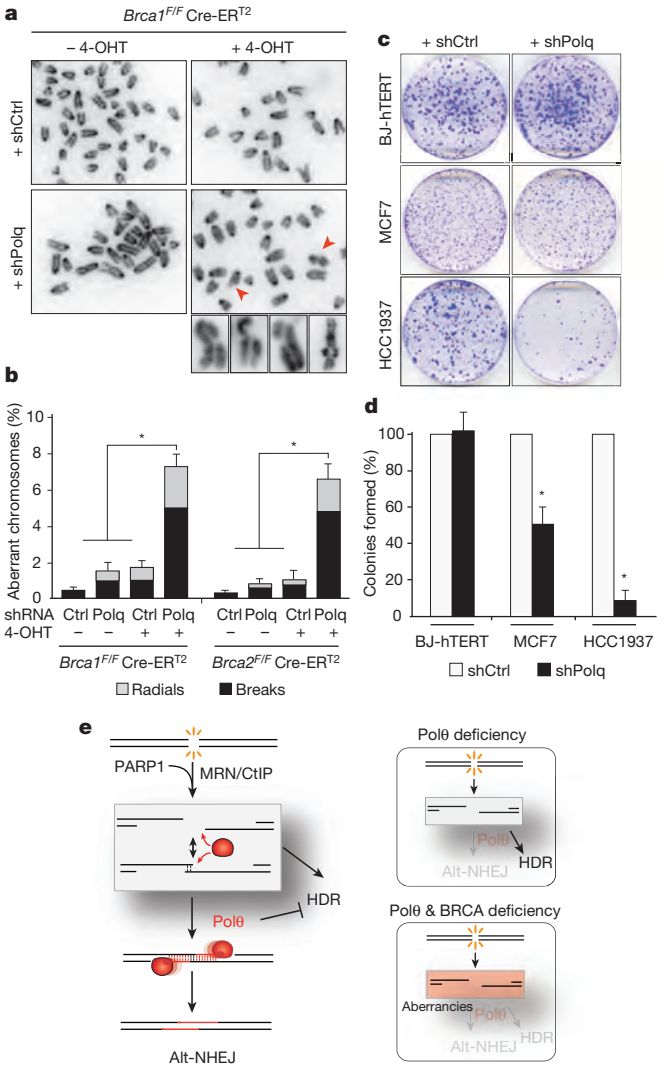

Figure 4 | *Polq* inhibition in *Brca*-mutant cells leads to increased chromosomal aberrancies and reduced cellular survival. **a**, Analysis of genomic instability in metaphase spreads from *Brca1*$^{F/F}$ Cre-ER^{T2} MEFs treated with shRNA against *Polq* or vector control. **b**, Quantification of breaks (chromatid and chromosome) and radials in *Brca1*$^{F/F}$ Cre-ER^{T2} and *Brca2*$^{F/F}$ Cre-ER^{T2} MEFs with the indicated treatment. Mean values are presented with error bars denoting ± s.d. from three independent experiments. **c**, Clonogenic survival after *Polq* depletion. Crystal violet staining of BJ-hTERT, MCF7 and HCC1937 cells treated with shRNA against *Polq* or vector control. **d**, Quantitative analyses of colony formation assay. Colonies in each control shRNA cell line were set to 100%. Colonies in shPolq-expressing cells are normalized to shCtrl. Mean values ± s.d. derived from three independent experiments. $*P < 0.05$, $**P < 0.01$; two-tailed Student's *t*-test. **e**, Schematic depicting our model for the function of Polθ during DSB repair (see Supplementary Information).

of the cell cycle, resection of DSBs by MRE11 and CtIP[20] potentially exposes micro-homology that allows spontaneous annealing of broken DNA ends (Fig. 4e). The binding of RPA antagonizes this annealing step to promote HDR-mediated repair[26,27]. An opposing activity is likely to be exerted by Polθ. Placing our finding in the context of recent biochemical experiments and genetic studies in model organisms[13–16], we ultimately propose a model in which Polθ exploits both its template-independent and template-dependent activities to stabilize the annealed intermediate structure and channel repair towards the alt-NHEJ pathway (Fig. 4e). Our findings that Polθ is critical for alt-NHEJ support this model, which provides a potential explanation as to how this polymerase counteracts HDR.

Finally, it is intriguing that although *POLQ* expression in normal human tissues is generally repressed[28], it is upregulated in a wide range of human cancers and associates with poor clinical outcome in breast tumours[29,30]. Our findings that cells with compromised HDR activity depend on this mutagenic polymerase for survival establish a rationale for the development of Polθ-targeted approaches for cancer treatment.

Online Content Methods, along with any additional Extended Data display items and Source Data, are available in the online version of the paper; references unique to these sections appear only in the online paper.

Received 28 July; accepted 16 December 2014.
Published online 2 February 2015.

1. Capper, R. *et al.* The nature of telomere fusion and a definition of the critical telomere length in human cells. *Genes Dev.* **21,** 2495–2508 (2007).
2. Sfeir, A. & de Lange, T. Removal of shelterin reveals the telomere end-protection problem. *Science* **336,** 593–597 (2012).
3. Rai, R. *et al.* The function of classical and alternative non-homologous end-joining pathways in the fusion of dysfunctional telomeres. *EMBO J.* **29,** 2598–2610 (2010).
4. Sfeir, A. Telomeres at a glance. *J. Cell Sci.* **125,** 4173–4178 (2012).
5. van Steensel, B., Smogorzewska, A. & de Lange, T. TRF2 protects human telomeres from end-to-end fusions. *Cell* **92,** 401–413 (1998).
6. Wang, H. *et al.* DNA ligase III as a candidate component of backup pathways of nonhomologous end joining. *Cancer Res.* **65,** 4020–4030 (2005).
7. Audebert, M., Salles, B., Weinfeld, M. & Calsou, P. Involvement of polynucleotide kinase in a poly(ADP-ribose) polymerase-1-dependent DNA double-strand breaks rejoining pathway. *J. Mol. Biol.* **356,** 257–265 (2006).
8. Yan, C. T. *et al.* IgH class switching and translocations use a robust non-classical end-joining pathway. *Nature* **449,** 478–482 (2007).
9. Simsek, D. *et al.* DNA ligase III promotes alternative nonhomologous end-joining during chromosomal translocation formation. *PLoS Genet.* **7,** e1002080 (2011).
10. Simsek, D. & Jasin, M. Alternative end-joining is suppressed by the canonical NHEJ component Xrcc4-ligase IV during chromosomal translocation formation. *Nature Struct. Mol. Biol.* **17,** 410–416 (2010).
11. Okamoto, K. *et al.* A two-step mechanism for TRF2-mediated chromosome-end protection. *Nature* **494,** 502–505 (2013).
12. Arana, M. E., Seki, M., Wood, R. D., Rogozin, I. B. & Kunkel, T. A. Low-fidelity DNA synthesis by human DNA polymerase theta. *Nucleic Acids Res.* **36,** 3847–3856 (2008).
13. Hogg, M., Sauer-Eriksson, A. E. & Johansson, E. Promiscuous DNA synthesis by human DNA polymerase θ. *Nucleic Acids Res.* **40,** 2611–2622 (2012).
14. Chan, S. H., Yu, A. M. & McVey, M. Dual roles for DNA polymerase theta in alternative end-joining repair of double-strand breaks in *Drosophila*. *PLoS Genet.* **6,** e1001005 (2010).
15. Roerink, S. F., van Schendel, R. & Tijsterman, M. Polymerase theta-mediated end joining of replication-associated DNA breaks in *C. elegans*. *Genome Res.* **24,** 954–962 (2014).
16. Koole, W. *et al.* A Polymerase Theta-dependent repair pathway suppresses extensive genomic instability at endogenous G4 DNA sites. *Nature Commun.* **5,** 3216 (2014).
17. Shima, N. *et al.* Phenotype-based identification of mouse chromosome instability mutants. *Genetics* **163,** 1031–1040 (2003).
18. Tang, J. *et al.* Acetylation limits 53BP1 association with damaged chromatin to promote homologous recombination. *Nature Struct. Mol. Biol.* **20,** 317–325 (2013).
19. Wang, M. *et al.* PARP-1 and Ku compete for repair of DNA double strand breaks by distinct NHEJ pathways. *Nucleic Acids Res.* **34,** 6170–6182 (2006).
20. Truong, L. N. *et al.* Microhomology-mediated End Joining and Homologous Recombination share the initial end resection step to repair DNA double-strand breaks in mammalian cells. *Proc. Natl Acad. Sci. USA* **110,** 7720–7725 (2013).
21. Bailey, S. M., Cornforth, M. N., Kurimasa, A., Chen, D. J. & Goodwin, E. H. Strand-specific postreplicative processing of mammalian telomeres. *Science* **293,** 2462–2465 (2001).
22. Certo, M. T. *et al.* Tracking genome engineering outcome at individual DNA breakpoints. *Nature Methods* **8,** 671–676 (2011).
23. Bindra, R. S., Goglia, A. G., Jasin, M. & Powell, S. N. Development of an assay to measure mutagenic non-homologous end-joining repair activity in mammalian cells. *Nucleic Acids Res.* **41,** e115 (2013).
24. Sakai, W. *et al.* Secondary mutations as a mechanism of cisplatin resistance in BRCA2-mutated cancers. *Nature* **451,** 1116–1120 (2008).
25. Fernandez-Vidal, A. *et al.* A role for DNA polymerase θ in the timing of DNA replication. *Nature Commun.* **5,** 4285 (2014).
26. Deng, S. K., Gibb, B., de Almeida, M. J., Greene, E. C. & Symington, L. S. RPA antagonizes microhomology-mediated repair of DNA double-strand breaks. *Nature Struct. Mol. Biol.* **21,** 405–412 (2014).
27. Chen, H., Lisby, M. & Symington, L. S. RPA coordinates DNA end resection and prevents formation of DNA hairpins. *Mol. Cell* **50,** 589–600 (2013).
28. Kawamura, K. *et al.* DNA polymerase theta is preferentially expressed in lymphoid tissues and upregulated in human cancers. *Int. J. Cancer* **109,** 9–16 (2004).
29. Higgins, G. S. *et al.* Overexpression of POLQ confers a poor prognosis in early breast cancer patients. *Oncotarget* **1,** 175–184 (2010).
30. Lemée, F. *et al.* DNA polymerase theta up-regulation is associated with poor survival in breast cancer, perturbs DNA replication, and promotes genetic instability. *Proc. Natl Acad. Sci. USA* **107,** 13390–13395 (2010).

Supplementary Information is available in the online version of the paper.

Acknowledgements We thank T. de Lange, R. Greenberg, J. Shay, N. Shima, C. Cazaux and R. Wood for providing key reagents for this study. We are grateful to M. Ji, L. Walton Masters, A. Phillips, A. Pinzaru, F. Yeung, P. Tonzi and J. Wong for technical assistance. We thank S. Kabir and F. Lottersberger for critical reading of the manuscript. This work was supported by a grant from the Breast Cancer Alliance (A.S.), V-foundation (A.S.), Department of Defense Breast Cancer Research Program BC134020 (P.A.M.-G.), Pew-Stewart Scholars Award (A.S.), Pew Scholars Award (E.L.-D.), Novartis Advanced Discovery Institute (E.L.-D.), and a grant from the National Institutes of Health (NIH) AG038677 (E.L.-D.). The A.S. laboratory was supported by start-up funds from the Helen L. and Martin S. Kimmel Center for Stem Cell Biology. The K.M.M. laboratory was supported in part by start-up funds from the University of Texas at Austin and from the Cancer Prevention Research Institute of Texas (CPRIT, R116). K.M.M. is a CPRIT scholar.

Author Contributions A.S., E.L.-D. and P.A.M.-G. conceived the experimental design. P.A.M.-G. and A.S. performed the experiments and analysed the data. E.L.-D. and N.N. performed telomere-sequencing experiments. F.G. and K.M.M. performed experiments related to Polθ localization at DNA breaks. A.S. wrote the manuscript. All authors discussed the results and commented on the manuscript.

Author Information Sequence has been deposited with the BioProject database under accession PRJNA269507. Reprints and permissions information is available at www.nature.com/reprints. The authors declare no competing financial interests. Readers are welcome to comment on the online version of the paper. Correspondence and requests for materials should be addressed to A.S. (agnel.sfeir@med.nyu.edu).

METHODS

Cell culture procedures. *Trf2*$^{F/F}$ Cre-ER^{T2}, *Trf1*$^{F/F}$ *Trf2*$^{F/F}$ *Ku80*$^{-/-}$ Cre-ER^{T2} and *Trf1*$^{F/F}$ *Trf*$^{F/F}$ *Lig4*$^{-/-}$ Cre-ER^{T2} MEF lines were previously described[2,11]. *Polq*$^{+/+}$ and *Polq*$^{-/-}$ MEFs were a gift from N. Shima[17]. *Brca1*$^{F/F}$ Cre-ER^{T2} and *Brca2*$^{F/F}$ Cre-ER^{T2} MEFs and U2OS-DSB reporter cells[18] were a gift from R. Greenberg. *Trf1*$^{F/F}$ *Trf2*$^{F/F}$ *Lig4*$^{-/-}$ Cre-ER^{T2} MEFs were derived from mice that were deficient in p53. The remaining MEF lines were immortalized with pBabeSV40LargeT. MEFs were cultured in DMEM supplemented with 10–15% FBS (Gibco), 2 mM L-glutamine (Sigma), 100 U ml^{-1} penicillin (Sigma), 0.1 μg ml^{-1} streptomycin (Sigma), 0.1 mM non-essential amino acids (Invitrogen) and 1 mM sodium pyruvate (Sigma). Expression of Cre recombinase was induced by treating MEFs carrying the Cre-ER^{T2} allele with 0.5 μM 4-OHT (Sigma H7904) for 12 h. The $t = 0$ time point was set at the time of treatment with 4-OHT. BJ-hTERT and MCF7 cells were grown in DMEM supplemented with 10% FBS. HCC1937 cells were grown in RPMI medium (Gibco) containing 15% FBS. U2OS-DSB reporter cells were grown in DMEM supplemented with 10% BCS. Human HeLa cells were grown in DMEM supplemented with 10% FBS, 100 U ml^{-1} penicillin, 100 μg ml^{-1} streptomycin and 2 mM L-glutamine. Mouse embryonic stem cells were grown in DMEM supplemented with 15% FBS (ES-qualified FBS) (Gibco), 2 mM L-glutamine (Sigma), 100 U ml^{-1} penicillin (Sigma), 0.1 μg ml^{-1} streptomycin (Sigma), 0.1 mM non-essential amino acids (Invitrogen), leukaemia inhibitory factor (LIF) and 2-β-mercaptoethanol (Gibco 21985). For inhibitor experiments, PARPi (KU58948, Axon medchem), ATMi (KU-55933, Tocris) and ATRi (VE-821, Selleckchem) were all used at a final concentration of 10 μM, and were applied to culture medium 2–4 h before irradiation. For ionizing radiation treatment, cells were exposed to 1–10 Gy ionizing radiation by a Faxitron X-ray system (120 kV, 5 mA, dose rate 5 Gy min^{-1}) and recovered for 4 h before immunofluorescence analysis.

Lentiviral delivery of shRNA. shRNA treatments were carried out before 4-OHT treatment. shRNAs (see below for a list of sequences) were introduced by two lentiviral infections at 12 h intervals using supernatant from transfected 293T cells. Parallel infection with pLK0.1 was used as a negative control. Cells were selected with puromycin for 3 days.

TLR assay. Lentiviral constructs coding for TLR (31482) and I-Sce1 with donor e-GFP (31476) were purchased from Addgene[22]. To avoid the confounding effect of classical-NHEJ on the repair of I-Sce1-induced DNA breaks, we stably integrated the TLR construct into *Ku80*$^{-/-}$ and *Lig4*$^{-/-}$ MEFs. The plasmid was transduced by two lentiviral infections at 12 h intervals using supernatant from transfected 293T cells. Cells with integrated TLR were selected with puromycin for 5 days. Cells were then transduced with concentrated *Polq* shRNA lentiviral particles followed by I-Sce1. Cells were collected 72 h later without further antibiotic selection and analysed on a BD LSRII. eGFP fluorescence, which reflects HDR repair, was measured using a 488-nm laser for excitation and a 530/30 filter for detection. mCherry fluorescence, indicative of alt-NHEJ was measured by using a 561-nm laser for excitation and a 610/20 filter for detection. Data were analysed using FloJo software.

Detection of telomeric fusions. To enrich for telomeric DNA, genomic DNA was digested with two frequent cutters (AluI and MboI) and fragments greater than 10 kilobases (kb) were isolated. The resulting DNA was used to generate a library using the NEBNext Ultra Library Prep Kit and the NEBNext Multiplex Oligos for Illumina (NEB) following the manufacturer instructions. The resulting library was run on an Illumina HiSeq platform generating 100-base-pair (bp) indexed pair-end reads.

Transient transfection of cells and laser micro-irradiation. Full-length human *POLQ* was cloned into pLPC-Myc vectors. HeLa cells were plated on glass-bottomed dishes (Willco Wells). Myc–Polθ constructs were transfected into HeLa and U2OS-DSB reporter cells cell with HilyMax (Dojindo) according to the manufacturer's instruction. Then, 24 h after transfection, cells were pre-sensitized with 10 μM 5-bromo-2′-deoxyuridine (BrdU) in normal DMEM medium for 20 h. After indicated treatments, cells were damaged by laser micro-irradiation as previously described[31]. After laser micro-irradiation, cells were incubated for 1 h, then fixed and analysed by immunofluorescence and microscopic imaging as described below. For PARP1 siRNA experiments, cells were transfected with siCtrl (non-targeting pool, Thermo Scientific) or siPARP1 (GGGCAAGCACAGUGUCAAAUU, Sigma), for 24 h before *POLQ* transfections and subsequent treatments as described above.

Immunofluorescence and confocal microscopy. After the indicated treatments, cells were processed and analysed for immunofluorescence as previously described[32]. In brief, cells were fixed with 2% (v/v) paraformaldehyde for 15 min at room temperature. Cells were washed with PBS, permeabilized with 0.5% (v/v) Triton X-100 for 10 min, and blocked with PBS containing 3% BSA. Cells were incubated with the same buffer containing primary antibodies for 1 h at room temperature followed by secondary antibodies incubations for 1 h at room temp. Cells were imaged and analysed with *Z*-stacked setting using the FV10-ASW3.1 software on a Fluoview 1000 confocal microscope (Olympus). For laser line quantification, >50 cells were counted for all conditions from two independent experiments. The primary antibodies used for immunofluorescence were γ-H2AX (p Ser139) (rabbit polyclonal, Novus, NB100-384) and c-Myc (mouse monoclonal, Santa Cruz, sc-40). The secondary antibodies used for immunofluorescence were Alexa Fluor 594 (rabbit) (Invitrogen, A11037) and Alexa Fluor 488 (mouse) (Invitrogen, A11029). To analyse the recruitment of Polθ to double-stranded breaks, U2OS-DSB reporter cells expressing Myc–Polθ were analysed 4 h after treatment with shield and tamoxifen. Lastly, to analyse RAD51 foci formation and its co-localization with γ-H2AX (p Ser139) after ionizing radiation treatment, cells were treated with 0.2% Triton X-100 (in PBS) for 5 min on ice before fixation with paraformaldehyde. The primary antibodies used for RAD51 immunofluorescence were γ-H2AX (p Ser139) (mouse monoclonal, Novus, NB100-384) and RAD51 (rabbit polyclonal, Santa Cruz, sc-8349).

FISH. Cells were collected at 96 h after treatment with 4-OHT to analyse the frequency of telomere fusions. In brief, ~80% confluent MEFs were incubated for 2 h with 0.2 μg ml^{-1} colcemid (Sigma). The cells were collected by trypsinization, resuspended in 0.075 M KCl at 37 °C for 30 min, and fixed overnight in methanol/acetic acid (3:1) at 4 °C. The cells were dropped onto glass slides and the slides were dried overnight. The next day, the slides were rehydrated with PBS for 15 min then fixed with 4% formaldehyde for 2 min at room temperature. Slides were digested with 1 mg ml^{-1} pepsin, pH 2.2, at 37 °C for 10 min, washed three times with PBS and fixed again in 4% formaldehyde for 2 min at room temperature. After three PBS washes, the slides were incubated consecutively with 75%, 95% and 100% ethanol and allowed to air dry for 30 min before applying hybridization solutions (70% formamide, 1 mg ml^{-1} blocking reagent (Roche), 10 mM Tris-HCl, pH 7.2) containing TAMRA-OO-$(TTAGGG)_3$ PNA probes (Applied Biosystems). Slides were denatured by heating for 3 min at 80 °C and hybridized for 2 h at room temperature. The next day, the slides were washed twice for 15 min each in 70% formamide, 10 mM Tris-HCl, followed by three 5-min washes in 0.1 M Tris-HCl, pH 7.0, 0.15 M NaCl and 0.08% Tween-20. Chromosomal DNA was counterstained with DAPI during the second PBS wash. Slides were mounted in antifade reagent (ProLong Gold, Invitrogen) and images were captured with a Nikon Eclipse TI microscope (see http://delangelab.rockefeller.edu/protocols).

CO-FISH. Cells were labelled with BrdU:BrdC (3:1, final concentration 10 μM) for 14–16 h. Two hours before collection by trypsinization, 0.2 μg ml^{-1} colcemid was added to the media. To fix the cells and drop metaphases on a glass slide, the same procedure that was applied for FISH was followed. Slides were treated with 0.5 mg ml^{-1} RNase A (in PBS, DNase-free) for 10 min at 37 °C, incubated with 0.5 μg ml^{-1} Hoechst 33258 (Sigma) in 2×SSC for 15 min at room temperature, and exposed to 365-nm ultraviolet light (Stratalinker 1800 UV irradiator) for 30 min. The slides were then digested twice with 800 U exonuclease III (Promega) at room temperature for 10 min each, washed with PBS and dehydrated through an ethanol series of 70%, 95% and 100%. After air-drying, slides were hybridized with Tamra-OO-$(TTAGGG)_3$ PNA probe in hybridization solution (70% formamide, 1 mg ml^{-1} blocking reagent (Roche) and 10 mM Tris-HCl, pH 7.2) for 2 h at room temperature. The slides were then washed for a few seconds with 70% formamide and 10 mM Tris-HCl, pH 7.2, and incubated with FITC-OO-$(CCCTAA)_3$ PNA probe in hybridization solution for 2 h. Slides were washed and mounted as described for FISH (see http://delangelab.rockefeller.edu/protocols).

Western blot analysis. Cells were collected by trypsinization, lysed in 2× Laemmli buffer (100 mM Tris-HCl, pH 6.8, 200 μM dithiothreitol, 3% SDS, 20% glycerol and 0.05% bromophenol blue) at 1×10^4 cells per microlitre. The lysate was denatured for 10 min at 95 °C, and sheared by forcing it through a 28-gauge insulin needle ten times. Lysate from 1×10^5 cells was loaded on an SDS–PAGE and transferred to a nitrocellulose membrane. The membrane was blocked in 5% milk in TBS with 0.1% Tween-20 and incubated with primary antibody in TBS, 5% milk and 0.1% Tween-20 for 2 h at room temperature. The following primary antibodies were used: Polθ (ab80906, Abcam); TRF1 (1449, rabbit polyclonal); RAP1 (1252, rabbit polyclonal); phospho-CHK2 (Thr68) (rabbit polyclonal, Cell Signaling); CHK2 (rabbit polyclonal, Cell Signaling); phospho-CHK1 (Ser 345) (mouse monoclonal, Cell Signaling); CHK1 (mouse monoclonal, Santa Cruz); LIG3 (mouse monoclonal, Santa Cruz); Myc (9E10; Calbiochem); and γ-tubulin (clone GTU-88, Sigma); PARP1 (polyclonal, Cell signaling). (See http://delangelab.rockefeller.edu/protocols.)

Chromosomal aberrancies. Cells were collected and dropped on microscope slides as described for the FISH protocol. After the slides had dried overnight, they were rehydrated in PBS, stained with 0.25 μg ml^{-1} DAPI, dehydrated in a 70%, 95% and 100% ethanol series, mounted and imaged using Nikon Eclipse TI microscope. Aberrancies were scored as a percentage of chromatid breaks, chromosome breaks, and chromosome radial structures compared to total number of chromosomes.

Chromosomal translocation assay. Induced pluripotent stem cells were derived from primary *Polq*$^{+/+}$ and *Polq*$^{-/-}$ MEFs according to standard Yamanaka protocol[33]. To perform the translocation assay, *Polq*$^{+/+}$ and *Polq*$^{-/-}$ induced pluripotent stem cells were transfected with 2 μg of Cas9-gRNA(Rosa26;H3f3b) plasmid per million cell. We constructed Cas9-gRNA(Rosa26;H3f3b) by introducing two guide RNAs

(5′-GTTGGCTCGCCGGATACGGG-3′ for H3f3b; 5′-ACTCCAGTCTTTCTAGAAGA-3′ for Rosa26) into pX330 (Addgene, 42230). After transfection, 1×10^4 cells were seeded per well in a 96-well plate, and lysed 3 days later in 40 µl lysis buffer (10 mM Tris, pH 8.0, 0.45% Nonidet P-40 and 0.45% Tween 20). The lysate was incubated with 200 µg ml^{-1} proteinase K for 2 h at 55 °C. Translocation detection was performed according to previously established protocol[9], using nested PCR. The primers used for the first PCR reaction were Tr6-11-Fwd: 5′-GCGGGAGAAATGGATATGAA-3′ and Tr6-11-Rev: 5′- TTGACGCCTTCCTTCTTCTG-3′ for der(6), and Tr11-6-Fwd: 5′-AACCTTTGAAAAAGCCCACA-3′ and Tr11-6-Rev: 5′-GCACGTTTCCGACTTGAGTT-3′, for der(11). For the second round of PCR amplification we used the primers Tr6-11NFwd: 5′-GGCGGATCACAAGCAATAAT-3′ and Tr6-11NRev: 5′-CTGCCATTCCAGAGATTGGT-3′, and Tr11-6NFwd: 5′-AGCCACAGTGCTCACATCAC-3′ and Tr11-6NRev: 5′TCCCAAAGTCGCTCTGAGTT-3′. The number of PCR-positive wells was used to calculate the translocation frequency as previously described[9]. Amplified products from positive wells were sequenced to verify translocations and determine the junction sequences.

Surveyor assay. Forty-eight hours after transfection, genomic DNA was extracted with GE Healthcare Illustra Genomic Prep Mini Spin Kit (28-9042-76). The genomic region encompassing the guide RNA target sites was amplified using Q5 High-Fidelity DNA polymerase (New England BioLabs) with the primers Rosa26-Fwd: 5′-TAAAACTCGGGTGAGCATGT-3′ and Rosa26-Rev: 5′-GGAGTTCTCTGCTGCCTCCTG-3′, and H3f3b-Fwd: 5′-GCGGCGGCTTGATTGCTCCAG-3′ and H3f3b-Rev: 5′-AGCAACTTGTCACTCCTGAGCCAC-3′. PCR fragments were gel purified and the surveyor assay was performed using a detection kit (Transgenomic), according to manufacturer's instructions. Agarose gels (2%) were used to visualize the bands after surveyor digestion.

Colony formation assay. After lentiviral transduction with shCtrl or (sequences listed below), cells were selected with puromycin (BJ: 0.5 µg ml^{-1}; MCF7 and HCC1937: 1 µg ml^{-1}; MEFs: 2 µg ml^{-1}) for 72 h and plated in 6-cm dishes (1,000 and 10,000 cells per plate). After 10–14 days, colonies were fixed with 3% paraformaldehyde (5 min), rinsed with PBS, and stained with crystal violet (Sigma-Aldrich).

CRISPR targeting to mutate *Polq* gene in mouse embryonic stem cells. To generate cells carrying a catalytic dead Polθ, two mutations at residues Asp2494Gly and Glu2495Ser (ref. 34) were introduced in the endogenous *Polq* locus in mouse embryonic stem cells using CRISPR/Cas9 gene targeting. Two guides RNAs were co-transfected with a Cas9-nickase (pX335-U6-Chimeric_BB-CBh-hSpCas9n(D10A)), and a donor cassette that introduces a SacII restriction site while replacing the two amino acid residues. Clonal cells lines were derived and genotyped to determine successful targeting. Two independent clonally derived lines were used for the analysis of translocation.

shRNA target sequence (pLK0.1 vector). shPolm: 5′-CTCACCTCTCACACACCATAA-3′; shPolk: 5′-GCCCTTAGAAATGTCTCATAA-3′; shPolh: 5′-GCTCGATTCTCCAGCTTACAA-3′; shPoli: 5′-AGTGAAGAAGATACGTTTAAA-3′; shPolb: 5′-CCAAAGTTGTTACATCGTGTT-3′; shPoln: 5′-CCTACTCACATGAAGGACATT-3′; shLig3 (mouse): 5′-CCAGACTTCAAACGTCTCAAA-3′; shLIG3 (human): 5′-CCGGATCATGTTCTCAGAAAT-3′; shPolq-1 (mouse): 5′-CGGCGGAGTATGAGAACTATT-3′; shPolq-2(mouse): 5′-CCAGGAATCAAAGACGACAAT-3′; shPolq-3(mouse): 5′-CCTGGCTGAATGCTGAACTTT-3′; shPOLQ (human): 5′-CGGGCCTCTTTAGATATAAAT-3′; shBrca1(mouse): 5′-GCTCAGTGTATGACTCAGTTT-3′.

Primers for quantitative PCR. BRCA1Fwd: 5′-CTGCCGTCCAAATTCAAGAAGT-3′ and BRCA1Rev: 5′-CTTGTGCTTCCCTGTAGGCT-3′; BRCA2Fwd: 5′-TGTGGTAGATGTTGCTAGTCCGCC-3′ and BRCA2Rev: 5′-GCTTTTCTCGTTGTAGTACTGCC-3′; POLbFwd: 5′-TGAACCATCATCAACGAATTGGG-3′ and POLbRev: 5′-CCATGTCTCCACTCGACTCTG-3′; POLmFwd: 5′-AGGCTTCCGCGTCCTAGAT-3′ and POLmRev: 5′-GTGGGGAGAGCATCCATGTT-3′; POLkFwd: 5′-AGCTCAAATTACCAGCCAGCA-3′ and POLkRev: 5′-GGTTGTCCCTCATTTCCACAG-3′; POLhFwd: 5′-ATCGAGTGGTTGCTCTTGTAGA-3′ and POLhRev: 5′-CCAAATGCTCGGGCTTCATAG-3′; POLiFwd: 5′-GCAGTCAAGGGCCACCTAC-3′ and POLiRev: 5′-AGGTCTGTCCTTTAATTCTGGGT-3′; POLnFwd: 5′-AGCTGATGGATGCTCTCAAGCAGG-3′ and POLnRev: 5′-GAGTCAGAGTGCTGTTGCCTACATGG-3′; LIG3(mouse)Fwd: 5′-GAAGAAAGCTGCTGTCCAGG-3′ and LIG3(mouse)Rev: 5′-CAGAGTTGTTGGGTTTTGCTG-3′; LIG3(human)Fwd: 5′-GAAGAGCTGGAAGATAATGAGAAGG-3′ and LIG3(human)Rev: 5′-AGTGGTTGTCAACTTAGCCTGG-3′; POLQ(mouse)Fwd: 5′-CAAGGTTTCATTCGGGTCTTGG-3′ and POLQ (mouse)Rev: 5′-CGAGCAGGAAGATTCACTCCAG-3′; POLQ(human) Fwd: 5′-CAGCCCTTATAGTGGAAGAAGC-3′ and POLQ(human) Rev: 5′-GCACATGGATTCCATTGCACTC-3′.

Statistical analysis. Results are presented as mean ± s.d. of two or three independent experiments unless otherwise stated. $P < 0.05$ was considered statistically significant, and P values were calculated using the two-tailed Student's t-test. No statistical methods were used to predetermine sample size.

31. Shee, C. *et al.* Engineered proteins detect spontaneous DNA breakage in human and bacterial cells. *Elife* **2,** e01222 (2013).
32. Leung, J. W. *et al.* Nucleosome acidic patch promotes RNF168- and RING1B/BMI1-dependent H2AX and H2A ubiquitination and DNA damage signaling. *PLoS Genet.* **10,** e1004178 (2014).
33. Takahashi, K. & Yamanaka, S. Induction of pluripotent stem cells from mouse embryonic and adult fibroblast cultures by defined factors. *Cell* **126,** 663–676 (2006).
34. Prasad, R. *et al.* Human DNA polymerase θ possesses 5′-dRP lyase activity and functions in single-nucleotide base excision repair in vitro. *Nucleic Acids Res.* **37,** 1868–1877 (2009).
35. Celli, G. B. & de Lange, T. DNA processing is not required for ATM-mediated telomere damage response after TRF2 deletion. *Nature Cell Biol.* **7,** 712–718 (2005).
36. Sfeir, A., Kabir, S., van Overbeek, M., Celli, G. B. & de Lange, T. Loss of Rap1 induces telomere recombination in the absence of NHEJ or a DNA damage signal. *Science* **327,** 1657–1661 (2010).

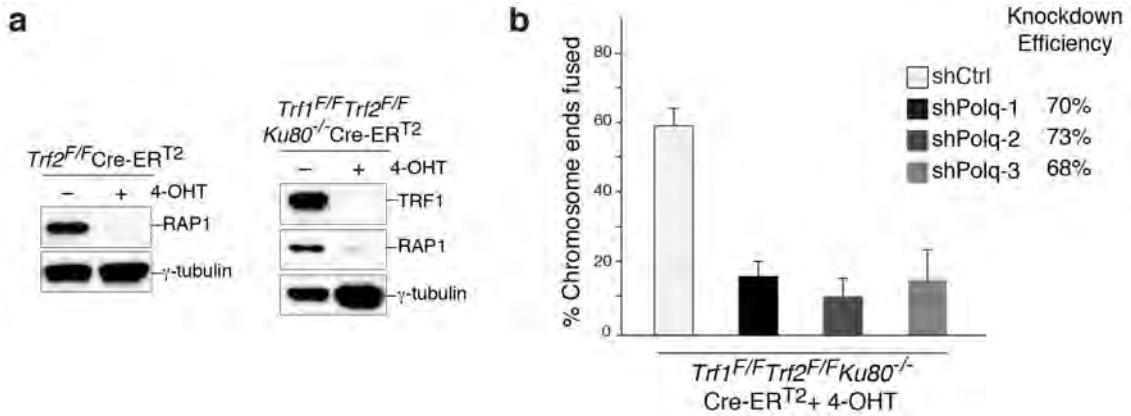

Extended Data Figure 1 | Polθ promotes alt-NHEJ repair at dysfunctional telomeres. (Related to Fig. 1.) **a**, Immunoblots for TRF1 and RAP1 after 4-OHT-induced depletion of TRF2 from *Trf2*$^{F/F}$ Cre-ER^{T2} MEFs and co-depletion of TRF1 and TRF2 from *Trf1*$^{F/F}$ *Trf2*$^{F/F}$ *Ku80*$^{-/-}$ Cre-ER^{T2} cells. Loss of TRF2 is confirmed by the disappearance of RAP1; a TRF2-interacting protein the stability of which depends on TRF2 (refs 35, 36). **b**, To validate the effect of *Polq* depletion on alt-NHEJ we monitored the frequency of telomere fusions in shelterin-free *Ku80*-null cells treated with three independent shPolq vectors. shPolq-1 was used in Fig. 2. Mean values are presented with error bars denoting ± s.e.m. from two independent experiments.

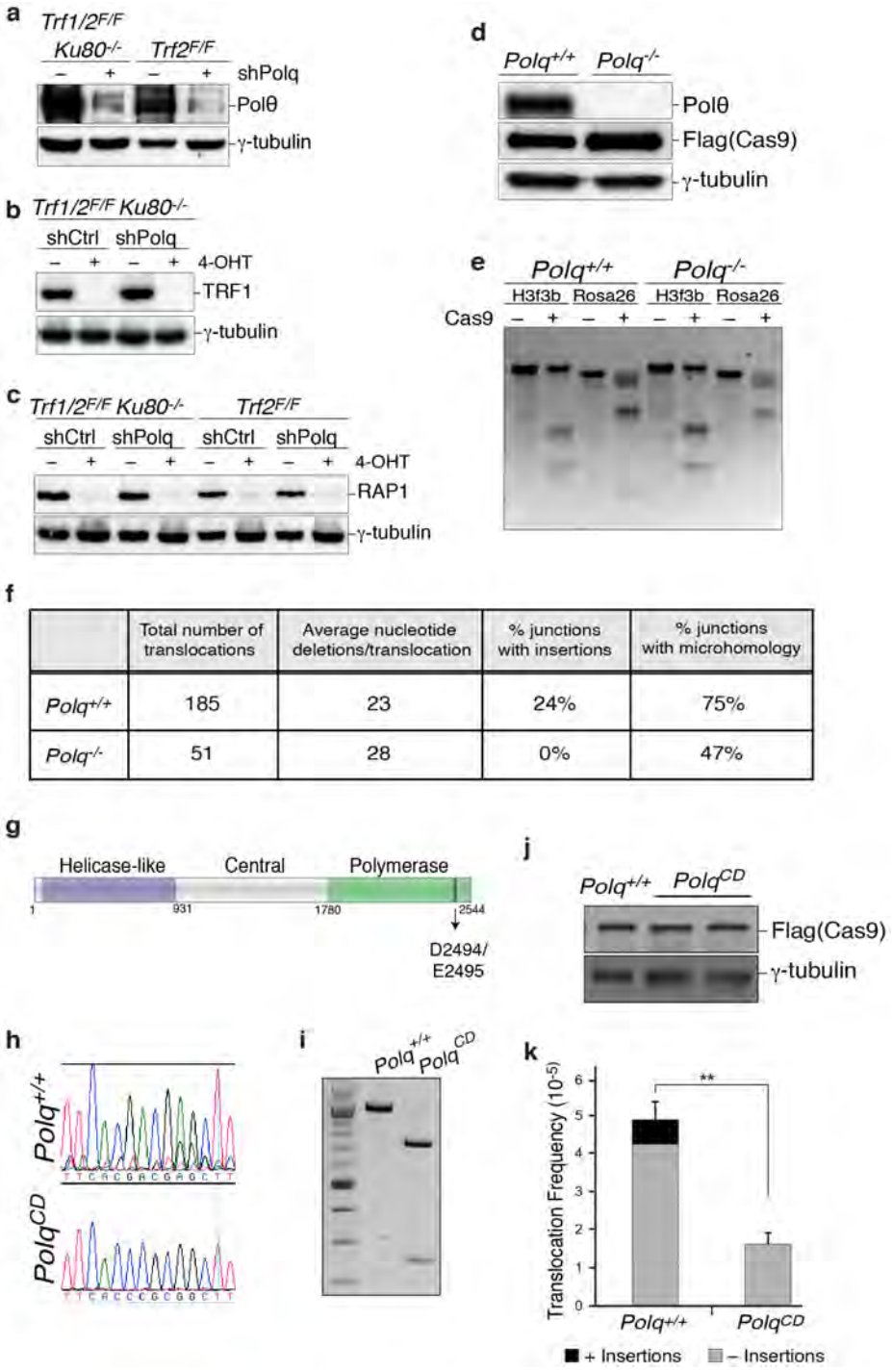

	Total number of translocations	Average nucleotide deletions/translocation	% junctions with insertions	% junctions with microhomology
Polq$^{+/+}$	185	23	24%	75%
Polq$^{-/-}$	51	28	0%	47%

Extended Data Figure 2 | Polθ drives chromosomal translocations in mouse cells. (Related to Fig. 2.) **a**, Immunobloting for Polθ in MEFs with the indicated genotype and treatment. **b**, Immunoblot for TRF1 in MEFs with the indicated genotype. Cells were analysed 96 h after Cre induction. **c**, RAP1 immunoblot (similar to **b**). **d**, Western blot analysis for Polθ and Flag–Cas9 in lysates prepared from *Polq*$^{-/-}$ and *Polq*$^{+/+}$ cells after Cas9 expression. Tubulin serves as a loading control. **e**, Surveyor nuclease assay for *Polq*$^{-/-}$ and *Polq*$^{+/+}$ cells expressing Cas9-gRNA(Rosa26;H3f3b) plasmid. Genomic DNA isolated from cells with the indicated genotype was used as a template to amplify across the cleavage site at either the Rosa26 or the H3f3b locus to assess intra-chromosomal NHEJ. Amplification products were denatured and then re-annealed to form heteroduplexes between unmodified and modified sequences from imprecise NHEJ. The mismatched duplex was selectively cleaved by the Surveyor nuclease at the loops that form at mismatches. **f**, Signature of translocations in *Polq*$^{-/-}$ and *Polq*$^{+/+}$ cells (see Extended Data Figs 3–5 for complete list of sequences). Table records the total number of translocation events identified following CRISPR-Cas9 induced-cleavage. On average, the same number of nucleotides was deleted at the fusion junction in *Polq*$^{-/-}$ and *Polq*$^{+/+}$ cells. No nucleotide insertions were found in the absence of *Polq*. Lastly, the percentage of junctions exhibiting microhomology was significantly reduced in cells lacking *Polq*. **g**, Scheme depicting Polθ domains. CRISPR/Cas9 gene targeting was used to create two base substitutions at Asp2494Gly and Glu2495Ser, and generate a catalytic-dead polymerase[34]. **h**, Sequence analysis of targeted cells. **i**, Genotyping PCRs of *Polq*$^{+/+}$ and *Polq*^{CD} (catalytically dead allele of *Polq*) after SacII digestion. **j**, Immunoblotting to analyse Cas9 expression in *Polq*$^{+/+}$ and two independently derived *Polq*^{CD} clonal cell lines. **k**, Frequency of chromosomal translocations (der(6)) in *Polq*$^{+/+}$ and *Polq*^{CD} cells. Bars represent mean of four independent experiments ± s.d. (two experiments per clonal cell line). $^{**}P = 0.006$; two-tailed Student's *t*-test. PCR products were sequenced to confirm translocation and identify possible insertions.

Extended Data Figure 3 | Sequence analysis of translocation junctions in *Polq*$^{+/+}$ cells. (Related to Fig. 2.) Sequences of der(11) breakpoint junction from *Polq*$^{+/+}$ cells. Predicted fusion breakpoint based on CRISPR cutting indicated by an arrow. Reference sequence highlighted at the top. The remaining lines represent individual translocations recovered by PCR and subject to Sanger sequencing. Nucleotide insertions are marked in red. In cases where insertions extended beyond the sequence included in the lane, the length of the insertion was noted in parenthesis (red). Gaps in the sequence represent nucleotide deletions. The average length of the deletions was noted in Extended Data Fig. 2f. Micro-homology is denoted by blue boxes. Micro-homology embedded in DNA extending beyond the enclosed sequence was noted in parentheses (blue).

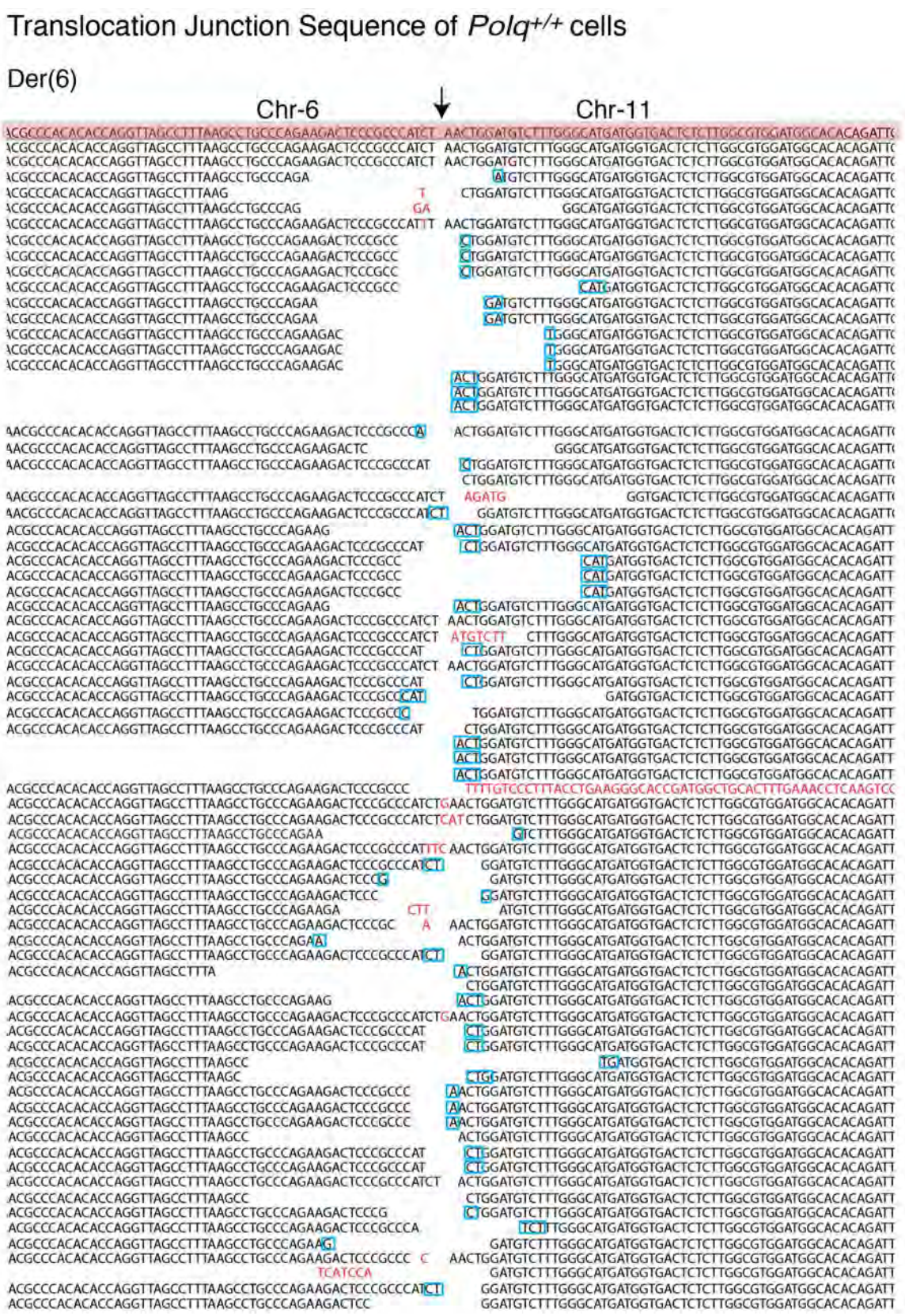

Extended Data Figure 4 | Sequence analysis of translocation junctions in *Polq*$^{+/+}$ cells. (Related to Fig. 2.) Sequences of der(6) breakpoint junction from *Polq*$^{+/+}$ cells. Predicted fusion breakpoint based on CRISPR cutting indicated by an arrow. Reference sequence highlighted at the top. The remaining lines represent individual translocations recovered by PCR and subject to Sanger sequencing.

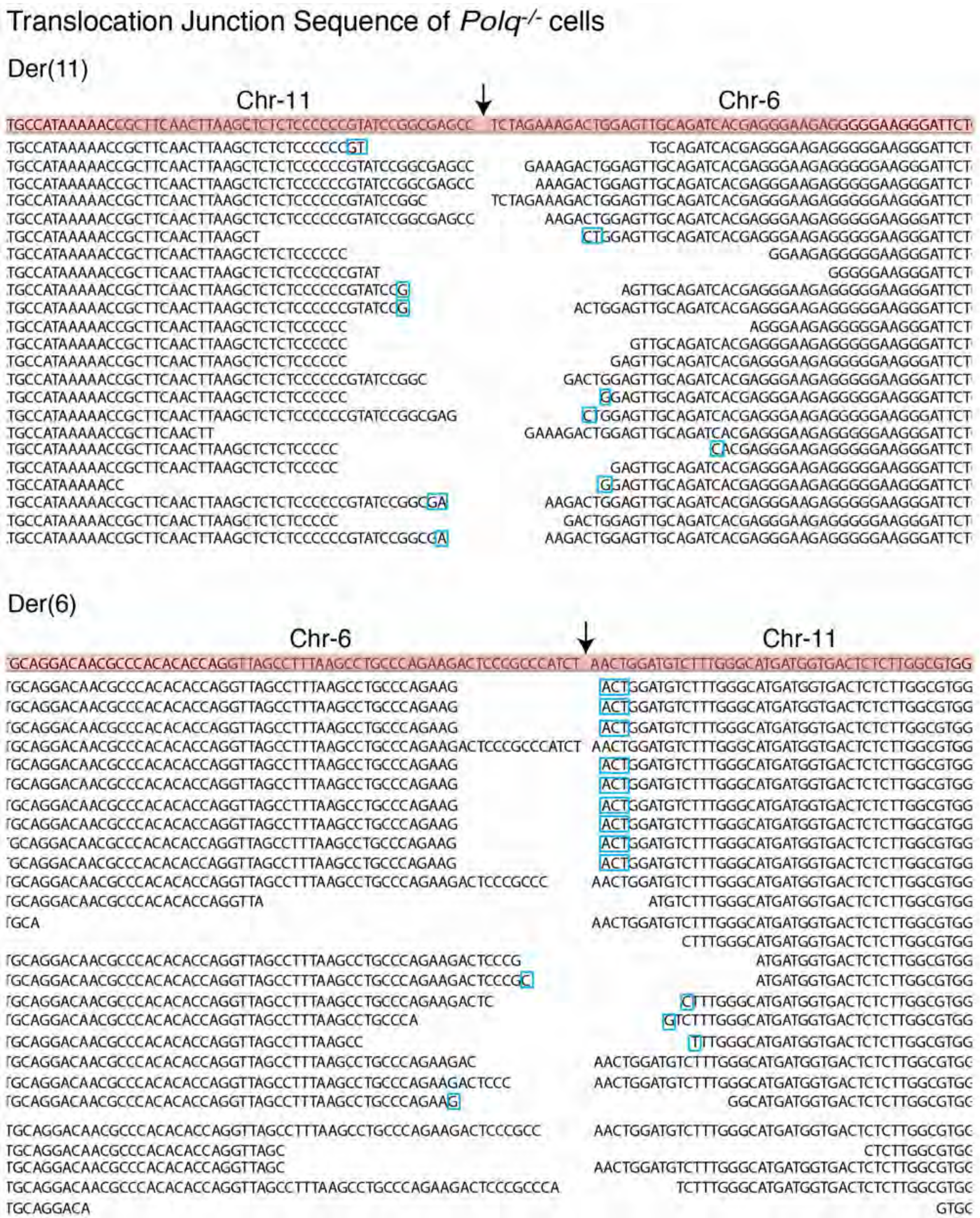

Extended Data Figure 5 | Sequence analysis of translocation junctions in *Polq*$^{-/-}$ cells. (Related to Fig. 2.) Sequences of der(11) and der(6) breakpoint junction from *Polq*$^{-/-}$ cells. Predicted fusion breakpoint based on CRISPR cutting indicated by an arrow. Reference sequence is highlighted at the top. The remaining lines represent individual translocations recovered by PCR and subject to Sanger sequencing. It is important to note that insertions were completely lacking at the fusions junctions in *Polq*$^{-/-}$ cells.

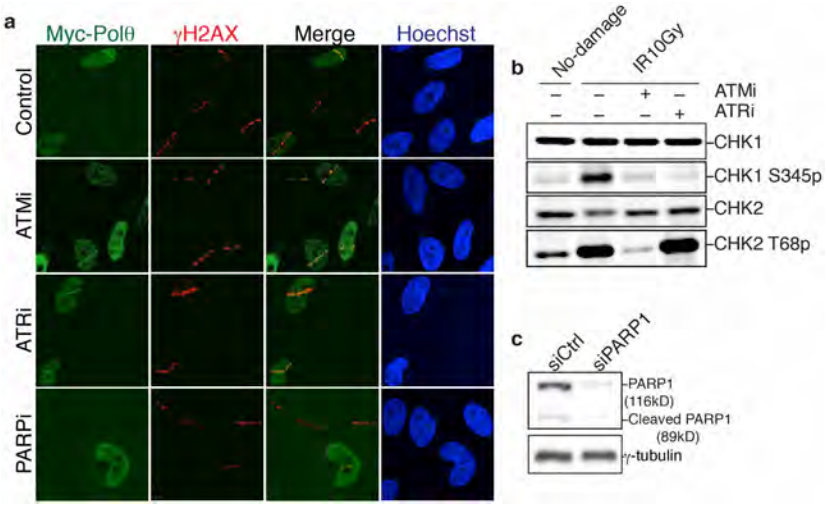

Extended Data Figure 6 | Polθ recruitment to DNA breaks. (Related to Fig. 3.) **a**, Laser micro-irradiation experiment using HeLa cells expressing Myc–Polθ and treated with ATM inhibitor (KU55933), ATR inhibitor (VE-821) or PARP inhibitor (KU58948). **b**, Western blot analysis for CHK1 and CHK2 phosphorylation. Cells with the indicated treatment were analysed 2 h after irradiation. **c**, Immunoblot for PARP1. HeLa cells were treated with PARP1 siRNA and analysed 72 h after siRNA transfection for efficiency of knockdown.

a

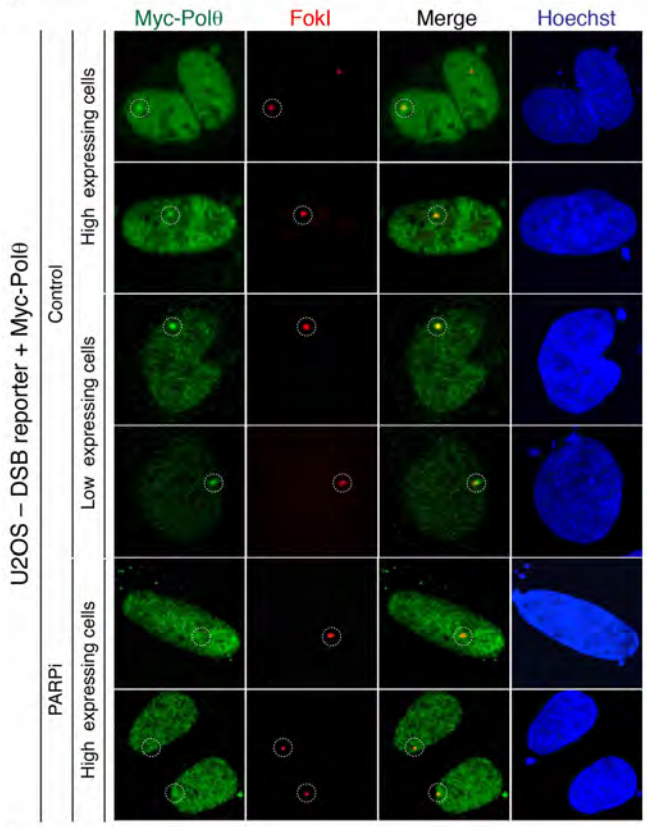

b

		# Cells Polθ+/FokI+	# cells with Polθ /FokI colocalization	% cells with Polθ /FokI colocalization
Experiment 1	Control	217	55	25.3%
	PARPi	213	23	10.8%
Experiment 2	Control	247	66	26.7%
	PARPi	240	25	10.4%

Extended Data Figure 7 | PARP1-dependent Polθ recruitment to DNA double-stranded breaks (DSBs). (Related to Fig. 3.) **a**, Results from immunofluorescence performed 4 h after induction (1 μM Shield1 ligand, Clontech 631037; 0.5 μM 4-OH tamoxifen) of DSBs by mCherry-LacI-FokI in the U2OS-DSB reporter cells[18] transfected with the Myc–Polθ and treated with PARP inhibitor (KU58948). The mCherry signal is used to identify the area of damage and to assess the recruitment of Myc–Polθ to cleaved LacO repeats. **b**, Table displaying quantification related to **a.**

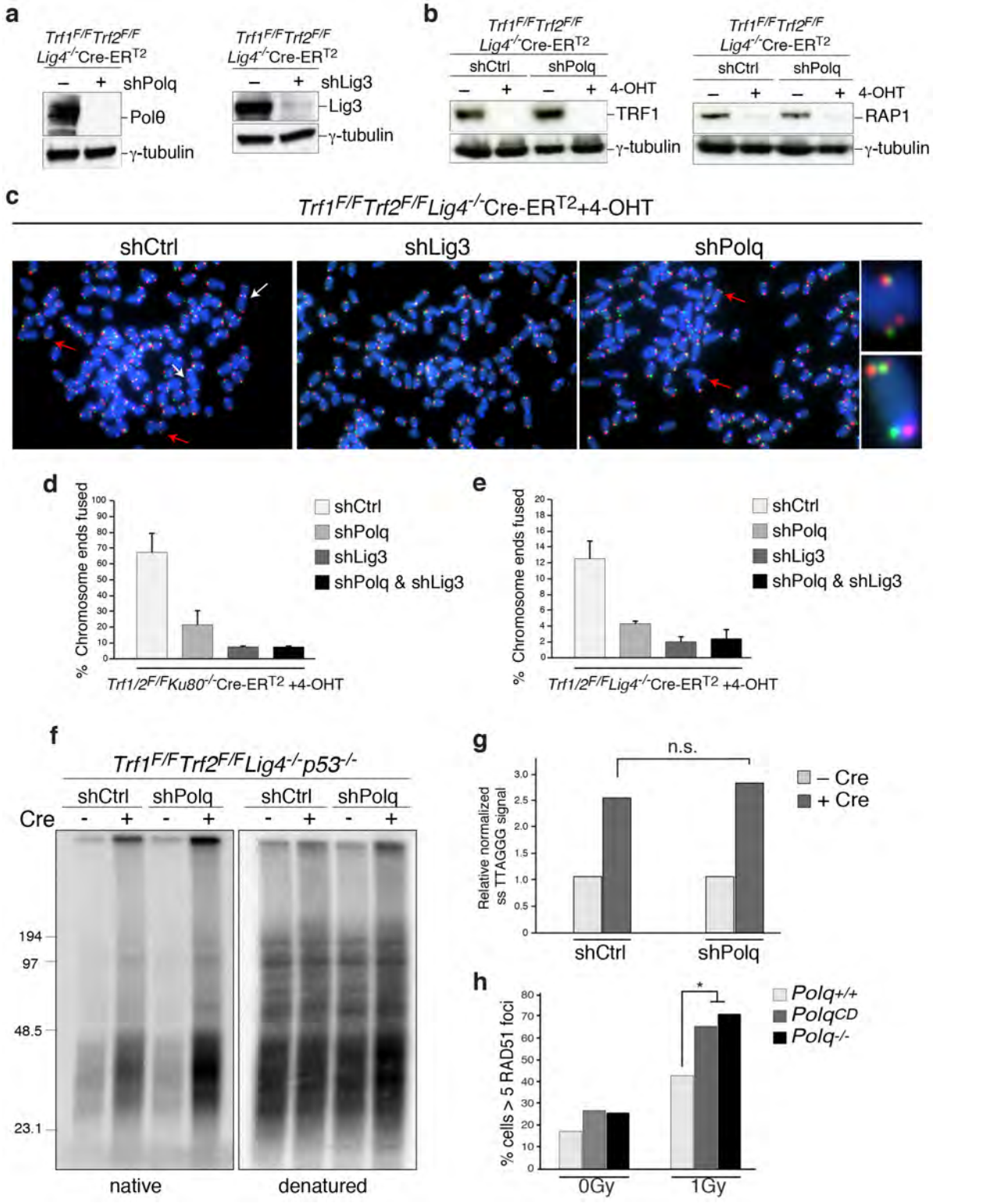

Extended Data Figure 8 | Polθ suppresses homology-directed repair at dysfunctional telomeres. (Related to Fig. 3.) **a**, Western blot analysis for Polθ and LIG3 in shelterin-free *Lig4*-null MEFs. **b**, Western blot for TRF1 and RAP1 after 4-OHT treatment of shelterin-free *Lig4*-deficient cells. **c**, Metaphase spreads from $Trf1^{F/F}Trf2^{F/F}Lig4^{-/-}$ Cre-ER^{T2} MEFs, with the indicated shRNA treatment, 96 h after Cre expression. CO-FISH assay was performed using a FITC-OO-$(CCCTAA)_3$ PNA probe (green) and a Tamra-OO-$(TTAGGG)_3$ PNA probe (red). DAPI in blue. Examples of alt-NHEJ-mediated fusion and T-SCE events (HDR) are indicated by white and red arrows, respectively. Examples of T-SCE events reflective of increased HDR in cells treated with shPolq are on the right. **d**, **e**, Quantification of telomere fusions by alt-NHEJ in MEFs with the indicated genotype and shRNA treatment. Bars represent mean of two independent experiments ± s.e.m. **f**, Representative in-gel hybridization to assess 3′ overhang of $Trf1^{F/F}Trf2^{F/F}Lig4^{-/-}$ Cre-ER^{T2} MEFs with the indicated shRNA treatment after Cre deletion. **g**, Quantification of the gel in **f**. The single-stranded DNA/total signal ratios of the '+Cre' samples are expressed relative to the '−Cre' samples for each shRNA treatment. Mean of two independent experiments. **h**, Graph representing RAD51 accumulation after ionizing radiation treatment of $Polq^{CD}$, $Polq^{+/+}$ and $Polq^{-/-}$ embryonic stem cells. Bars represent mean of two independent experiments. *$P > 0.05$; two-tailed Student's *t*-test.

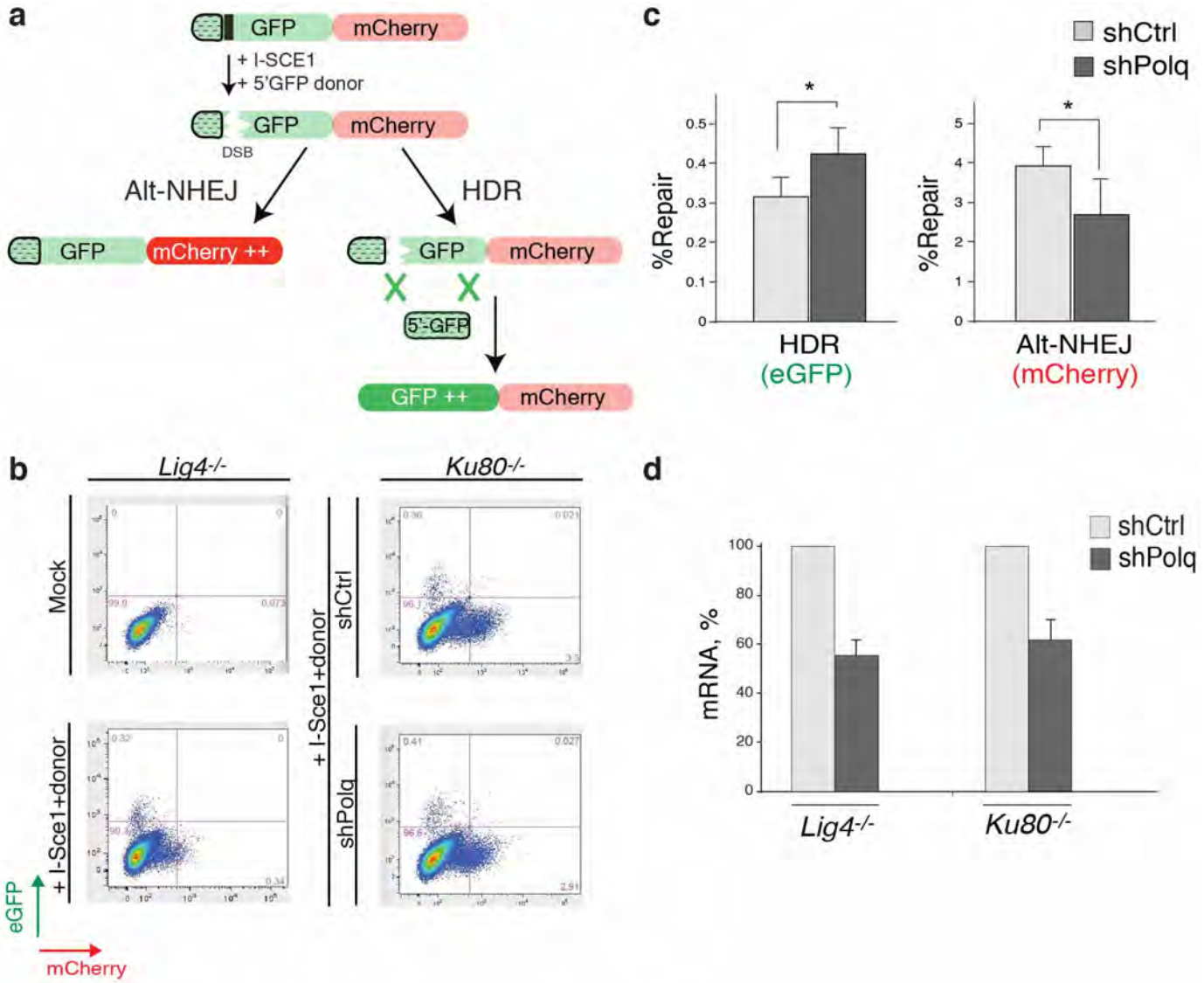

Extended Data Figure 9 | Polθ promotes alt-NHEJ and inhibits homology-directed repair at I-SceI-induced DNA breaks. (Related to Fig. 3.) **a**, Polθ represses recombination at DSBs induced by I-Sce1. The TLR system was used to measure the relative ratio of end-joining (mCherry) and HDR (enhanced green fluorescent protein (eGFP)) repair of a DSB. A diagram of the TLR is represented. **b**, The TLR construct was stably integrated into *Lig4*$^{-/-}$ and *Ku80*$^{-/-}$ MEFs to avoid the confounding effect of C-NHEJ, and limit end-joining reactions to the alt-NHEJ pathway. Expression of mCherry and eGFP was assessed by flow cytometry 72 h after I-Sce1 and 5′ eGFP donor transduction in cells with the indicated shRNA construct. Percentages of cells are indicated in the plot. **c**, Quantification of alt-NHEJ and HDR of TLR containing *Ku80*$^{-/-}$ MEFs after expression of I-Sce1 and 5′ eGFP together with the indicated shRNA construct. Bar graphs represent the mean of three independent experiments ± s.d. *$P = 0.03$; two-tailed Student's *t*-test. **d**, Real-time PCR to monitor the knockdown efficiency of *Polq* in *Ku80*$^{-/-}$ and *Lig4*$^{-/-}$ MEFs. The FACS analysis reported in **e** and **f** was carried out without selecting for cells expressing the shRNA-containing plasmid.

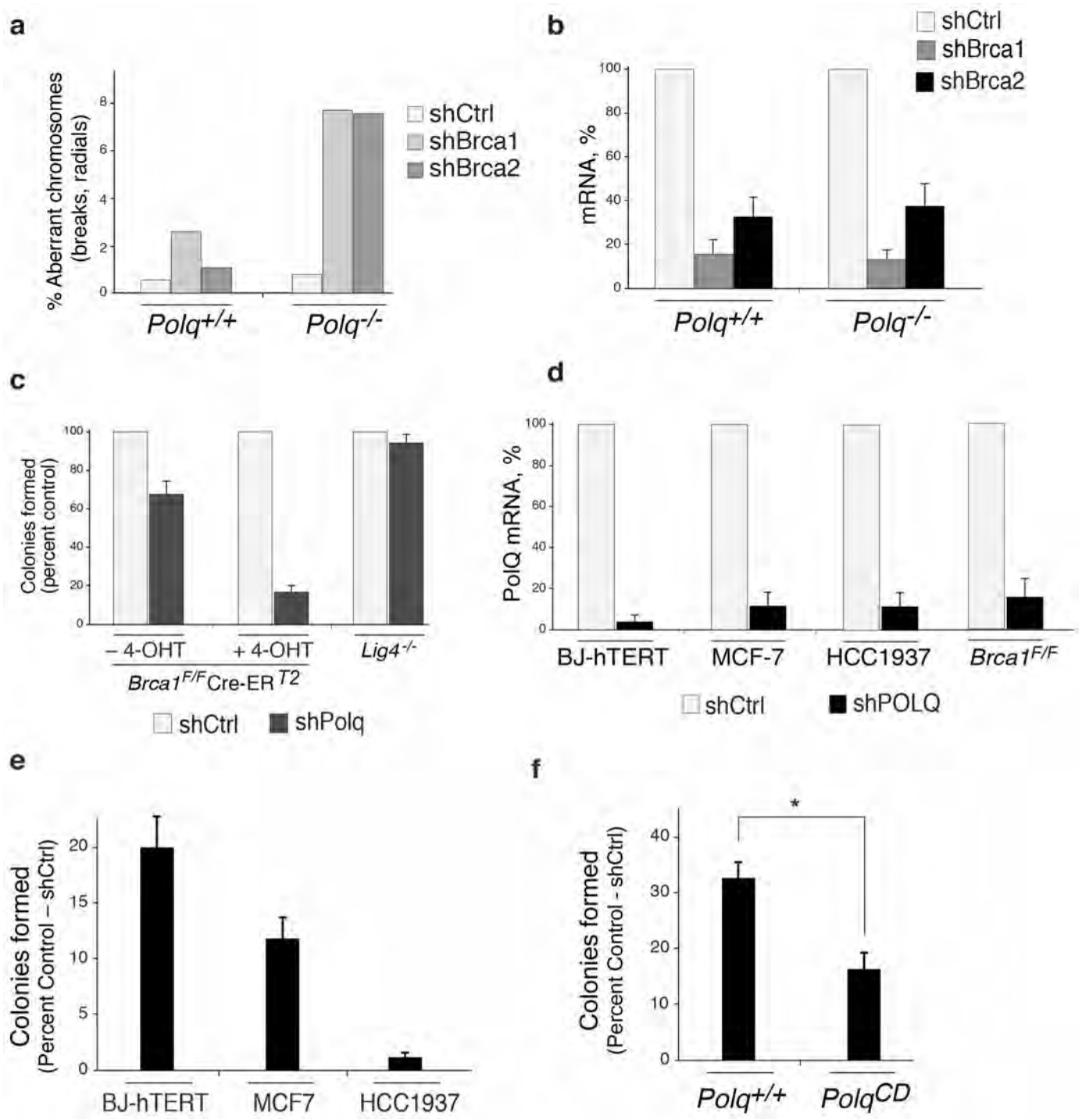

Extended Data Figure 10 | Polθ is required for survival of recombination-deficient cells. (Related to Fig. 4.) **a**, Accumulation of chromosomal aberrancies after *Brca1* and *Brca2* knockdown in $Polq^{-/-}$ and $Polq^{+/+}$ MEFs. Quantification of chromosomal aberrancies (chromatid breaks, chromosome breaks and radials) in MEFs stably transduced with lentiviral vectors expressing the indicated shRNA. **b**, Real-time PCR to confirm the knockdown of *Brca1* and *Brca2* as in **a**. **c**, Quantitative analysis of colony formation in $Brca1^{F/F}$ Cre-ER^{T2} and $Lig4^{-/-}$ cells after *Polq* depletion. The number of colonies in control shRNA-treated cells was set to 100%. Mean values are presented with error bars denoting ± s.d. from three independent experiments. **d**, Real-time PCR to measure the knockdown efficiency of human *POLQ* in BJ-hTERT, MCF7 and HCC1937 cells and mouse *Polq* in $Brca1^{F/F}$ Cre-ER^{T2} cells. **e**, Quantitative analyses of colony formation in BJ-hTERT, MCF7 and HCC1937 cells after LIG3 inhibition. The number of colonies in control-shRNA-treated cells was set to 100%. The knockdown efficiency for *Lig3* was ~85%. Bars represent mean of two independent experiments ± s.e.m. **f**. Quantitative analyses of colony formation in $Polq^{CD}$ and $Polq^{+/+}$ embryonic stem cells after *BRCA1* inhibition. The number of colonies in control-shRNA-treated cells was set to 100%. The knockdown efficiency for *BRCA1* was >80%. Bars represent mean of two independent experiments ± s.e.m. *$P = 0.05$; two-tailed Student's *t*-test.

The helicase domain of Polθ counteracts RPA to promote alt-NHEJ

Pedro A. Mateos-Gomez[1], Tatiana Kent[2], Ekaterina Kashkina[2], Richard T Pomerantz[2], and Agnel Sfeir[1*]

1 – Skirball Institute of Biomolecular Medicine, New York University School of Medicine, New York, USA.
2 – Temple University Lewis Katz School of Medicine, Philadelphia, USA.

Keywords: *POLQ*, Polθ, RPA, Alternative-NHEJ, homologous recombination, CRISPR/Cas9 targeting, translocations.

[*] Correspondence: Agnel Sfeir
Skirball Institute/NYU Langone Medical center
540 First Avenue
4th floor/ Lab3
New York, NY 10016
Phone: (646) 501 6742
agnel.sfeir@med.nyu.edu

Abstract

Mammalian polymerase theta (Polθ; encoded by *POLQ*) is a unique multifunctional enzyme that promotes error-prone DNA repair by alternative-NHEJ (alt-NHEJ). Here we perform structure-function analyses and report that, in addition to the polymerase domain, the helicase activity plays a central role during Polθ-mediated double-stranded break (DSB) repair. Our results show that Polθ-helicase promotes chromosomal translocations by alt-NHEJ in mouse embryonic stem cells. In addition, the helicase activity suppresses CRISPR/Cas9 mediated gene targeting by homologous recombination (HR). *In vitro* experiments reveal that Polθ–helicase displaces RPA to facilitate the annealing of complementary DNA during alt-NHEJ. Consistent with an antagonistic role for RPA during alt-NHEJ, we show that the inhibition of RPA1 subunit enhances end-joining and suppresses recombination at telomeres. Taken together, our results reveal that the balance between HR and alt-NHEJ is regulated by opposing activities of Polθ and RPA, providing critical insight into the mechanism that control DSB repair pathway choice in mammalian cells.

Introduction

Double strand break (DSB) repair is essential for cellular survival and maintenance of genome integrity. In addition to the two canonical DSB repair pathways of homologous recombination (HR) and classical non-homologous end-joining (C-NHEJ), an error-prone and mechanistically distinct pathway termed alternative-NHEJ (alt-NHEJ) covalently joins DNA ends[1]. Alt-NHEJ was initially thought to act as a back-up mechanism[2], however, recent studies indicated that it operates even when HR and C-NHEJ are intact[3], and is a major repair pathway during early vertebrate development[4]. Moreover, when HR and C-NHEJ are impaired, mammalian cells become highly dependent on alt-NHEJ for survival[5-7]. Whether alt-NHEJ comprises one or multiple overlapping mechanisms is still a matter of debate, yet a significant fraction of its events are characterized by the presence of microhomology, as well as deletions and insertions that scar DNA repair sites[1]. Whole genome sequence analysis of BRCA1/2 mutated tumors identified a genomic signatures with features (insertions and microhomology) that are highly reminiscent of alt-NHEJ repair[8-10]. The source of mutagenic insertions during alt-NHEJ has been attributed to the activity of polymerase theta (Polθ – encoded by *POLQ*), a unique enzyme found only in metazoans[11].

Polθ was originally identified in *D. melanogaster* through the analysis of mus308 mutants that displayed hypersensitivity to agents that induce DNA interstrand cross-links (ICL)[12]. The activity of Polθ was first linked to alt-NHEJ during P-element transposition in flies[13], and later found to promote end-joining in response to different DSB-inducing agents in plants[14], worms[15], fish[4], and mammals[5,6,16-18]. Mammalian Polθ stimulates alt-NHEJ in response to endonuclease-cleaved reporter constructs[5,6,16,17], drives the fusion of dysfunctional telomeres[5], and promotes chromosomal translocations in mouse embryonic stem cells[5]. In addition to promoting alt-NHEJ, recent evidences suggested that Polθ negatively regulates HR[5,17]. The accumulation of IR-induced Rad51 foci was significantly enhanced upon suppression of Polθ[5,6]. In addition, increased recombination in response to Polθ inhibition was noted at dysfunctional telomeres and using I-SceI-based reporter assays[5,6].

Polθ is a multifunctional enzyme that is composed of a superfamily 2 (SF2) Hel308-type helicase domain at the N-terminus, a low fidelity A-family polymerase domain at the C-terminus, and a non-structured central domain[11]. The role of the polymerase domain (Polθ–polymerase) during alt-NHEJ was elucidated through a series of biochemical studies[5,17,19-23]. Polθ–polymerase is capable of oscillating between templated and non-templated activities to promote alt-NHEJ. Templated nucleotides are primarily copied from regions flanking the break sites in *cis* and in *trans*, while non-templated extensions by Polθ–polymerase are driven by its template-independent terminal transferase activity[17,19]. The biochemical and biological functions of the helicase domain (Polθ–helicase), which is similar in sequence to Hel308 and RecQ type helicases, remain poorly understood. Analysis of the crystal structure revealed that the helicase domain of Polθ forms a tetramer, an arrangement that was also observed in solution[24]. It has been

proposed that the helicase domain acts together with the Rad51 interaction motif within the central region to antagonize strand invasion during HR[6]. Analysis of alt-NHEJ in *D. melanogaster* indicated that cells harboring mutations in the ATPase motif display less microhomology at repair junctions, albeit the overall efficiency of end-joining was not affected[13]. Similar results were obtained upon studying the repair of breaks incurred on episomal end-joining substrates in mouse cells overexpressing inactive Polθ–helicase[7]. So far, biochemical analysis failed to show any DNA unwinding activities, yet its Polθ–ATPase activity is readily detectable and stimulated by DNA[23,25]. Despite that presence of the helicase at the N-terminus of *POLQ* s conserved among metazoans, the mechanism by which it influences DSB repair remains unknown.

How cells choose between erroneous alt-NHEJ and accurate HR is critical, yet poorly understood. Both pathways are maximally active in S and G2 phases of the cell cycle, with alt-NHEJ processing 10-20% of breaks incurred during S phase in HeLa cells[3]. As in HR, the initial step of alt-NHEJ involves DNA end-resection by the Mre11–Rad50–Nbs1 (MRN) complex and CtIP to create short single-stranded DNA (ssDNA) overhangs[3,26,27]. Resection exposes microhomology internal to break sites, which could facilitate spontaneous annealing of ssDNA to form a synapsed intermediate that is essential for end-joining. The stability of the synapsis is governed by the extent of microhomology and influenced by factors acting at break sites. For example, in *S. cerevisiae*, where the frequency of alt-NHEJ activity is very low, end-joining requires 5-12 base-pairs (bp) of homology[28,29,30]. Furthermore, the binding of the replication protein A (RPA) complex to resected ends prevents spontaneous annealing between microhomologous overhangs, thereby hindering alt-NHEJ in yeast[31]. Whether the function of RPA as a negative regulator of alt-NHEJ is conserved in mammalian cells remains unknown. Furthermore, the factors and mechanisms that promote and stabilize annealed intermediates with little microhomology (i.e. ~2 bp)[32], typical of mammalian alt-NHEJ, have yet to be determined.

In this study, we identify a crucial role for Polθ–helicase in promoting alt-NHEJ and counteracting HR. Our data demonstrate that the function of Polθ–helicase is consistent with an ATP-dependent annealing helicase that counteracts RPA to drive alt-NHEJ. Lastly, we show that inactivation of RPA subunit 1 enhances alt-NHEJ at the expense of HR. Altogether, our results indicate that opposing activities of RPA and Polθ–helicase at DSBs regulate the balance between alt-NHEJ and HR. As such, the outcome of this interplay will have profound impact on the stability of mammalian genomes and the proliferation of HR-deficient cancer cells.

Results:

Mutational analysis uncovers the function of independent domains within Polθ

Polθ is the only known eukaryotic DNA polymerase that contains an intrinsic helicase domain, which lies at the N-terminus[23]. Three putative Rad51 interaction motifs were identified within the unstructured central domain of human Polθ, however, only one motif is evolutionary conserved. The function of the

different Polθ domains in mammalian cells has been primarily investigated using cellular-based assays that involve overexpression of various truncated alleles of Polθ, such as the helicase domain[6,7,16]. The cellular levels of Polθ in cells are low[33] and *POLQ* overexpression altered DNA replication and triggered a DNA damage response[34]. As such, it is imperative to address the function of its different domains in the context of physiological Polθ levels. To that end, we exploited CRISPR/Cas9 gene editing and targeted the endogenous *Polq* locus in mouse embryonic stem (mES) cells. We generated independent cell lines with inactivating mutations in the conserved ATPase (K120G)[7] and polymerase (D2494P, E2495R)[35] domains (Figure 1a). In addition, we engineered mouse ES cells harboring a 47 aa deletion (ΔD844-M890) that eliminated the conserved Rad51 binding site (Figure 1a). For each mutant, we isolated multiple clonally-derived cell lines and confirmed successful bi-allelic targeting by Sanger sequencing (Figure S1a).

Polθ expression is essential for the proliferation of HR-defective cells[5,6], including ones lacking *BRCA1* and *BRCA2*. To examine the function of the different Polθ domains, we treated $Polq^{\Delta Hel}$, $Polq^{\Delta Pol}$, $Polq^{\Delta Rad51}$, and control $Polq^{+/+}$ cells with shRNA targeting *BRCA1*. We then compared the survival of *BRCA1* depleted cells to those treated with control shRNA (Figure 1b and S1b). The results of the colony formation assay indicated that the growth of *BRCA1* depleted $Polq^{\Delta Hel}$ and $Polq^{\Delta Pol}$ cells was significantly compromised when compared to $Polq^{+/+}$ cells (Figure 1b). The findings are in agreement with previous reports that have implicated Polθ helicase and polymerase activities in the survival of cancer cells[5,6,16]. On the other hand, the survival of $Polq^{\Delta Rad51}$ cells following *BRCA1* depletion was similar to wildtype cells (Figure 1b). These results suggest that both polymerase and helicase enzymatic activities are important for proper Polθ function, whereas its interaction with Rad51 is dispensable for the survival of HR defective ES cells.

Polθ–helicase activity promotes efficient repair by alt-NHEJ

We next set out to investigate the involvement of the different Polθ domains during alt-NHEJ. To that end, we tested whether the *Polq* mutations impair chromosomal translocation formation in mES cells, an event that was previously reported to be mediated by alt-NHEJ[36] and dependent on Polθ[5]. The quantitative chromosomal translocation assay involves simultaneous cleavage of the Rosa26 (chromosome 6) and the H3f3B (chromosome 11) loci with CRISPR/Cas9 (Figure 1c and S1c). Cells transfected with Cas9-gRNA(Rosa26:H3f3b) plasmid were seeded in 96-well plates and a nested PCR was performed to detect breakpoint junctions of chromosomal translocations in each well. We calculated the translocation frequency based on the ratio of positive wells relative to the total number of transfected cells. It is necessary to monitor translocation frequency on the basis of individual wells since population-based PCR methods preferentially amplify shorter transcripts and bias against translocations with larger inserts.

We analyzed translocations in *Polq* mutant cells, and found that cells lacking the Rad51 interaction motif exhibited similar translocation frequencies as wild-type cells (Figure 1d). On the other hand, we observed a significant reduction in the frequency of translocations in $Polq^{\Delta Hel}$ as well as $Polq^{\Delta Pol}$ cells (Figure 1d). In summary, these data indicate that in addition to the previously established role for the polymerase activity during alt-NHEJ[5,7,16,17], the Polθ–helicase domain is essential for efficient joining of DNA ends in mammalian cells.

To gain additional insight into the function of the different Polθ activities, we examined the sequence of fusion breakpoints at derivative chromosome 6 (Der (6)). We categorized the different translocation events and assigned an alt-NHEJ-signature score based on the presence of insertions and microhomologies (Figure S1d). Interestingly, the alt-NHEJ signature was enriched at translocation events retrieved from wild-type cells but significantly reduced in cells with compromised Polθ– helicase and polymerase functions. Specifically, translocations in $Polq^{\Delta Hel}$ and $Polq^{\Delta Pol}$ cells exhibited a significant decrease in the frequency of microhomology and nucleotide insertions (>2 nts) (Figure 1e). In contrast, $Polq^{\Delta Rad51}$ displayed a similar translocation profile as wild type cells, further confirming that the Rad51 interaction motif is dispensable for Polθ function in alt-NHEJ (Figure 1e and Table S1-9).

Enhanced HR-driven genome editing by CRISPR/Cas9 upon Polθ inhibition

Having established a role for both Polθ–helicase and polymerase during alt-NHEJ, we next investigated the involvement of these enzymatic activities during suppression of HR, a key phenotype associated with Polθ overexpression and observed in many cancers[5,6]. Using mES cells harboring the different *Polq* mutations, we first measured the formation of IR-induced Rad51 foci, an indirect readout for HR. We detected a significant increase in Rad51 foci in $Polq^{\Delta Hel}$ and $Polq^{\Delta Pol}$ cells. On the other hand, the accumulation of Rad51 in $Polq^{\Delta Rad51}$ cells was similar to wildtype cells (Figure S2a). The latter finding is inconsistent with recent observations implicating the Rapd51 interaction domain in the suppression of HR by polθ[6]. This discrepancy might be attributed to differences in the requirements of Polθ-mediated repair between tumor cells and mouse ES cells. Alternatively, given that the overall levels of Rad51 in cells exceed those of Polθ, it is possible that Polθ can only impact Rad51 function when the polymerase is overexpressed, as is the case in high grade ovarian cancers[6].

In an independent set of experiments, we aimed to investigate the function of Polθ during HR using a more direct assay. To do so, we investigated whether Polθ inhibition increases HR-mediated gene targeting stimulated by CRISPR/Cas9. We designed a gene targeting assay in which the coding sequence of a Zsgreen fluorescent protein was integrated at the 3' end of the housekeeping *Hsp90* gene (Figure 2a and S2b-c). Based on this assay, cells that have undergone productive HR are stably marked with green fluorescence and distinguished by fluorescence-activated cell sorting (FACS). Notably, FACS analysis

revealed two distinct populations of Zsgreen positive cells (Figure 2b) corresponding to mono-allelic and bi-allelic targeting (Figure 2c). We noticed that targeting of the *Hsp90* locus in MEFs and mES cells was minimally responsive to DNA-PKcs inhibition, suggesting that C-NHEJ is not a major barrier to gene editing at this locus (Figure S2d). Interestingly, we observed a significant increase in the efficiency of *Hsp90* targeting in *Polq*$^{-/-}$ cells relative to *Polq*$^{+/+}$ *cells* (Figure 2d-e and S2d). Furthermore, a similar increase in mono- and bi-allelic targeting of the *Hsp90* locus was detected in *Polq*$^{\Delta Hel}$ and *Polq*$^{\Delta Pol}$ cells (Figure 2e).

We then employed a similar CRISPR/Cas9 strategy to target the highly transcribed *Sox2* gene in mouse ES cells. In contrast to targeting of the *Hsp90* locus, we observed an increase in the percentage of cells expressing green fluorescent protein from the *Sox2* locus in response to DNA-PKcs inhibition, suggesting that this particular locus is more amenable to repair by C-NHEJ (Figure S2e-h). However, depletion of *Polq* did not yield enhanced gene targeting (Figure S2e-h), possibly denoting a minor role for alt-NHEJ in the repair of DSBs incurred at this locus. It was recently reported that the nature of the Cas9-induced lesion influences repair pathway choice, whereby lesions with overhangs preferentially provoke HR and alt-NHEJ over C-NHEJ[37]. We therefore tested the effect of Polθ depletion on HR-mediated repair of breaks triggered using Cas9 nickase (D10A) and a pair of gRNAs that cleave on opposite DNA strands, thereby generating single stranded overhangs. Consistent with previous reports[37], we noticed a tenfold increase in *Sox2* gene targeting by HR when breaks were induced by Cas9 nickase (Figure S2h-i). In addition, we noticed a small but significant increase in efficiency of gene targeting in *Polq*$^{-/-}$, *Polq*$^{\Delta Hel}$, and *Polq*$^{\Delta Pol}$ cells compared to control cells (Figure S2i). In summary, the data obtained from the gene targeting assay demonstrate that both, helicase and polymerase activities, are essential for suppression of HR by Polθ. In addition, our data suggest that Polθ inhibition could enhance precise genome editing by canonical HR, albeit in locus-specific manner and its effect is influenced by the nature of the ends generated by Cas9 cleavage. Genome-wide-based approaches will be necessary to systematically query the genome and identify specific loci that would yield increased gene targeting in response to Polθ inactivation.

Polθ–helicase dissociates RPA to promote the annealing of complementary DNA

To investigate the molecular mechanism by which Polθ–helicase, which lacks detectable DNA unwinding activities, promotes alt-NHEJ, we performed a set of *in vitro* experiments. Consistent with previous reports, purified human Polθ–helicase (aa 1-894) displayed robust ATPase activity (Figure S3a-b)[23]. Considering that alt-NHEJ likely requires active annealing between 3' ssDNA overhangs, we examined whether Polθ–helicase functions as an annealing helicase. For example, helicases such as HARP1/SMARCAL1 have been shown to promote ssDNA annealing in the presence of RPA which acts as a physical and energetic barrier to annealing[38]. Given the previously reported role for replication protein A (RPA) acting as a negative regulator of alt-NHEJ in yeast[31], we hypothesized that Polθ–helicase utilizes the energy of ATP to overcome the RPA barrier to annealing, in a similar manner to HARP1/SMARCAL1.

To test this hypothesis, we performed ssDNA annealing in the presence of RPA and Polθ–helicase as follows: A 33-nucleotides ssDNA was pre-incubated with RPA in the presence or absence of ATP using standard buffer with $MgCl_2$ (Figure 3a). Next, increasing amounts of Polθ – helicase was added for 15 min, followed by the addition of ^{32}P-labelled complementary ssDNA for 10 min. Reactions were then terminated and resolved on non-denaturing gels. As previously reported[31,39], pre-loading of RPA onto ssDNA prevented spontaneous annealing of the complementary DNA substrate (Figure. 3b). Strikingly, the addition of Polθ–helicase to the reaction stimulated DNA annealing in an ATP-dependent manner (Figure 3b). We compared ssDNA annealing reactions with ATP versus a non-hydrolyzable ATP analog (AMP-PNP). The results show that Polθ–helicase annealing occurs in the presence of ATP, but not AMP-PNP, which demonstrates that ATP hydrolysis is required to promote annealing in the presence of RPA (Figure 3b). These data suggest that the helicase enzymatically dissociates RPA from ssDNA in order to promote annealing. Lastly, to address the specificity of Polθ–helicase annealing activity, we performed the annealing reactions using E. coli single-strand binding protein (SSB). In contrast to the results with RPA, Polθ–helicase was unable to promote annealing in the presence of SSB (Figure S3c), which suggests that the helicase was selected to act with RPA during annealing.

Polθ–helicase utilizes the energy of ATP to promote alt-NHEJ

The results outlined above implicate Polθ–helicase involvement in the synapsis of resected DSBs and underscore opposing activities exerted by RPA and Polθ–helicase during alt-NHEJ. To gain further insight into the interplay between these two repair factors, we investigated end-joining *in vitro*. To that end, we used partially resected model substrates containing 6 bases of terminal microhomology, previously shown to support efficient end-joining by Polθ–polymerase *in vitro* (Figure 3c)[17]. Consistent with previous results[17], Polθ–polymerase joined these substrates together forming double-size products in the presence of deoxyribonucleoside triphosphates (dNTPs) as observed in a native gel (Figure 3d). Since RPA suppresses alt-NHEJ in yeast, we tested whether human RPA inhibits end-joining *in vitro*. Indeed, Polθ–polymerase end-joining was significantly reduced when the resected substrates were pre-bound by RPA (Figure 3d and S3d). In contrast, Polθ–polymerase activity was completely resistant to RPA when tested in a traditional primer-template assay (Figure S3e). Taken together, these data demonstrate that the initial ssDNA annealing/synapse step is suppressed by RPA, whereas polymerase extension of the minimally paired overhangs, which is essential for stabilizing the end-joining product, is refractory to RPA binding. To assess whether Polθ–helicase catalytic activity overcomes the RPA block to Polθ–polymerase end-joining, we repeated the reaction in the presence of the helicase domain. Notably, the data demonstrate that the helicase reduces the RPA barrier to end-joining exclusively in the presence of ATP (Figure 3d). The stimulation of DNA annealing by Polθ–helicase was observed under multiple concentrations of RPA and Polθ–helicase (Figure S3d). Altogether, our data indicate that RPA negatively regulates alt-NHEJ by

blocking the initial ssDNA annealing/synapse step which is essential for subsequent extension of the minimally paired overhangs by Polθ–polymerase. Notably, Polθ–polymerase alone can promote end-joining in the absence of RPA (Figure 3d and [17]). In this case, the polymerase presumably takes advantage of transiently and spontaneously annealed/synapsed overhangs which does not require an enzymatic annealing function. However, in the presence of RPA which blocks spontaneous annealing/synapse formation, Polθ–helicase enzymatic activity is needed to reduce this energetic barrier in order to facilitate overhang pairing/synapsis and subsequent Polθ–polymerase extension (Figure 3d and S3d).

Mammalian RPA inhibits alt-NHEJ *in vivo* and is counteracted by Polθ–helicase

Our *in vitro* data indicated that RPA prevents DNA synapse formation during alt-NHEJ, and that this inhibition is overcome by Polθ–helicase activity to promote end-joining. As mentioned earlier, inhibition of alt-NHEJ by RPA was first detected in *S. cerevisiae*. Specifically, a hypomorphic *rfa1*-D228Y allele that is unable to unwind secondary DNA structures – including ones that resemble synapsed DNA[39,40] – triggered a 350 fold increase in the frequency of alt-NHEJ[31]. RPA binds ssDNA with similar affinity across eukaryotes and the aspartic acid residue (D228 in budding yeast) is highly conserved (Figure S4a), prompting us to ask whether mammalian RPA (D258 in mice) prevents alt-NHEJ *in vivo*. To that end, we examined DSB repair in the context of dysfunctional telomeres. It has been previously established that upon depletion of the protective shelterin complex from *TRF1*$^{F/F}$*TRF2*$^{F/F}$*Lig4*$^{-/-}$Cre-ER^{T2} MEFs, ~10% of telomeres ends are processed by alt-NHEJ and ~5% undergo telomere sister chromatid exchange (T-SCE), indicative of HR[41]. As expected, we observed a significant reduction in the frequency of T-SCEs following shelterin loss in MEFs with reduced levels of RPA1 (Figure 4a and Figure S4b-c). In addition, depletion of RPA1 lead to a concomitant increase in alt-NHEJ, denoted by the accumulation of chromosome end-to-end fusions (Figure 4b and S4b-c). We then transduced shelterin-free MEFs with shRNA-resistant RPA1 allele harboring a D258Y mutation, prior to deletion of endogenous RPA1. Analysis of metaphase chromosomes revealed that the expression of mutant RPA failed to rescue the telomere phenotypes associated with RPA1 depletion. In a control experiment, we observed that the expression of a wildtype RPA1 allele restored telomere recombination and prevented the increase in alt-NHEJ (Figure 4a-b and S4a-e). Lastly, we showed that the inhibition of HR through depletion of *Rad51*, which acts downstream of RPA, resulted in a reduction in the frequency of telomere recombination without impacting the levels of alt-NHEJ (Figure S4f-g). In conclusion, these results suggest that RPA acts as a specific regulator of repair pathways choice, promoting error-free repair by HR, while preventing repair by alt-NHEJ.

Finally, we sought to examine the effect of Polθ–helicase on the accumulation of RPA at DSBs *in vivo*. In order to visualize RPA at break sites, we turned to the previously established TRF1-Fok1 system that triggers multiple DSBs per telomeres[42]. It was recently noted that Fok1-induced telomere breaks were not processed by C-NHEJ, but fixed by HR and alt-NHEJ[43], which renders them ideal substrates to examine

the interplay between RPA and Polθ-helicase *in vivo*. The expression of TRF1-FokI fusion protein in U2OS cells lead to significant co-localization of Myc-RPA1 at damaged telomeres (Figure 4c). Interestingly, we observed a small, but significant reduction in the accumulation of RPA1 at telomere breaks in cells expressing Polθ–helicase (Figure 4c and Figure S4h-i). Importantly, expression of a helicase-defective Polθ allele (K121M) did not impact the formation of RPA1 foci at telomere breaks (Figure 4c and Figure S4h-i). Taken together, these results highlight a role for Polθ–helicase in displacing RPA from ssDNA while catalyzing overhang annealing, thereby facilitating alt-NHEJ at the expense of HR.

Discussion

Error-prone repair by alt-NHEJ can destabilize the genome due to the accumulation of insertions and deletions at break sites. Alternatively, repair of similar lesions by HR will lead to a safer outcome. Paradoxically, both pathways display maximal activity in S and G2 and share the initial resection step. The underlying mechanism(s) that regulate the choice between HR and alt-NHEJ following the resection is poorly understood. In this study, we provide evidence in support of an antagonistic interplay between Polθ and RPA that orchestrates DSB repair. Specifically, our results highlight a crucial role for the helicase domain within Polθ to promote alt-NHEJ during chromosomal translocation in ES cells, and suppress HR mediated gene editing. In addition, our data establish that Polθ–helicase offsets the inhibitory role of RPA to foster the annealing of microhomologous sequences between opposing ssDNA overhangs generated at DSBs. Finally, we show that inhibition of RPA, or expression of an RPA-D258Y mutant that is unable to block spontaneous ssDNA annealing, leads to significant inhibition of HR and a concomitant enhancement in alt-NHEJ.

Based on our observations, we propose a model in which a key commitment step to repairing breaks by HR versus alt-NHEJ is executed at the level of DNA end synapsis (Figure. 5). The first decision point during DSB repair is achieved through 5'-3' DNA resection by MRN-CtIP to block C-NEHJ[3,44,45]. The binding of RPA to the resulting short ssDNA overhangs stimulates further resection by BLM/EXO1 to facilitate subsequent steps during HR[46,47]. In addition, RPA inhibits the spontaneous annealing of microhomologous sequences exposed by end resection[31,39,48]. On the other hand, Polθ–helicase actively dissociates RPA to promote DNA end-synapsis; a critical commitment step for alt-NHEJ (Figures 3 and 4). In effect, the antagonistic activities between Polθ–helicase and RPA define a second decision point during DSB repair immediately following initial end-resection. When Polθ–helicase prevails, the minimally paired ssDNA overhangs are subsequently extended by Polθ–polymerase which is essential for stabilizing the alt-NHEJ intermediate and filling in the gaps prior to covalent joining of DNA by Lig3, or Lig1 (to a lesser extent)[49].

The helicase domain of Polθ is most closely related to HelQ, also known as Hel308, an ATP-dependent helicase that unwinds replication fork DNA substrates to mediate replication-coupled DNA repair in response to ICL inducing agents[50,51]. In contrast, Polθ is thought to lack DNA unwinding activity[23,24,52] and mammalian cells lacking *POLQ* are not sensitive to ICL[16,33], thus highlighting significant functional divergence between the two helicases. The annealing function of Polθ–helicase is highly reminiscent to that displayed by HARP/SMARCAL1, an annealing helicase that is recruited to sites of replication stress *via* an interaction with RPA to minimize the amount of ssDNA and protect stalled replication forks[38,53,54]. We were unable to detect a direct interaction between RPA and Polθ (data not shown), suggesting that the recruitment of Polθ to DSBs is independent of the RPA complex. Whether Polθ utilizes its annealing activity to allow cancer cells to better tolerate replication stress[55] remains to be addressed.

RPA is a major eukaryotic ssDNA binding protein that has been shown to unwind secondary structure and antagonize annealing of complementary oligonucleotides[31]. Consistent with this activity, yeast strains carrying RPA1 mutations exhibited enhanced alt-NHEJ activity[31]. Our results demonstrate that the inhibitory role for RPA during alt-NHEJ is conserved in higher eukarotes. Nonetheless, there remain significant differences between alt-NHEJ in yeast and mammals. One difference is illustrated by the degree of microhomoloqy required for joining broken DNA. Alt-NHEJ events in budding yeast requires >5 bp of microhomoloqy and are less tolerant to mismatches[28,29,30], whereas joining in mammals can take place with as little as one nucleotide of homology[32]. The thermostability of base pairing might be sufficient to promote end-joining in yeast. Alternatively, metazoans acquired an essential and dedicated activity – that of Polθ – to enzymatically promote annealing/synapse of ssDNA overhangs with limited microhomoloqy and rapidly stabilize these minimally paired ends via their extension by the polymerase domain. Given that yeast lack a *Polq* gene, it will be interesting to test whether the expression of Polθ alleviates the requirement for extensive microhomoloqy during alt-NHEJ–mediated repair in S. *cerevisiae*.

POLQ is frequently overexpressed in human cancers[11,56], and its overexpression is linked to poor prognosis in breast cancer[34]. Furthermore, *POLQ* expression confers resistance to DSB forming agents, including ionizing irradiation and chemotherapy drugs[16,18]. Lastly, Polθ-mediated alt-NHEJ was proposed to be an adaptive mechanism that allows the survival of cells with defective HR or C-NHEJ, including *BRCA1*/2 mutated breast and ovarian cancer cells[5-7]. As a result, Polθ has emerged as a novel cancer drug target. Our findings that both enzymatic activities support Polθ function during DSB repair highlight more opportunities for targeting this unique enzyme in cancer.

Figure legends:

Figure 1. Structure-function analysis reveals the function of Polθ–helicase during alt-NHEJ. (a) Top

– schematic representation depicting the different domains of Polθ. Three Rad51 binding domains were identified in human *POLQ*, however, only one motif is conserved in mouse (highlighted in blue). The polymerase domain contains three conserved unique insertion loops (highlighted in grey) that are involved in DNA synthesis. Bottom – CRISPR/Cas9 gene targeting was carried out in mouse ES cells (CCE) to introduce two base substitutions (Asp2494 and Glu2495) that inactivate the polymerase domain. In addition, independent gene editing was carried out to inactivate the ATPase activity (Lys120) and delete the conserved Rad51 interaction motif (residues 844-890). (b) Quantitative analysis of colony formation assay in mES cells carrying the indicated *Polq* mutant alleles and treated with sh*BRCA1*. In each cell line, colonies were normalized to cells treated with shControl. Bars represent means of three independent experiments ± S.D. For every experiment, two independent clonally derived cells lines were analyzed. * p<0.05; two-tailed Student's t-test. **(c)** Schematic of chromosomal translocation assay in which DSBs are induced at the Rosa26 and H3f3b loci. Generation of derivative chromosomes Der(6) is detected by nested PCR. **(d)** Frequency of chromosomal translocation in $Polq^{+/+}$, $Polq^{\Delta Pol}$, $Polq^{\Delta Hel}$, and $Polq^{\Delta Rad51}$ cells. Bars represent mean ± S.D. Two independent experiments, each was carried out using two clonally-derived cells lines. *p<0.05; two-tailed Student's t-test. **(e)** Table summarizing the analysis of nucleotide composition at the junction of translocation events in (**d**).

Figure 2. Polθ inhibition increase the efficiency of HR-mediated CRISPR-Cas9 gene targeting. (a) Scheme depicting gene targeting assay at the Hsp90 locus. The donor plasmid contains a Zsgreen coding sequence and 600 base pairs of homology arms. (**b**) (FACS) analysis to determine the percentage of ZsGreen positive cells. Three distinct populations were isolated (highlighted as 1, 2 and 3). (**c**) Genotyping PCR for *Hsp90* on DNA corresponding to the three highlighted populations of cells (indicated in (**b**)). (**d**) Gene-targeting efficiency at the *Hsp90* locus in $Polq^{-/-}$ and $Polq^{+/+}$ MEFs. Bars represent mean ± S.D. (n = 3). (**e**) Gene-targeting efficiency at the *Hsp90* locus in mES cells with the indicated genotype. Bars represent mean ± S.D. (n = 3). **p<0.01; two-tailed Student's t-test.

Figure 3. Polθ–helicase antagonizes RPA to promote annealing and alt-NHEJ *in vitro.* (a) Diagram of the annealing assay used to investigate whether Polθ–helicase (Polθ-hel) promotes pairing of complementary ssDNA bound by RPA. ssDNA is incubated with RPA, prior to addition of Polθ–helicase. End-labeled complementary ssDNA (indicated with asterisk) is then added, the reaction terminated, and DNA analyzed in non-denaturing gels following protein degradation. (**b**) Representative non-denaturing gels displaying ssDNA annealing in the presence and absence of ATP/AMP-PNP and indicated amounts of Polθ–helicase. % dsDNA indicated. (**c**) Schematic of Polθ–polymerase (Polθ-pol) mediated alt-NHEJ assay. Partially resected DNA model substrates containing 3' terminal microhomology (6 bases) were used as described[17]. (**d**) Non-denaturing gels showing Polθ–polymerase mediated alt-NHEJ in the presence of the indicated proteins and ATP. % end-joining indicated.

Figure 4. Mammalian RPA inhibits alt-NHEJ. (a) Quantification of telomere sister-chromatid exchanges (T-SCEs), reflective of telomere recombination events in *TRF1*$^{F/F}$*TRF2*$^{F/F}$*Lig4*$^{-/-}$Cre-ER^{T2} cells with the indicated treatments. Top – Representative examples of T-SCE events (white arrows). Error bars denote S.E.M. from two independent experiments. *P < 0.05, **P < 0.01; two-tailed Student's t-test. **(b)** Quantification of telomere fusions by alt-NHEJ in cells with the indicated treatment. Top – Examples of chromosomes fusion events denoted by white arrows. Bars represent mean ± S.D. from three independent experiments. *P < 0.05 and **P < 0.01; two-tailed Student's t-test. (**c**) Immunofluorescence for Myc-RPA1 and TRF1-FokI-mCherry in U2OS cells expressing the indicated alleles. TRF1-Fok1-mCherry expression was induced upon treatment with doxycycline, shield-1, and 4-OHT. (**d**) Graph representing the quantification of Myc-RPA1 accumulation in cells expressing TRF1-FokI (as in c). Bars represent mean ± S.D. from three independent experiments. *P < 0.05 and **P < 0.01; two-tailed Student's t-test.

Figure 5. The interplay between Polθ and RPA determine the outcome of DSB repair. Schematic depicting our model for the interplay between Polθ and RPA during DSB repair. Binding of the RPA complex to resected DSB ends block alt-NHEJ and promote HR. The helicase activity of Polθ perturbs the binding of RPA to ssDNA and stimulate the annealing of resected DSBs. Annealed intermediates are then stabilized upon fill-in synthesis by Polθ-polymerase and ultimately joined by Lig3/Lig1.

Authors contribution:

Experiments were designed by A.S., R.T.P., P.A. M-G. and T.K. T.K. performed in vitro experiments. T.K. and E.K. purified proteins. P.A.M-G. performed all other experiments. A.S. wrote the manuscript. All authors discussed the results and commented on the manuscript.

Acknowledgements:

We thank R. Greenberg and T. de Lange for providing key reagents. We are grateful to Sarah Deng, Alexandra Pinzaru, and Raymond Barry for providing comments on the manuscript. This work was supported by grants from Pershing Square Sohn cancer research alliance (A.S.), the V-foundation (A.S.), Pew-Stewart scholars award (A.S.), and the National Institutes of Health award 1R01GM115472-01 (R.T.P.). P.A. M-G. is supported by a fellowship from the Department of Defense (BC134020).

References

1 Sfeir, A. & Symington, L. S. Microhomology-Mediated End Joining: A Back-up Survival Mechanism or Dedicated Pathway? *Trends in biochemical sciences*, doi:10.1016/j.tibs.2015.08.006 (2015).

2 Boulton, S. J. & Jackson, S. P. Saccharomyces cerevisiae Ku70 potentiates illegitimate DNA double-strand break repair and serves as a barrier to error-prone DNA repair pathways. *The EMBO journal* **15**, 5093-5103 (1996).

3 Truong, L. N. *et al.* Microhomology-mediated End Joining and Homologous Recombination share the initial end resection step to repair DNA double-strand breaks in mammalian cells. *Proceedings of the National Academy of Sciences of the United States of America* **110**, 7720-7725, doi:10.1073/pnas.1213431110 (2013).

4 Thyme, S. B. & Schier, A. F. Polq-Mediated End Joining Is Essential for Surviving DNA Double-Strand Breaks during Early Zebrafish Development. *Cell reports*, doi:10.1016/j.celrep.2016.03.072 (2016).

5 Mateos-Gomez, P. A. *et al.* Mammalian polymerase theta promotes alternative NHEJ and suppresses recombination. *Nature* **518**, 254-257, doi:10.1038/nature14157 (2015).

6 Ceccaldi, R. *et al.* Homologous-recombination-deficient tumours are dependent on Poltheta-mediated repair. *Nature* **518**, 258-262, doi:10.1038/nature14184 (2015).

7 Wyatt, D. W. *et al.* Essential Roles for Polymerase theta-Mediated End Joining in the Repair of Chromosome Breaks. *Molecular cell* **63**, 662-673, doi:10.1016/j.molcel.2016.06.020 (2016).

8 Nik-Zainal, S. *et al.* Mutational processes molding the genomes of 21 breast cancers. *Cell* **149**, 979-993, doi:10.1016/j.cell.2012.04.024 (2012).

9 Davies, H. *et al.* HRDetect is a predictor of BRCA1 and BRCA2 deficiency based on mutational signatures. *Nature medicine* **23**, 517-525, doi:10.1038/nm.4292 (2017).

10 Alexandrov, L. B. *et al.* Signatures of mutational processes in human cancer. *Nature* **500**, 415-421, doi:10.1038/nature12477 (2013).

11 Wood, R. D. & Doublie, S. DNA polymerase theta (POLQ), double-strand break repair, and cancer. *DNA repair* **44**, 22-32, doi:10.1016/j.dnarep.2016.05.003 (2016).

12 Harris, P. V. *et al.* Molecular cloning of Drosophila mus308, a gene involved in DNA cross-link repair with homology to prokaryotic DNA polymerase I genes. *Molecular and cellular biology* **16**, 5764-5771 (1996).

13 Chan, S. H., Yu, A. M. & McVey, M. Dual roles for DNA polymerase theta in alternative end-joining repair of double-strand breaks in Drosophila. *PLoS genetics* **6**, e1001005, doi:10.1371/journal.pgen.1001005 (2010).

14 van Kregten, M. *et al.* T-DNA integration in plants results from polymerase-theta-mediated DNA repair. *Nat Plants* **2**, 16164, doi:10.1038/nplants.2016.164 (2016).

15 Koole, W. *et al.* A Polymerase Theta-dependent repair pathway suppresses extensive genomic instability at endogenous G4 DNA sites. *Nature communications* **5**, 3216, doi:10.1038/ncomms4216 (2014).

16 Yousefzadeh, M. J. *et al.* Mechanism of suppression of chromosomal instability by DNA polymerase POLQ. *PLoS genetics* **10**, e1004654, doi:10.1371/journal.pgen.1004654 (2014).

17 Kent, T., Chandramouly, G., McDevitt, S. M., Ozdemir, A. Y. & Pomerantz, R. T. Mechanism of microhomology-mediated end-joining promoted by human DNA polymerase theta. *Nature structural & molecular biology* **22**, 230-237, doi:10.1038/nsmb.2961 (2015).

18 Higgins, G. S. *et al.* A small interfering RNA screen of genes involved in DNA repair identifies tumor-specific radiosensitization by POLQ knockdown. *Cancer research* **70**, 2984-2993, doi:10.1158/0008-5472.CAN-09-4040 (2010).

19 Kent, T., Mateos-Gomez, P. A., Sfeir, A. & Pomerantz, R. T. Polymerase theta is a robust terminal transferase that oscillates between three different mechanisms during end-joining. *Elife* **5**, doi:10.7554/eLife.13740 (2016).

20 Kent, T. *et al.* DNA polymerase theta specializes in incorporating synthetic expanded-size (xDNA) nucleotides. *Nucleic acids research* **44**, 9381-9392, doi:10.1093/nar/gkw721 (2016).

21 Zahn, K. E., Averill, A. M., Aller, P., Wood, R. D. & Doublie, S. Human DNA polymerase theta grasps the primer terminus to mediate DNA repair. *Nature structural & molecular biology* **22**, 304-311, doi:10.1038/nsmb.2993 (2015).

22 Hogg, M., Sauer-Eriksson, A. E. & Johansson, E. Promiscuous DNA synthesis by human DNA polymerase theta. *Nucleic acids research* **40**, 2611-2622, doi:10.1093/nar/gkr1102 (2012).

23 Seki, M., Marini, F. & Wood, R. D. POLQ (Pol theta), a DNA polymerase and DNA-dependent ATPase in human cells. *Nucleic acids research* **31**, 6117-6126 (2003).

24 Newman, J. A., Cooper, C. D., Aitkenhead, H. & Gileadi, O. Structure of the Helicase Domain of DNA Polymerase Theta Reveals a Possible Role in the Microhomology-Mediated End-Joining Pathway. *Structure* **23**, 2319-2330, doi:10.1016/j.str.2015.10.014 (2015).

25 Newman, J. A. *et al.* Crystal structure of the Bloom's syndrome helicase indicates a role for the HRDC domain in conformational changes. *Nucleic acids research* **43**, 5221-5235, doi:10.1093/nar/gkv373 (2015).

26 Xie, A., Kwok, A. & Scully, R. Role of mammalian Mre11 in classical and alternative nonhomologous end joining. *Nature structural & molecular biology* **16**, 814-818, doi:10.1038/nsmb.1640 (2009).

27 Rass, E. *et al.* Role of Mre11 in chromosomal nonhomologous end joining in mammalian cells. *Nature structural & molecular biology* **16**, 819-824, doi:10.1038/nsmb.1641 (2009).

28 Villarreal, D. D. *et al.* Microhomology directs diverse DNA break repair pathways and chromosomal translocations. *PLoS genetics* **8**, e1003026, doi:10.1371/journal.pgen.1003026 (2012).

29 Decottignies, A. Microhomology-mediated end joining in fission yeast is repressed by pku70 and relies on genes involved in homologous recombination. *Genetics* **176**, 1403-1415, doi:10.1534/genetics.107.071621 (2007).

30 Daley, J. M. & Wilson, T. E. Rejoining of DNA double-strand breaks as a function of overhang length. *Molecular and cellular biology* **25**, 896-906, doi:10.1128/MCB.25.3.896-906.2005 (2005).

31 Deng, S. K., Gibb, B., de Almeida, M. J., Greene, E. C. & Symington, L. S. RPA antagonizes microhomology-mediated repair of DNA double-strand breaks. *Nature structural & molecular biology* **21**, 405-412, doi:10.1038/nsmb.2786 (2014).

32 Simsek, D. & Jasin, M. Alternative end-joining is suppressed by the canonical NHEJ component Xrcc4-ligase IV during chromosomal translocation formation. *Nature structural & molecular biology* **17**, 410-416, doi:10.1038/nsmb.1773 (2010).

33 Shima, N., Munroe, R. J. & Schimenti, J. C. The mouse genomic instability mutation chaos1 is an allele of Polq that exhibits genetic interaction with Atm. *Molecular and cellular biology* **24**, 10381-10389, doi:10.1128/MCB.24.23.10381-10389.2004 (2004).

34 Lemee, F. *et al.* DNA polymerase theta up-regulation is associated with poor survival in breast cancer, perturbs DNA replication, and promotes genetic instability. *Proceedings of the National Academy of Sciences of the United States of America* **107**, 13390-13395, doi:10.1073/pnas.0910759107 (2010).

35 Prasad, R. *et al.* Human DNA polymerase theta possesses 5'-dRP lyase activity and functions in single-nucleotide base excision repair in vitro. *Nucleic acids research* **37**, 1868-1877, doi:10.1093/nar/gkp035 (2009).

36 Simsek, D. *et al.* DNA ligase III promotes alternative nonhomologous end-joining during chromosomal translocation formation. *PLoS genetics* **7**, e1002080, doi:10.1371/journal.pgen.1002080 (2011).

37 Bothmer, A. *et al.* Characterization of the interplay between DNA repair and CRISPR/Cas9-induced DNA lesions at an endogenous locus. *Nature communications* **8**, 13905, doi:10.1038/ncomms13905 (2017).

38 Yusufzai, T. & Kadonaga, J. T. HARP is an ATP-driven annealing helicase. *Science* **322**, 748-750, doi:10.1126/science.1161233 (2008).

39 Audry, J. *et al.* RPA prevents G-rich structure formation at lagging-strand telomeres to allow maintenance of chromosome ends. *The EMBO journal* **34**, 1942-1958, doi:10.15252/embj.201490773 (2015).

40 Sugiyama, T., New, J. H. & Kowalczykowski, S. C. DNA annealing by RAD52 protein is stimulated by specific interaction with the complex of replication protein A and single-stranded DNA. *Proceedings of the National Academy of Sciences of the United States of America* **95**, 6049-6054 (1998).

41 Sfeir, A. & de Lange, T. Removal of shelterin reveals the telomere end-protection problem. *Science* **336**, 593-597, doi:10.1126/science.1218498 (2012).

42 Tang, J. *et al.* Acetylation limits 53BP1 association with damaged chromatin to promote homologous recombination. *Nature structural & molecular biology* **20**, 317-325, doi:10.1038/nsmb.2499 (2013).

43 Doksani, Y. & de Lange, T. Telomere-Internal Double-Strand Breaks Are Repaired by Homologous Recombination and PARP1/Lig3-Dependent End-Joining. *Cell reports* **17**, 1646-1656, doi:10.1016/j.celrep.2016.10.008 (2016).

44 Lee-Theilen, M., Matthews, A. J., Kelly, D., Zheng, S. & Chaudhuri, J. CtIP promotes microhomology-mediated alternative end joining during class-switch recombination. *Nature structural & molecular biology* **18**, 75-79, doi:10.1038/nsmb.1942 (2011).

45 Symington, L. S. & Gautier, J. Double-strand break end resection and repair pathway choice. *Annual review of genetics* **45**, 247-271, doi:10.1146/annurev-genet-110410-132435 (2011).

46 Cejka, P. *et al.* DNA end resection by Dna2-Sgs1-RPA and its stimulation by Top3-Rmi1 and Mre11-Rad50-Xrs2. *Nature* **467**, 112-116, doi:10.1038/nature09355 (2010).

47 Niu, H. *et al.* Mechanism of the ATP-dependent DNA end-resection machinery from Saccharomyces cerevisiae. *Nature* **467**, 108-111, doi:10.1038/nature09318 (2010).

48 Chen, H., Lisby, M. & Symington, L. S. RPA coordinates DNA end resection and prevents formation of DNA hairpins. *Molecular cell* **50**, 589-600, doi:10.1016/j.molcel.2013.04.032 (2013).

49 Audebert, M., Salles, B. & Calsou, P. Involvement of poly(ADP-ribose) polymerase-1 and XRCC1/DNA ligase III in an alternative route for DNA double-strand breaks rejoining. *The Journal of biological chemistry* **279**, 55117-55126, doi:10.1074/jbc.M404524200 (2004).

50 Adelman, C. A. *et al.* HELQ promotes RAD51 paralogue-dependent repair to avert germ cell loss and tumorigenesis. *Nature* **502**, 381-384, doi:10.1038/nature12565 (2013).

51 Richards, J. D. *et al.* Structure of the DNA repair helicase hel308 reveals DNA binding and autoinhibitory domains. *The Journal of biological chemistry* **283**, 5118-5126, doi:10.1074/jbc.M707548200 (2008).

52 Maga, G. *et al.* Human DNA polymerase lambda functionally and physically interacts with proliferating cell nuclear antigen in normal and translesion DNA synthesis. *The Journal of biological chemistry* **277**, 48434-48440, doi:10.1074/jbc.M206889200 (2002).

53 Yusufzai, T., Kong, X., Yokomori, K. & Kadonaga, J. T. The annealing helicase HARP is recruited to DNA repair sites via an interaction with RPA. *Genes & development* **23**, 2400-2404, doi:10.1101/gad.1831509 (2009).

54 Driscoll, R. & Cimprich, K. A. HARPing on about the DNA damage response during replication. *Genes & development* **23**, 2359-2365, doi:10.1101/gad.1860609 (2009).

55 Goullet de Rugy, T. *et al.* Excess Poltheta functions in response to replicative stress in homologous recombination-proficient cancer cells. *Biol Open* **5**, 1485-1492, doi:10.1242/bio.018028 (2016).

56 Kawamura, K. *et al.* DNA polymerase theta is preferentially expressed in lymphoid tissues and upregulated in human cancers. *International journal of cancer. Journal international du cancer* **109**, 9-16, doi:10.1002/ijc.11666 (2004).

Figure 1

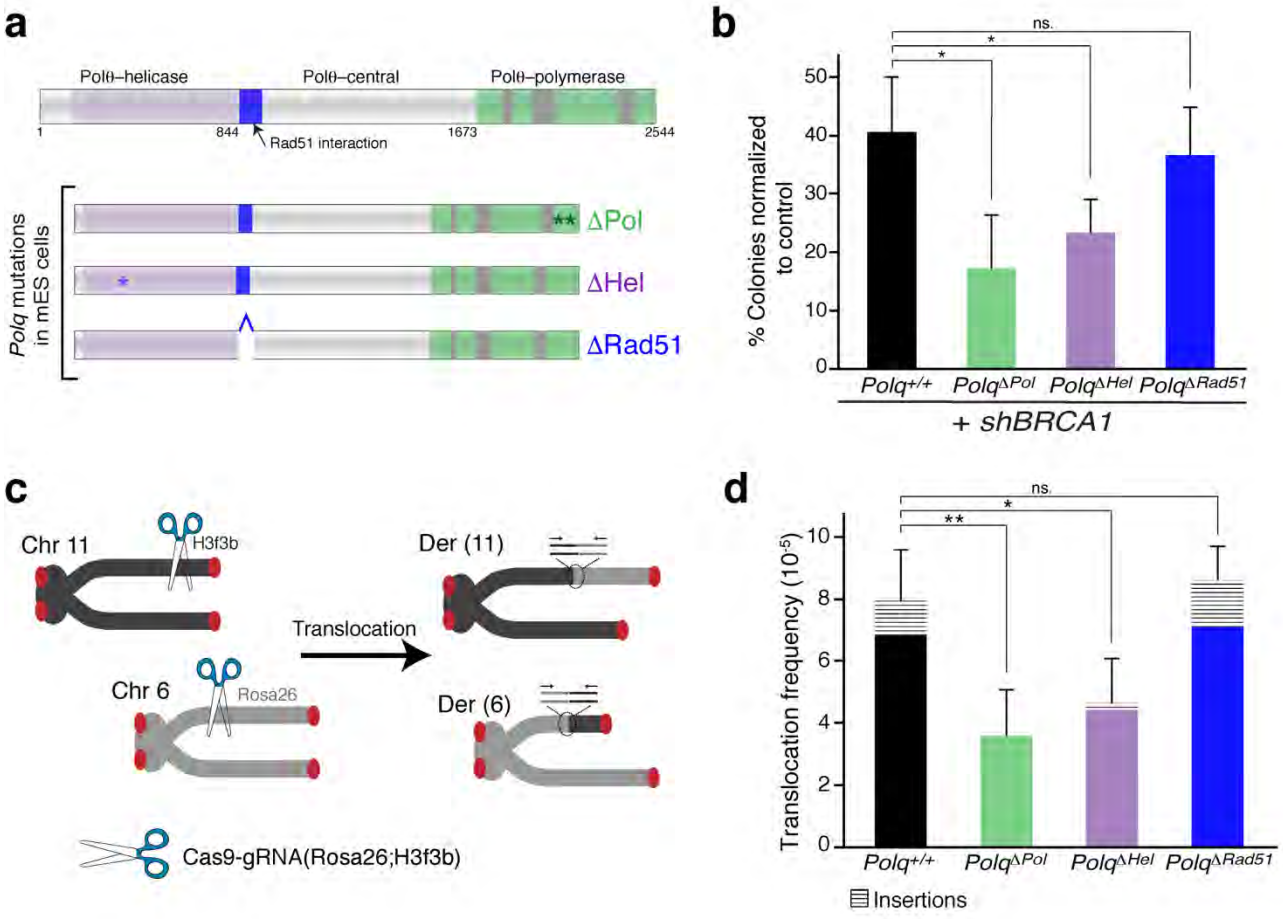

e

Der (6)	*Polq*$^{+/+}$	*Polq*$^{\Delta Pol}$	*Polq*$^{\Delta Hel}$	*Polq*$^{\Delta Rad51}$
% translocation with alt-NHEJ signature	63.7	24.2	31.2	57.1
% translocation with >2nt insertions	14.3	0.0	4.9	14.3
% translocation with microhomology	72.6	32.0	47.0	67.4
% translocation with deletion	83.1	90.3	72.1	82.9

Figure 2

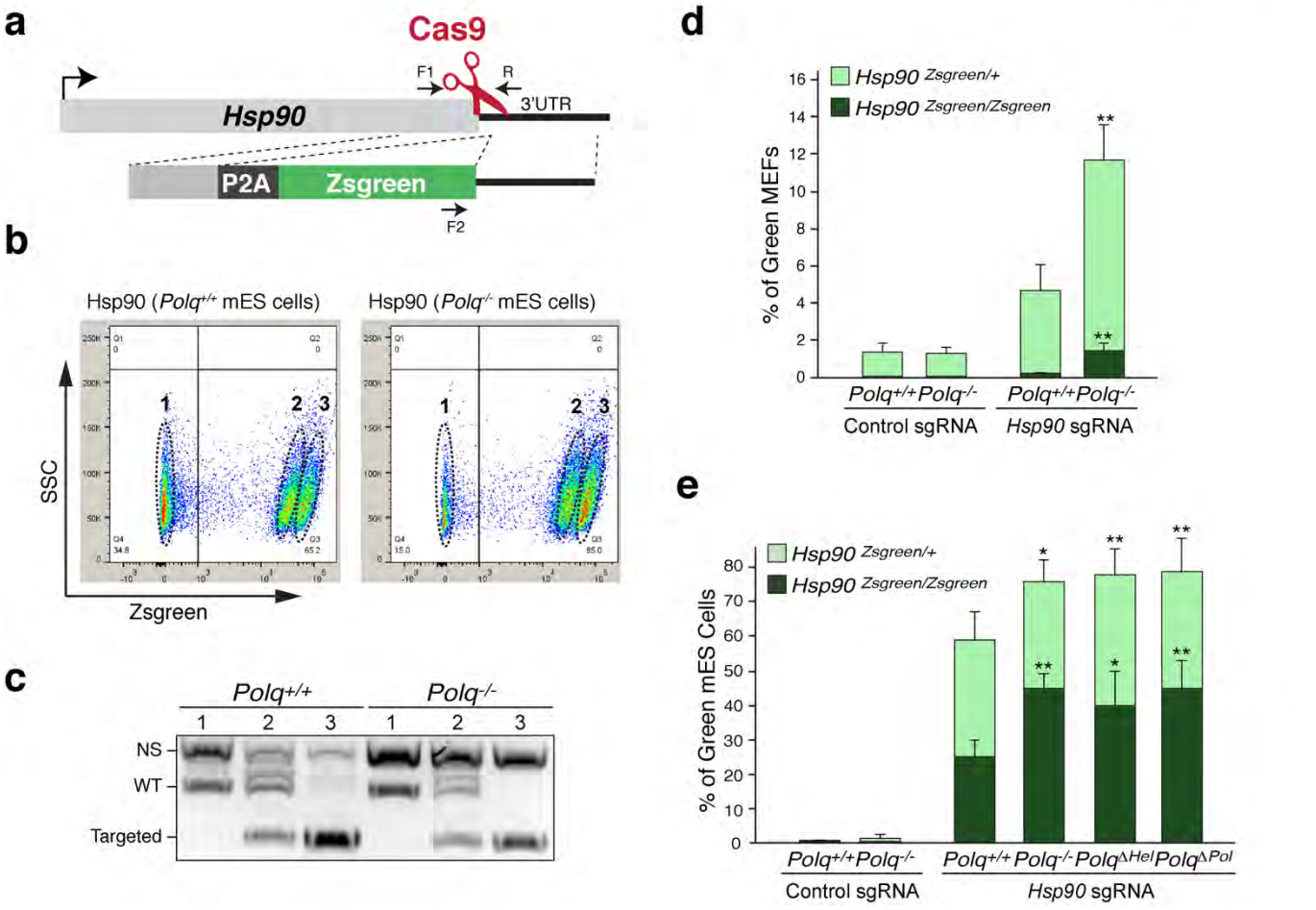
a
Cas9
F1
R
3'UTR
Hsp90
P2A
Zsgreen
F2
b
Hsp90 (Polq+/+ mES cells)
Hsp90 (Polq-/- mES cells)
SSC
Zsgreen
1
2
3
c
Polq+/+
Polq-/-
1
2
3
NS
WT
Targeted
d
Hsp90 Zsgreen/+
Hsp90 Zsgreen/Zsgreen
% of Green MEFs
Polq+/+ Polq-/-
Control sgRNA
Polq+/+ Polq-/-
Hsp90 sgRNA
e
Hsp90 Zsgreen/+
Hsp90 Zsgreen/Zsgreen
% of Green mES Cells
Polq+/+ Polq-/-
Control sgRNA
Polq+/+ Polq-/- PolqΔHel PolqΔPol
Hsp90 sgRNA

Figure 3

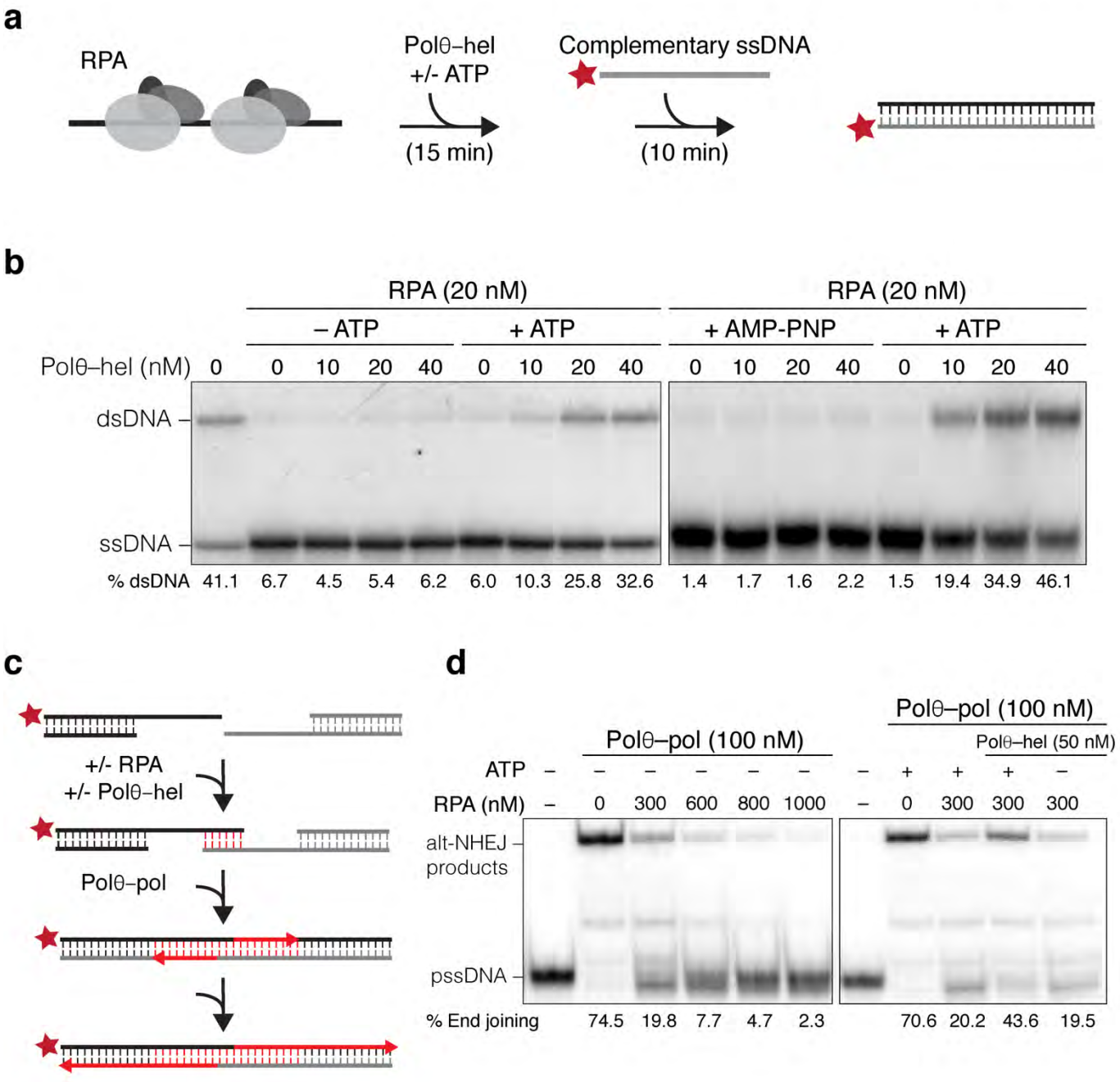
a
RPA
Polθ–hel
+/- ATP
(15 min)
Complementary ssDNA
(10 min)
b
RPA (20 nM)
RPA (20 nM)
– ATP
+ ATP
+ AMP-PNP
+ ATP
Polθ–hel (nM) 0 0 10 20 40 0 10 20 40 0 10 20 40 0 10 20 40
dsDNA
ssDNA
% dsDNA 41.1 6.7 4.5 5.4 6.2 6.0 10.3 25.8 32.6 1.4 1.7 1.6 2.2 1.5 19.4 34.9 46.1
c
+/- RPA
+/- Polθ–hel
Polθ–pol
d
Polθ–pol (100 nM)
Polθ–pol (100 nM)
Polθ–hel (50 nM)
ATP – – – – – – – + + + –
RPA (nM) – 0 300 600 800 1000 – 0 300 300 300
alt-NHEJ products
pssDNA
% End joining 74.5 19.8 7.7 4.7 2.3 70.6 20.2 43.6 19.5

Figure 4

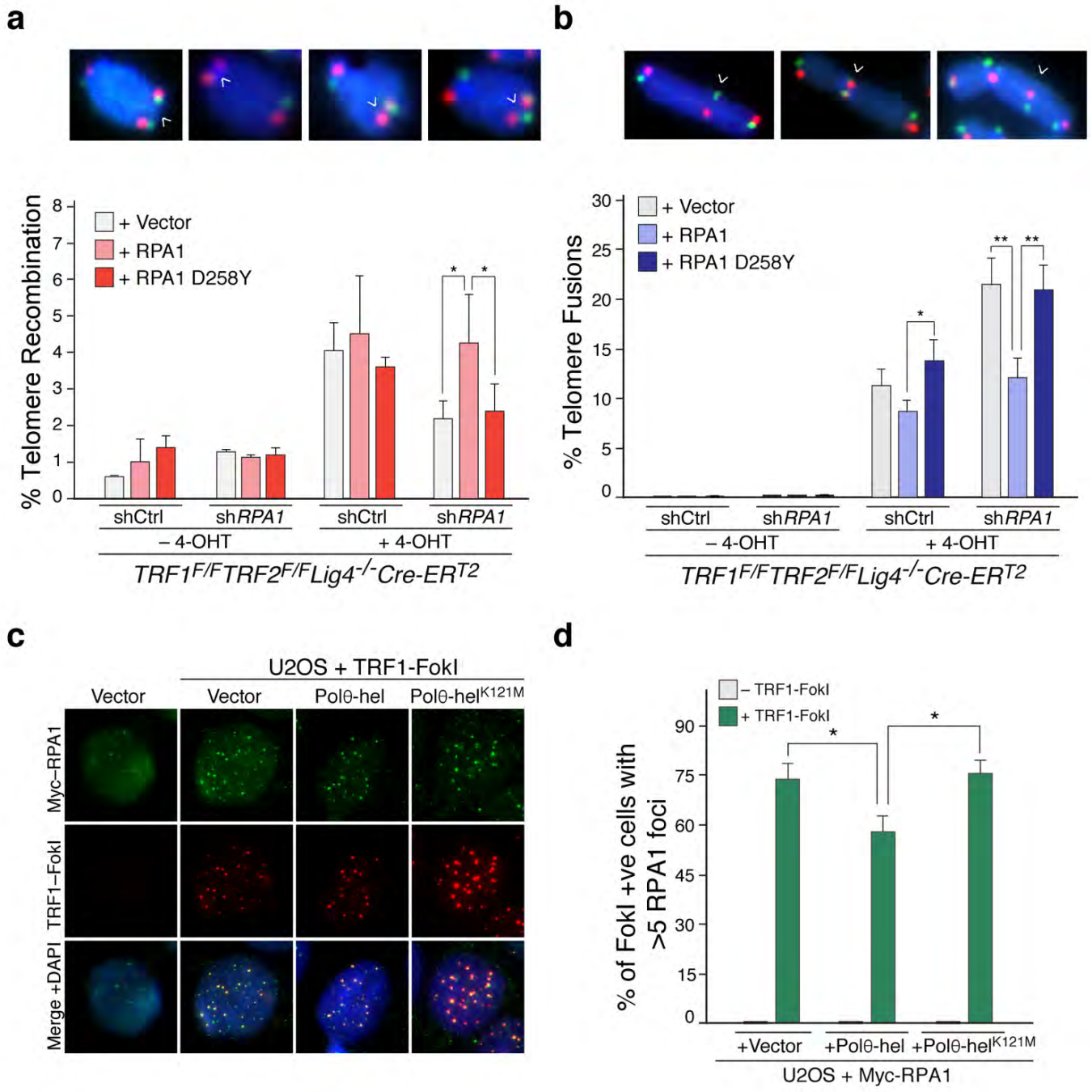
a
b
% Telomere Recombination
+ Vector
+ RPA1
+ RPA1 D258Y
shCtrl
shRPA1
– 4-OHT
+ 4-OHT
TRF1F/FTRF2F/FLig4-/-Cre-ERT2
% Telomere Fusions
c
U2OS + TRF1-FokI
Vector
Polθ-hel
Polθ-helK121M
Myc–RPA1
TRF1–FokI
Merge +DAPI
d
– TRF1-FokI
+ TRF1-FokI
% of FokI +ve cells with >5 RPA1 foci
+Vector
+Polθ-hel
+Polθ-helK121M
U2OS + Myc-RPA1

Figure 5

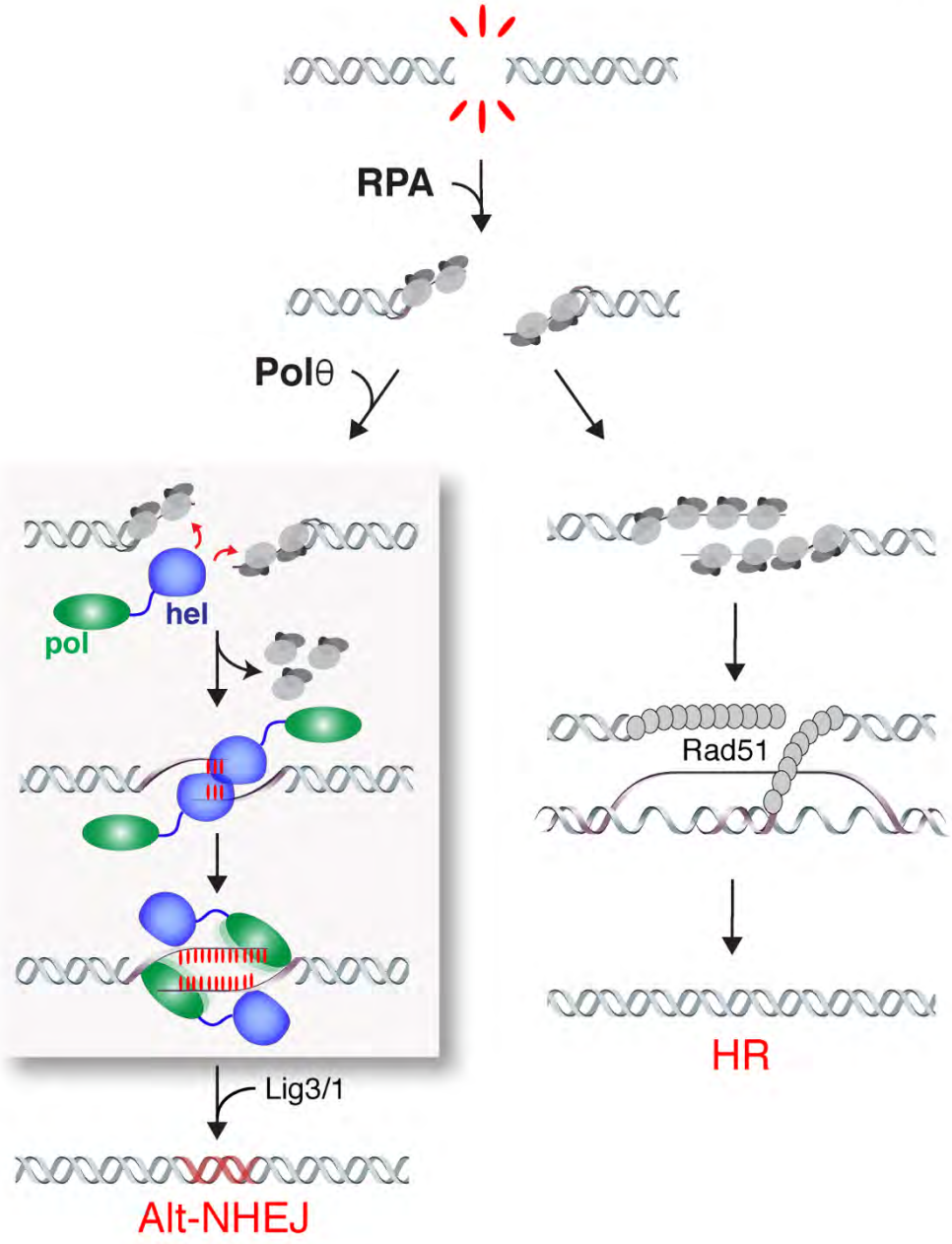

Supplementary Information

Material and Methods

Cells culture procedures

Polq$^{+/+}$ and *Polq*$^{-/-}$ mouse embryonic fibroblast (MEFs) were derived from 13.5 day embryos and immortalized with pBABE-SV40LT. *TRF1*$^{F/F}$*TRF2*$^{F/F}$*Lig4*$^{-/-}$Cre-ER^{T2} MEFs were previously established[1]. *PolQ*$^{+/+}$ and *PolQ*$^{-/-}$ mouse embryonic stem (mES) cells were derived from embryos and adapted to feeder-free growth conditions. CCE mouse embryonic feeder-free stem cells were derived from 129/Sv mouse[2]. U2OS cells expressing inducible TRF1-FokI-ER^{T2} cells were a gift from the lab of R. Greenberg[3]. MEFs and U2OS cells were cultured in Dulbecco's Modified Eagle Medium (DMEM) supplemented with 10% fetal bovine serum (FBS) (Gibco), 2 mM L-glutamine (Sigma), 100 U/ml penicillin (Sigma), 0.1 μg/ml streptomycin (Sigma), 0.1 mM non-essential amino acids (Invitrogen), and 1 mM sodium pyruvate (Sigma). mES cells were grown in DMEM supplemented with 15% fetal bovine serum (ES qualified FBS) (Gibco), 2 mM L-glutamine (Sigma), 100 U/ml penicillin (Sigma), 0.1 μg/ml streptomycin (Sigma), 0.1 mM non-essential amino acids (Invitrogen), leukemia inhibitory factor (LIF), 2-Betamercaptoethanol (Gibco 21985), MEK inhibitor 1μM (PD03259010, Sigma) and GDK-3 inhibitor (CHIR99021, R&D Systems). Expression of Cre recombinase was induced by treating MEFs expressing Cre-ER^{T2} allele with 0.5 μM 4-OH tamoxifen (4-OHT; Sigma H7904) for 12 hours. t=0 time-point was set at the time of treatment with 4-OHT.

Generating *Polq* mutations in mouse embryonic stem cells (mECs) by CRISPR/Cas9 targeting

CCE-mESc were targeted to obtain catalytically inactive polymerase (*Polq*$^{\Delta Pol}$)[4] and helicase (*Polq*$^{\Delta Hel}$). Targeting was also performed to deleted a conserved Rad51 interaction motif (*Polq*$^{\Delta Rad51}$) and to generate *Polq* knockout cells. Briefly, two gRNAs were co-expressed from a plasmid that also codes for a Cas9-nickase plasmid (pX335-U6-Chimeric_BB-CBh-hSpCas9n(D10A)), were transfected together with a donor cassette. The template plasmids included 600 base pair of homology arms and carried mutations for the gRNA site. To generate *Polq*$^{\Delta Hel}$, lysine-120 was replaced and a silent mutation was introduced to create a BamHI restriction site. 141 nucleotides were deleted in *Polq*$^{\Delta Rad51}$ cells. *Polq* $^{-/-}$ cells were generated by deleting exon-3 (121 nt), which then introduced 3 stop codons in exon 4. Clonal cell lines were derived and genotyping PCR was performed to identify ones with homozygous targeting.

Analysis of CRISPR/Cas9 HR-mediated gene editing efficiency

MEFs, mouse ES cells, and CCEs were used to target the *Hsp90* (ab1) and *Sox2* genes. The 3' terminus of both genes were targeted to introduce a P2A-ZsGreen cassette preceding the STOP codon, allowing flow cytometry readout for successful targeting. DSBs were induces with a Cas9-nuclease (pX330-U6-Chimeric_BB-CBh-hSpCas9) and Cas9-nickase plasmid (pX335-U6-Chimeric_BB-CBh-hSpCas9n(D10A)) expressing one or two gRNAs, respectively. The plasmids were co-transfected with the template plasmid that included a P2A-ZsGreen and homology arms encoding for 600 nucleotides flanking the STOP codon. For reverse transfection, cells were incubated in fresh media 6 hours prior to transfection. Cells were trypsinized, pelleted, and resuspended in 100 µl of opti-men (Gibco) containing the plasmids and Lipofectamine 3000 (Invitrogen) according to the manufacturers instruction. One million cells were transfected with 200 ng of Cas9 and 800 ng of template plasmids (1 to 10 molar ratio). After incubation for 10 minutes, fresh media was added and cells were plated. Puromycin was added 16-hours post transfection to enrich for transfected cells (MEFs: 2 µg/ml for 48 hours, mES cells: 1 µg/ml for 24 hours, and CCE: 2 µg/ml for 24 hours). FACS analysis was performed 8 days post transfection using a BD^{TM} LSRII HTS cell analyzer. DNA was extracted from sorted cells to perform genotyping PCR. 50ng DNA was amplified using Q5 polymerase (NEB) and an annealing temperature of 60^{o}C. PCR-Primers indicated below.

Chromosomal translocation assay

To perform the translocation assay, 7*10^5 *PolQ*$^{+/+}$, *PolQ*$^{\Delta Hel}$, *PolQ*$^{\Delta Pol}$ and *PolQ*$^{\Delta Rad51}$ CCE cells were transfected with 2 µg of Cas9-gRNA(Rosa26;H3f3b) using Lipofectamine 2000 (Invitrogen). We constructed Cas9-gRNA(Rosa26;H3f3b) by introducing two guide RNAs (GTTGGCTCGCCGGATACGGG, for H3f3b; ACTCCAGTCTTTCTAGAAGA, for Rosa26) into pX330-U6-Chimeric_BB-CBh-hSpCas9. After transfection, 2*10^5 cells were used to assess Cas9 expression and 5*10^5 cells were seeded in a 96-well plate (10^4 cells/well). Cells were lysed (60 hours post plating) in 40ul lysis buffer/well (10mM Tris pH 8.0, 0.45% Nonidet P-40, 0.45% Tween 20). The lysates were incubated with 200ug/ml Proteinase K for 2 hours at 55°C. Translocation detection was performed according to previously established protocol using nested PCR[5]. To detect Der(6) the following primers were used in the first PCR reaction: Tr6-11-Fwd:5′-GCGGGAGAAATGGATATGAA-3′; Tr6-11-Rev: 5′- TTGACGCCTTCCTTCTTCTG -3′. For the second round of PCR amplification we used the primers: Tr6-11NFwd: 5′-GGCGGATCACAAGCAATAAT-3′; Tr6-11NRev: 5′-CTGCCATTCCAGAGATTGGT-3′. The number of PCR-positive wells was used to calculate the translocation frequency. Amplified

products from positive wells were sequenced to verify translocations and determine the junction sequences.

Colony Formation Assay

Following lentiviral transduction with sh*Ctrl* or sh*BRCA1* (sequence listed below), CCE mES cells were selected with Puromycin (2 μg/ml) for 24 hours and plated in 6cm dishes (200 and 400 cells per plate). 12 days later, colonies were fixed with 4% PFA (5 minutes), rinsed with PBS, and stained with crystal violet (Sigma-Aldrich).

CO-FISH

TRF1$^{F/F}$ *TRF2*$^{F/F}$ *Lig4*$^{-/-}$ Cre-ER^{T2} MEF were infected with concentrated lentivirus to ensure 100% transduction of sh*Ctrl,* sh*RPA1* or sh*Rad51* (sequence listed below). 6 hours post-infection, cells were treated with 4-OHT to induce the expression of CRE and subsequent loss of shelterin. For the CO-FISH assay, ~50% confluent MEFs were labeled with BrdU:BrdC (3:1, final concentration: 10 μM) for 14-16 hours and then incubated for 2 hours with 0.2 μg/ml colcemid (Sigma). Cells were harvested by trypsinization 110 hours after 4-OHT addition, washed with PBS, resuspended in 0.075 M KCl at 37°C for 30 minutes, and fixed overnight in methanol/acetic acid (3:1). Fixed ells were then dropped onto glass slides and the slides were dried overnight. The next day, the slides were rehydrated with PBS for 5 min, treated with 0.5 mg/ml RNase A (in PBS, DNase free) for 10 min at 37°C, incubated with 0.5 μg/ml Hoechst 33258 (Sigma) in 2XSSC for 15 min at room temperature, and exposed to 365-nm UV light (Stratalinker 1800 UV irradiator) for 30 min. The slides were then digested twice with 800 U Exonuclease III (Promega) at room temperature for 10 min each, washed with PBS and dehydrated through an ethanol series of 70%, 95%, 100%. After air-drying, slides were hybridized with Tamra-OO-[TTAGGG]3 PNA probe in hybridization solution (70% formamide, 1 mg/ml blocking reagent (Roche), 10 mM Tris-HCl pH 7.5) for 2 hours at room temperature. The slides were then washed for few seconds with 70% formamide-10 mM Tris-HCl pH 7.5 and incubated with FITC-OO-[CCCTAA]$_3$ PNA probe in hybridization solution for 2 hours. Slides were washed twice for 15 min each in 70% formamide-10 mM Tris-HCl, followed by three 5 min washes in 0.1 M Tris-HCl, pH 7.5, 0.15 M NaCl and 0.08% Tween-20. Chromosomal DNA was counterstained with 4,6-diamidino-2-phenylindole (DAPI) during the second PBS wash. Slides were mounted in antifade reagent (ProLong Gold, Invitrogen) and imaged using a Nikon Eclipse TI microscope.

Western blot analysis

Cells were harvested by trypsinization, lysed in 2X Laemmli buffer (100 mM Tris-HCl pH 6.8, 200 μM DTT, 3% SDS, 20% glycerol, 0.05% bromophenol blue) at 10^4 cell/μl. The lysate was denatured for 10 min at 95ºC, and sheared by forcing it through a 28-gauge insulin needle 5 times. Lysates from 10^5 cells were loaded on an SDS/PAGE and transferred to a nitrocellulose membrane. The membrane was blocked in 5% milk in TBS with 0.1%Tween-20 and incubated with primary antibody in TBS/5% milk/0.1% Tween-20 for 2 hours at room temperature. The following primary antibodies were utilized: Myc (9E10; Calbiochem); γ-tubulin (clone GTU-88, Sigma); Flag (anti-Flag M2, Sigma); Rad51 (H2 sc8349, Santa Cruz); RPA1 (A300-241A, Bethyl).

Immunofluorescence

Briefly, cells were fixed with 4% (v/v) paraformaldehyde for 10 minutes at room temperature. Cells were washed with PBS, permeabilized (0.5% Triton X 100, 20 mM Hepes-KOH pH7.9, 50 mM NaCl, 3 mM $MgCl_2$, 300 mM Sucrose) for 10 minutes, and blocked with PBS containing 3% BSA, 3% goat serum, 0.1% Triton X 100 and 1 mM EDTA for 30 minutes. Cells were incubated with the same buffer containing primary antibodies for 1.5 hours at room temperature, washed in PBS before incubation with secondary antibodies for 45 min and finally washed three times for 5 min in PBS. DNA was counterstained with 4,6-diamidino-2-phenylindole (DAPI) during the second PBS wash. Slides were mounted in antifade reagent (ProLong Gold, Invitrogen) and images were captured with a Nikon Eclipse TI microscope.

To analyze Rad51 foci formation and its co-localization with γ-H2AX, cells were exposed to 1 Gy IR by a Faxitron X-ray system (120kV, 5mA, does rate 5Gy/min) and recovered for 4 hours. Then cells were treated with 0.1% Triton-X 100 (in PBS) for 5 minutes on ice prior to a double fixation, paraformaldehyde for 10 minutes and with methanol fixation for 10 minutes at -20˚C. To monitor the recruitment of RPA1 to DNA double strand breaks at telomeres, U2OS-TRF1- FokI-ER^{T2} were nucleofected (4D-Nucleofector, Lonza) with RPA1-Myc-IRES-GFP and Flag-Polθ-Helicase-IRES-TdTomato, 48 hours prior to fixation. Polθ-Helicase comprised amino acid 1-1187. TRF1-FokI-ER^{T2} expression was induced by adding doxycycline (100 ng/ml) for 15 hours prior to treatment with 1 μM shield-1 (Clontech) and 0.5 μM 4-OH-tamoxifen for 7 hours. The treated cells were pre-extracted with 0.1% Triton-X 100 (in PBS) for 5 minutes on ice prior to fixation.The primary antibodies used for IF were: Myc (9B11; Cell Signaling); γ-H2AX [p Ser139] (mouse monoclonal, Novus, NB100-384), Rad51 (Rabbit polyclonal, Santa Cruz, sc-8349).

Protein purification

Polθ-helicase domain: pE-SUMOstar vector (Life Sensors) containing the Polθ-helicase cDNA (aa 1-894) was transformed into Rosetta2(DE3)/pLysS cells (Stratagene). Freshly grown colonies were picked from a plate and re-suspended in 20 ml LB broth. 1 ml of re-suspended cells was added to 1 L of auto-induction medium (1X Terrific Broth (USB Corporation), 0.5% w/v glycerol, 0.05% w/v dextrose, 0.2% w/v alpha-lactose, 100 µg/ml ampicillin and 34 µg/ml chloramphenicol) in a 2.8 L Fernbach flask. The flasks were shaken at 20° C for 60 hours. 6 L of culture were grown and resulting E. coli pellets were stored at −80° C.

Frozen pellets were thawed on ice and re-suspended in buffer containing 50 mM HEPES pH 8.0, 500 mM NaCl, 10% (v/v) glycerol, 10 mM imidazole pH 8.0, 1.5 % (v/v) Igepal CA-630 (Sigma), 5 mM 2-β-mercaptoethanol (BME), 10 mM PMSF, and 1 tablet of Complete EDTA-free protease inhibitors cocktail (Roche) per every 50 ml at a volume of 5 ml of buffer per gram of cell pellet. The resuspended cells were sonicated on ice with constant stirring then centrifuged at 27,000 g. The clarified cell lysate was loaded onto a 5 ml HisTrap FF Crude column (GE Lifesciences) and washed with buffer A (50 mM HEPES pH 8.0, 450 mM NaCl, 10% (v/v) glycerol, 10 mM imidazole pH 8.0, 5 mM BME and 0.005% v/v Igepal CA-630). Bound protein was then eluted with a gradient from buffer A to buffer B (50 mM HEPES pH 8.0, 450 mM NaCl, 10% (v/v) glycerol, 0.005% (v/v) Igepal CA-630, 5 mM BME and 250 mM imidazole pH 8.0). Fractions containing Polθ–helicase were pooled, mixed with with 25 units of SUMOStar protease (LifeSensors, #4110) and dialyzed against buffer C (50 mM HEPES pH 8.0, 450 mM NaCl, 10% (v/v) glycerol, 5 mM DTT and 0.005% v/v Igepal CA-630) overnight at 4° C. The protein mixture was then loaded onto a 5 ml HisTrap HP column and washed with buffer C. Cleaved Polθ-helicase was separated from uncleaved protein and the protease by applying a gradient to buffer B. Fractions containing cleaved Polθ–helicase were concentrated and stored in aliquots at −80° C. All steps of the purification process were performed at 4° C.

RPA: Hexa-histidine-tagged RPA expression vector was transformed into Rosetta2(DE3)/pLysS cells (Stratagene). Freshly grown colonies were inoculated into 50 ml of LB with 50 µg ml^{-1} ampicillin and 34 µg ml^{-1} chloramphenicol and incubated overnight at 37˚ C with agitation. The pre-culture was then diluted 100-fold into 6 L of LB with 50 µg ml^{-1} ampicillin and 34 µg ml^{-1} chloramphenicol and incubated at 37˚ C with agitation until O.D. at 600 nm reached 0.6. The was cooled to 16˚ C then protein expression was induced with 1 mM IPTG at 16˚ C for 16-18 h. Cells were harvested by centrifugation for 15 min at 5,000 x g. Cell pellets were frozen and stored at -80˚ C.

The frozen cell paste corresponding to 6 L of starter culture was thawed on ice and resuspended in buffer containing 40 mM Tris-HCl pH 7.5, 500 mM NaCl, 10% (v/v) glycerol, 10 mM imidazole pH 8, 5 mM 2-β-mercaptoethanol (BME), 10 mM PMSF, and 1 tablet of Complete EDTA-free protease inhibitors (Roche) cocktail per every 50 ml at a volume of 10 ml of buffer per gram of cell pellet. The resuspended cells were sonicated on ice with constant stirring and then centrifuged 27,000 g. The clarified cell lysate was loaded onto a 5 ml HisTrap FF Crude column (GE Lifesciences) and washed with buffer A (20 mM Tis-HCl pH 7.5, 250 mM NaCl, 10% (v/v) glycerol, 10 mM imidazole pH 8 and 5 mM BME). Bound fractions were then eluted with a gradient to 100% of elution buffer B (20 mM Tris-HCl pH 7.5, 250 mM NaCl, 500 mM imidazole pH 8.0, 10% glycerol and 5 mM BME). Fractions containing trimeric RPA were pooled and dialyzed against buffer C (20 mM Tris-HCl pH 7.5, 50 mM NaCl, 10% (v/v) glycerol and 5 mM BME) for overnight at 4° C. Next, the protein was were loaded onto a 5 ml HiTrap Q HP column (GE Lifesciences), washed with buffer C, then eluted with a gradient to 100% buffer D (20 mM Tris-HCl pH 7.5, 500 mM NaCl, 5 mM BME, 10% glycerol). Fractions were resolved and analyzed in a 4-15% SDS-PAGE gel (BioRad). Pure RPA fractions containing equimolar amounts of each subunit were pooled and dialyzed against 2 L of storage buffer (20 mM Tris-HCl pH 7.5, 250 mM NaCl, 5 mM BME, 10% glycerol) overnight at 4˚ C, then stored in aliquots at -80˚ C.

Polθ-polymerase was purified as previously described[6].

ATPase Assay

The indicated amounts of Polθ–helicase were incubated with 10 μM ATP, 2 μCi of γ-^{32}P-ATP and 100 nM ssDNA (29 nt poly-dT) in 5 μl of buffer (50 mM Tris-HCl, pH 7.5, 10 mM $MgCl_2$, 5 mM DTT, 0.1 mg/ml bovine serum albumin, and 10% v/v glycerol) at room temp for 20 min. The reaction mixture was then spotted onto a TLC plate on PEI cellulose, which was developed in a buffer containing 1 M acetic acid and 0.25 M $LiCl_2$ for 1.5 h. Plates were allowed to dry then visualized by phosphorimager.

Polθ–helicase ssDNA annealing

4 nM of ssDNA RP246 (5'-GCTCTGATGCCGCATAGTTAAGCCAGCCCCGACACCCG-3') was pre-incubated with 0 or 20 nM RPA or SSB (Sigma) for 5 min at 37º C in the buffer (25 mM Tris-HCl pH 7.5, 0.01% NP-40, 1 mM DTT, 4 mM $MgCl_2$). Samples were supplemented with or without 1 mM ATP or AMP-PNP (Sigma). Next, Polθ–helicase was added at indicated concentrations and reactions were incubated for a further 15 min at 37º C. Finally, 4 nM of the radio-labeled complementary ssDNA was added and incubated for an additional 10 min at 37º C. Reactions

were terminated by the addition of the stop solution with final concentrations as follows: 16 mM EDTA, 0.2% SDS, 20 mM Tris-HCl pH 7.5, 80 nM complementary ssDNA (without radio-label), Proteinase K 80 U/ml. Resulting nucleic acids were resolved in non-denaturing polyacrylamide gels and visualized by autoradiography. All concentrations are listed as final.

***In vitro* alt-NHEJ assay**

100 nM 5′-^{32}P radio-labeled pssDNA template (^{32}P-RP344/RP343) was pre-incubated at 37° C in buffer (25 mM Tris-HCl, pH 8.8, 10% glycerol, 1 mM DTT, 0.01% NP-40, 10 mM $MgCl_2$, and 0.1 mg/ml BSA) then mixed with indicated concentrations of RPA for 10 min. Next, 100 nM Polθ–polymerase (aa 1792-2590)[6] was added for 10 min, followed by the addition of 100 μM dNTPs for another 30 min at 37° C in a total volume of 20 μl. In reactions including Polθ–helicase (i.e. Fig. 3d, right panel), indicated concentrations of the helicase domain were added for 5 min in the presence or absence of 1 mM ATP or AMP-PNP prior to the addition of Polθ–polymerase. Reactions were terminated by the addition of 4 μl of non-denaturing stop buffer (0.5 M Tris-HCl, pH 7.5, 10 mg/ml proteinase K, 80 mM EDTA, and 1.0% SDS) followed by 15–30 min incubation at 37° C. The resulting nucleic acids were then resolved in non-denaturing polyacrylamide gels and visualized by autoradiography. All concentrations are listed as final with the exception of the stop buffer. RP344, 5'-CACTGTGAGCTTAGGGTTAGCCCGGG-3' (underline indicates microhomology); RP343, 5'-CTAAGCTCACAGTG-3'.

Polθ–polymerase primer-template extension

100 nM 5′-^{32}P radio-labeled primer-template (^{32}P-RP167/RP266) was pre-incubated at 37° C in buffer (25 mM Tris-HCl, pH 8.8, 10% glycerol, 1 mM DTT, 0.01% NP-40, 10 mM $MgCl_2$, and 0.1 mg/ml BSA) then mixed with indicated concentrations of RPA for 5 min. 100 nM Polθ was then added for another 10 min followed by the addition of 100 μM dNTPs for another 30 min at 37° C in a total volume of 20 μl. Reactions were terminated by the addition of 25 mM EDTA and 45% formamide, and DNA was resolved in denaturing (urea) polyacrylamide gels with 15% formamide and analyzed by autoradiography. RP167 (5'-CACAGATTCTGGCAGGCTGCAGAT-3'); RP266 (5'-TTTTTTTTTTTTTTTTTTGCGATCTGCAGCCTGCCAGAATCTGTG-3'). All concentrations are listed as final.

gRNA sequence

Mouse Hsp90ab1 nuclease Rev: 5'-CGATGAGGATGCCTCGCGCA-3'
Mouse Sox2 nuclease Rev: 5'-CAGCCCTCACATGTGCGACA-3'

Mouse Sox2 nickase Fwd: 5’-GTGAGGGCTGGACTGCGAAC-3’
Mouse Sox2 nickase Rev: 5’-TTAATGGCCGTGCCGGGCAC-3’

Primer sequence

Hsp90ab1 Fwd1: 5’-ACAAAGCTGTCAAGGACCTGGTGG-3’
Hsp90ab1 Rev: 5’-TGGCTCAGTATCAGCATACAGCAGAGG-3’
Hsp90ab1 Fwd2: 5’-AAGAACCAGAAGTGGCACCTGACC-3’
Sox2 Fwd: 5’-CGGCGGCAACCAGAAGAACAGC-3’
Sox2 Rev1: 5’-CAGATCTATACATGGTCCGATTCCC-3’
Sox2 Rev2: 5’-GGGGTTTTCTTCAACATCACCTGCTTGC-3’
BRCA1 Fwd: 5’-CTGCCGTCCAAATTCAAGAAGT-3’
BRCA1 Rev: 5’-CTTGTGCTTCCCTGTAGGCT-3’

shRNA target sequence using pLK0.1 vector

BRCA1 (mouse): GCTCAGTGTATGACTCAGTTT
RPA1 (mouse): GCCCTGAAGATCGCTAACAAA
Rad51-A (mouse): CGGTCAGAGATCATACAGATA
Rad51-B (mouse): GCTGAAGCTATGTTTGCCATT
Rad51-C (mouse): CCTGTGATGCTATACGGCTTT

Supplementary Figures

Figure S1

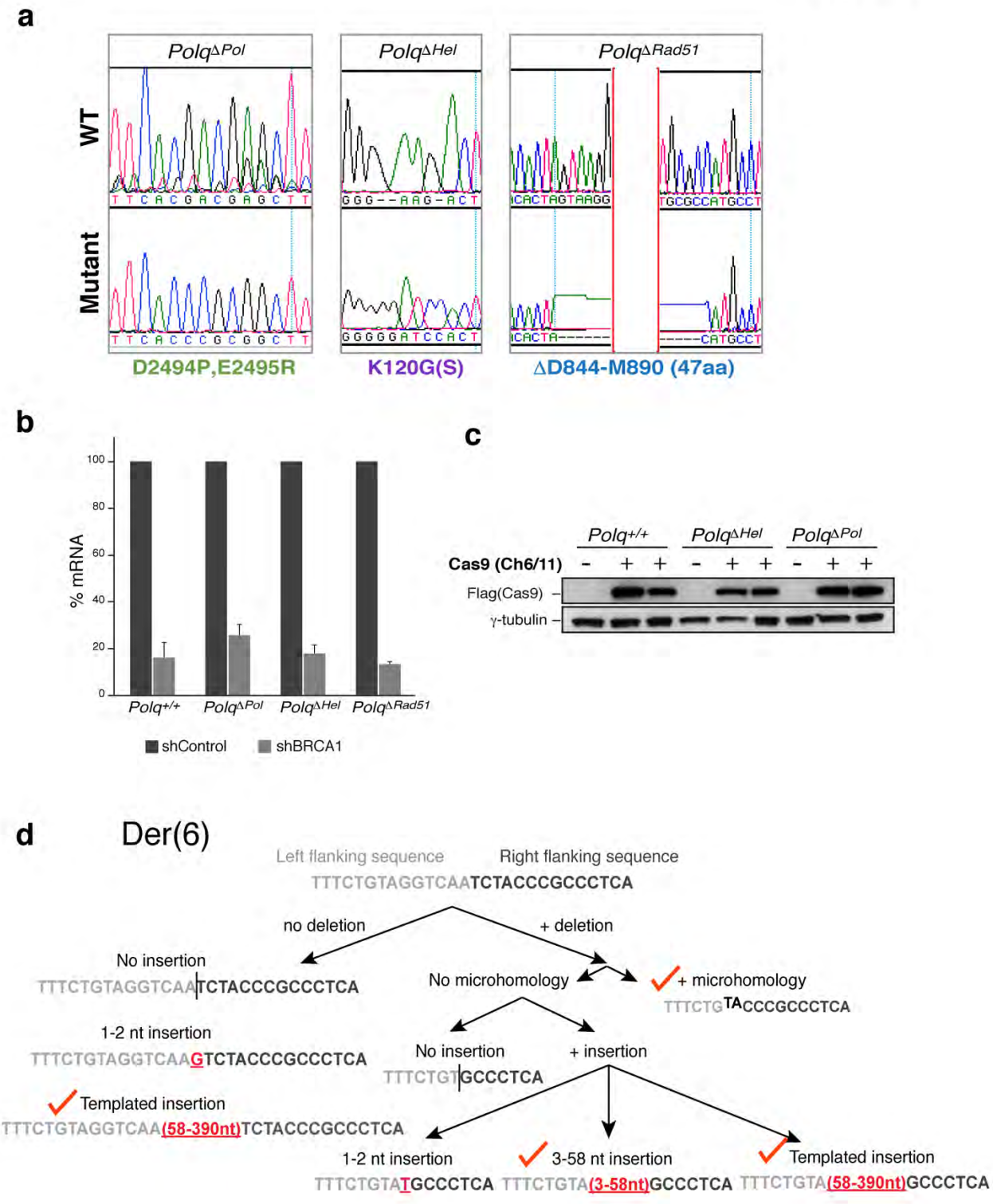
a
Polq^ΔPol
Polq^ΔHel
Polq^ΔRad51
WT
Mutant
D2494P,E2495R
K120G(S)
ΔD844-M890 (47aa)
b
% mRNA
Polq+/+
Polq^ΔPol
Polq^ΔHel
Polq^ΔRad51
shControl
shBRCA1
c
Cas9 (Ch6/11)
Flag(Cas9)
γ-tubulin
d
Der(6)
Left flanking sequence
Right flanking sequence
TTTCTGTAGGTCAATCTACCCGCCCTCA
no deletion
+ deletion
No insertion
TTTCTGTAGGTCAATCTACCCGCCCTCA
No microhomology
+ microhomology
TTTCTGTACCCGCCCTCA
1-2 nt insertion
TTTCTGTAGGTCAAGTCTACCCGCCCTCA
No insertion
TTTCTGTGCCCTCA
+ insertion
Templated insertion
TTTCTGTAGGTCAA(58-390nt)TCTACCCGCCCTCA
1-2 nt insertion
TTTCTGTATGCCCTCA
3-58 nt insertion
TTTCTGTA(3-58nt)GCCCTCA
Templated insertion
TTTCTGTA(58-390nt)GCCCTCA

Figure S1. Polθ structure-function analysis (**a**) Sequence analysis of the targeted CCE-mES cells with the indicated genotypes. (**b**) Relative quantification of BRCA1 mRNA in CCE-mES cells treated with shControl and sh*BRCA1*. (**c**) Western-blot analysis for Cas9 expression in cells with the indicated genotypes. (**d**) Examples of junction sequence for Der (6) retrieved from several translocation events and classified according to the presence of insertions, deletions and micro-homology. Junctions that fall in the category of “alt-NHEJ” signature are indicated with a check.

Figure S2

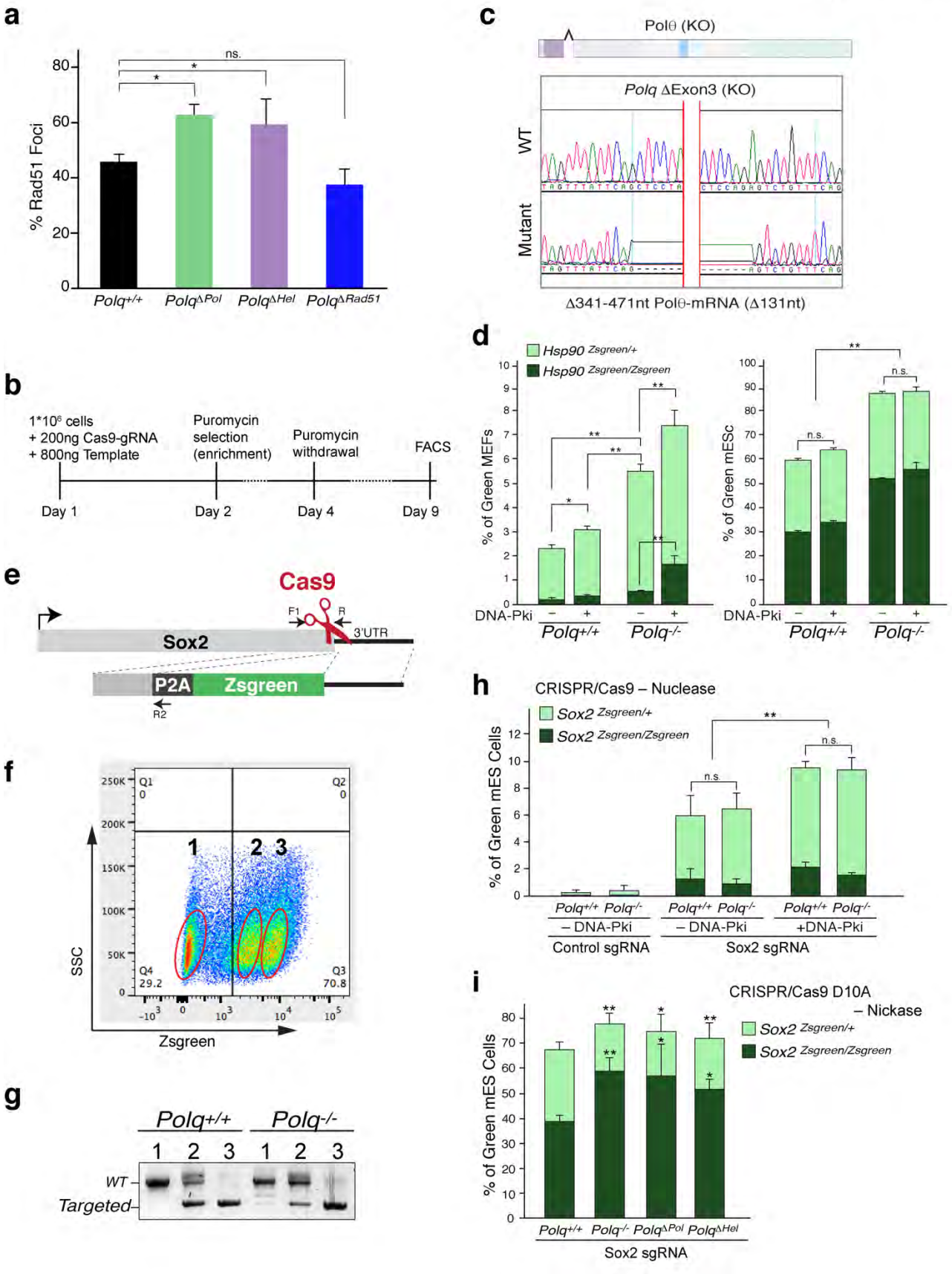
a
% Rad51 Foci
ns.
Polq+/+
PolqΔPol
PolqΔHel
PolqΔRad51
b
1*10⁶ cells
+ 200ng Cas9-gRNA
+ 800ng Template
Puromycin selection (enrichment)
Puromycin withdrawal
FACS
Day 1
Day 2
Day 4
Day 9
c
Polθ (KO)
Polq ΔExon3 (KO)
WT
Mutant
Δ341-471nt Polθ-mRNA (Δ131nt)
d
Hsp90 Zsgreen/+
Hsp90 Zsgreen/Zsgreen
% of Green MEFs
% of Green mESc
DNA-Pki
Polq+/+
Polq-/-
e
Cas9
F1
R
3'UTR
Sox2
P2A
Zsgreen
R2
f
Q1
Q2
Q3
Q4
29.2
70.8
SSC
Zsgreen
g
Polq+/+
Polq-/-
WT
Targeted
h
CRISPR/Cas9 – Nuclease
Sox2 Zsgreen/+
Sox2 Zsgreen/Zsgreen
% of Green mES Cells
– DNA-Pki
+DNA-Pki
Control sgRNA
Sox2 sgRNA
i
CRISPR/Cas9 D10A
– Nickase
Sox2 Zsgreen/+
Sox2 Zsgreen/Zsgreen
% of Green mES Cells
Polq+/+
Polq-/-
PolqΔPol
PolqΔHel
Sox2 sgRNA

Figure S2. The impact of Polθ-helicase and polymerase during HR (**a**) Accumulation of Rad51 in response to 1 Gy ionizing radiation of mES (CCE) cells with the indicated genotypes. Bars represent mean of two independent experiments. Two clonally-derived cell lines were used in each experiment. Two-tailed Student's t-test. (**b**) Scheme depicting the procedure used to investigate the impact of Polθ on the efficiency of gene targeting by HR. (**c**) Sequence analysis of the CCEs following CRISPR/Cas9 targeting to generate *Polq* knockout allele. (**d**) Quantification of CRISPR targeting at the *Hsp90* locus in *Polq* $^{+/+}$ and *Polq* $^{-/-}$ MEFs (left) and derived mES cells (right) in combination with DNA-PKc inhibitor. Bars represent the average of two experiments with SEM. Two-tailed Student's t-test. (**e**) Schematic of the strategy employed to target the *Sox2* locus. Primers used for genotyping are indicated. (**f**) FACS analysis to assess the frequency of CCE cells expressing Zsgreen from the *Sox2* locus following CRISPR/Cas9 targeting. Three independent population of cells were identified. (**g**) Genotyping PCR on sorted cells from (f) with the indicated genotypes. (**h**) Quantification of CRISPR targeting of *Sox2* using Cas9 nuclease in *Polq*$^{+/+}$ and *Polq*$^{-/-}$ mES cells (CCE). Bars represent the average of three experiments ± S.D. and two-tailed Student's t-test. (**i**) Quantification of CRISPR targeting with Cas9 nickase of *Sox2* in CCEswith the indicated genotypes. Bars represent mean ± S.D. from three independent experiments. *P < 0.05 and **P < 0.01; two-tailed Student's t-test.

Figure S3

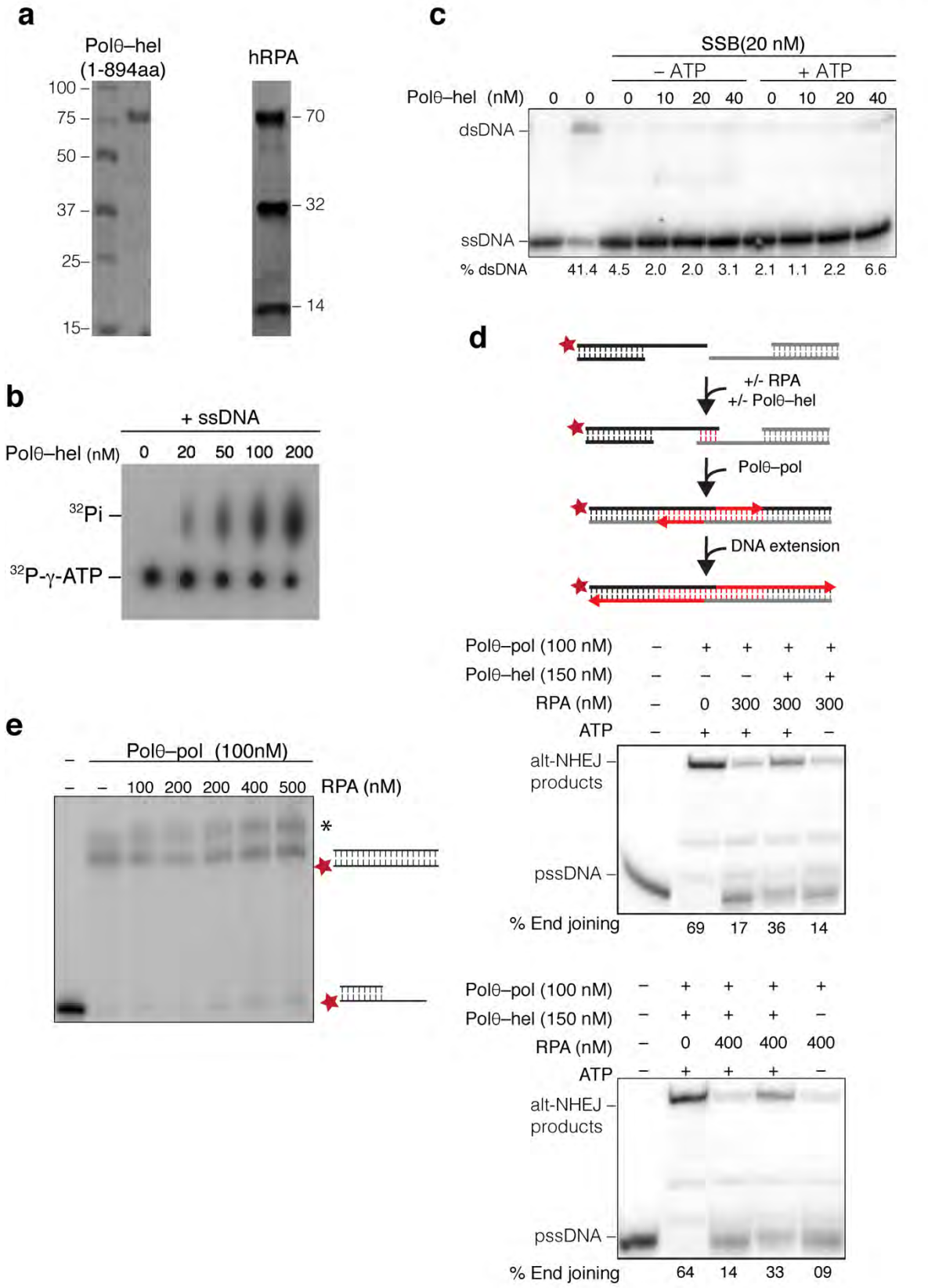
a
Polθ–hel (1-894aa)
hRPA
100
75
50
37
25
15
70
32
14
b
+ ssDNA
Polθ–hel (nM) 0 20 50 100 200
32Pi
32P-γ-ATP
c
SSB(20 nM)
– ATP
+ ATP
Polθ–hel (nM) 0 0 0 10 20 40 0 10 20 40
dsDNA
ssDNA
% dsDNA 41.4 4.5 2.0 2.0 3.1 2.1 1.1 2.2 6.6
d
+/- RPA
+/- Polθ–hel
Polθ–pol
DNA extension
Polθ–pol (100 nM) – + + + +
Polθ–hel (150 nM) – – – + +
RPA (nM) – 0 300 300 300
ATP – + + + –
alt-NHEJ products
pssDNA
% End joining 69 17 36 14
Polθ–pol (100 nM) – + + + +
Polθ–hel (150 nM) – + + + –
RPA (nM) – 0 400 400 400
ATP – + + + –
alt-NHEJ products
pssDNA
% End joining 64 14 33 09
e
Polθ–pol (100nM)
– – 100 200 200 400 500 RPA (nM)
*

Figure S3. *In vitro* analysis of Polθ-helicase function (**a**) Coomassie-stained SDS-page gel of purified Polθ–helicase (right) and the trimeric RPA complex (left) (**b**) Phosphorimager scan of thin layer chromatography plate containing results of Polθ ATPase assay in the presence of ssDNA. (**c**) Polθ–helicase is unable to promote annealing in the presence of SSB. Non-denaturing gel showing ssDNA annealing in the presence of indicated proteins and ATP. % dsDNA indicated. (**d**) Polθ–helicase promotes alt-NHEJ in the presence of RPA. Top panel: Schematic of Polθ–polymerase mediated alt-NHEJ assay. Bottom panels: Non-denaturing gels from two independent experiments showing alt-NHEJ products in reactions with the indicated proteins and ATP. (**e**) Polθ–polymerase template dependent activity is resistant to RPA binding of ssDNA. Denaturing gel showing Polθ–polymerase primer-template extension in the presence of the indicated amounts of RPA which were pre-incubated with the primer-template. Black asterisk marks template-independent extension of duplexed DNA by Polθ–polymerase.

Figure S4

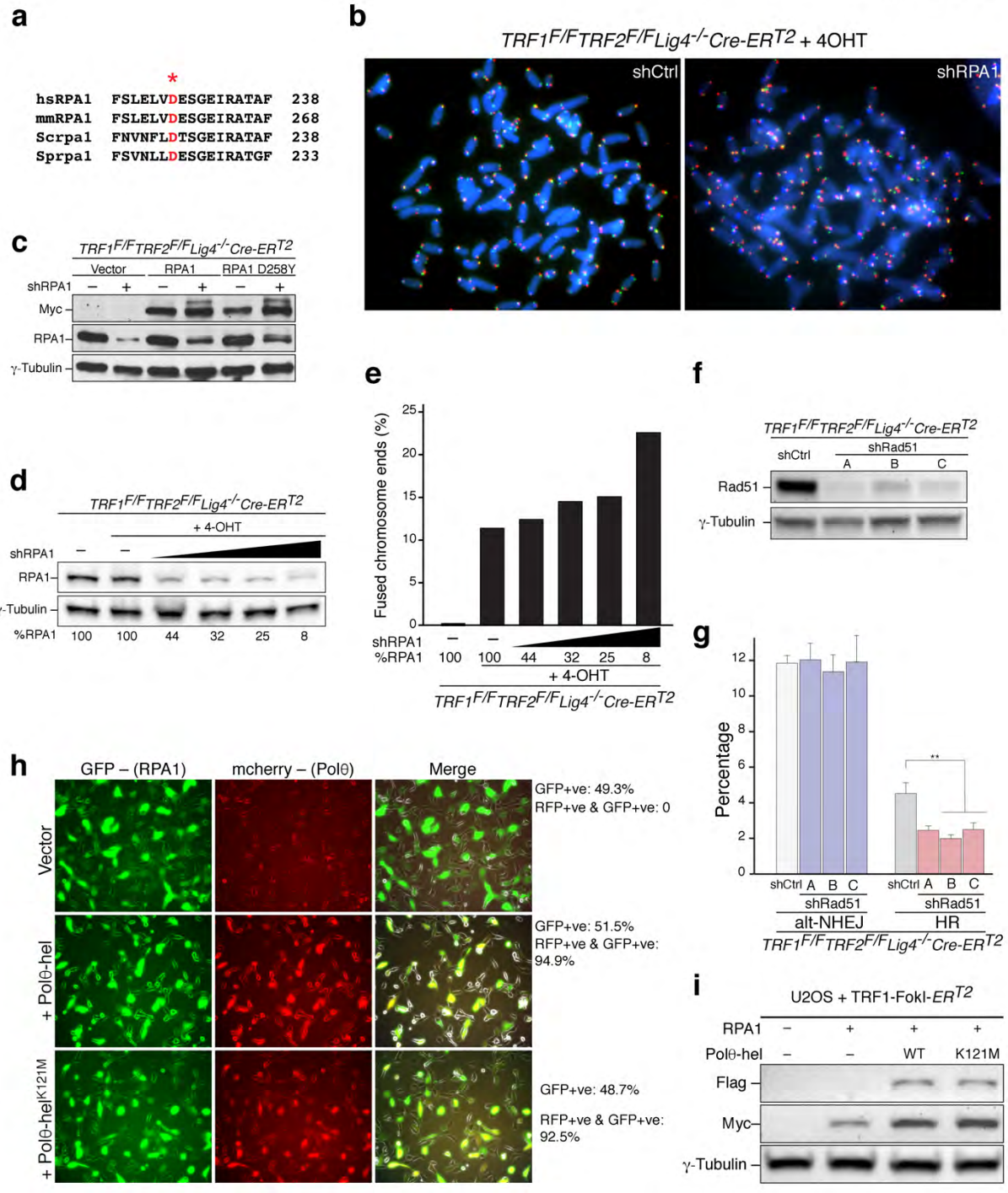
a
*
hsRPA1 FSLELVDESGEIRATAF 238
mmRPA1 FSLELVDESGEIRATAF 268
Scrpa1 FNVNFLDTSGEIRATAF 238
Sprpa1 FSVNLLDESGEIRATGF 233
b
TRF1F/FTRF2F/FLig4-/-Cre-ERT2 + 4OHT
shCtrl
shRPA1
c
TRF1F/FTRF2F/FLig4-/-Cre-ERT2
Vector
RPA1
RPA1 D258Y
shRPA1 – + – + – +
Myc
RPA1
γ-Tubulin
d
TRF1F/FTRF2F/FLig4-/-Cre-ERT2
+ 4-OHT
shRPA1 – –
RPA1
γ-Tubulin
%RPA1 100 100 44 32 25 8
e
Fused chromosome ends (%)
25
20
15
10
5
0
shRPA1 – –
%RPA1 100 100 44 32 25 8
+ 4-OHT
TRF1F/FTRF2F/FLig4-/-Cre-ERT2
f
TRF1F/FTRF2F/FLig4-/-Cre-ERT2
shCtrl
shRad51
A B C
Rad51
γ-Tubulin
g
Percentage
12
10
8
6
4
2
0
**
shCtrl A B C shCtrl A B C
shRad51 shRad51
alt-NHEJ HR
TRF1F/FTRF2F/FLig4-/-Cre-ERT2
h
GFP – (RPA1)
mcherry – (Polθ)
Merge
Vector
+ Polθ-hel
+ Polθ-helK121M
GFP+ve: 49.3%
RFP+ve & GFP+ve: 0
GFP+ve: 51.5%
RFP+ve & GFP+ve: 94.9%
GFP+ve: 48.7%
RFP+ve & GFP+ve: 92.5%
i
U2OS + TRF1-FokI-ERT2
RPA1 – + + +
Polθ-hel – – WT K121M
Flag
Myc
γ-Tubulin

Figure S4. Investigating the interplay between Polθ-helicase and RPA during alt-NHEJ (**a**) Representative metaphase spreads from *TRF1*$^{F/F}$*TRF2*$^{F/F}$*Lig4*$^{-/-}$Cre-ER^{T2} MEFs, with the indicated shRNA treatment, 96 h after Cre expression. CO-FISH assay was performed using a FITC-OO-(CCCTAA)3 PNA probe (green) and a Tamra-OO-(TTAGGG)3 PNA probe (red). DAPI in blue. (**b**) Western-blot analysis of Myc-RPA1, total RPA1 and tubulin in *TRF1*$^{F/F}$*TRF2*$^{F/F}$*Lig4*$^{-/-}$Cre-ER^{T2} MEFs treated with shControl and sh*RPA1*. (**c**) Western blot analysis for RPA1 in *TRF1*$^{F/F}$*TRF2*$^{F/F}$*Lig4*$^{-/-}$Cre-ER^{T2} treated with different amounts of shRPA1. Knock-down efficiency is quantified with image lab (Biorad). (**d**) Quantification of telomere fusions in shelterin-free cells treated with sh*RPA1* as in (d). (**e**) Alignment of RPA1 protein sequence from human, mouse, *S. cerevisiae* and *S. pombe*. Highlighted is the conserved aspartic acid residue at positions 228, 258, 228, and 223, respectively. (**f**) Western-blot analysis for the depletion of Rad51 in *TRF1*$^{F/F}$*TRF2*$^{F/F}$*Lig4*$^{-/-}$Cre-ER^{T2} MEFs. (**g**) Quantification of telomere fusion (alt-NHEJ) and T-SCE (HDR) in the indicated cells treated with shRNAs against Rad51 or control shRNA. Bars represent mean ± S.D. from three independent experiments. *P < 0.05 and **P < 0.01; two-tailed Student's t-test. (**h**) Representative images of U2OS cells expressing and inducible TRF1-FokI-ER^{T2} (mcherry) and co-transfected with Myc-RPA1-IRES-GFP and Flag-*Polq*-Helicase-IRES-TdTomato (wt or K121M). The percentage of cells expressing RPA1, and those co-expressing RPA1 and *Polq*-Helicase was determined prior to induction of TRF1-FokI with dox, shield and 4-OHT. (**i**) Western blot analysis of cells with the indicated treatment.

Table 1 – Translocation Junctions in *Polq*$^{+/+}$ cells

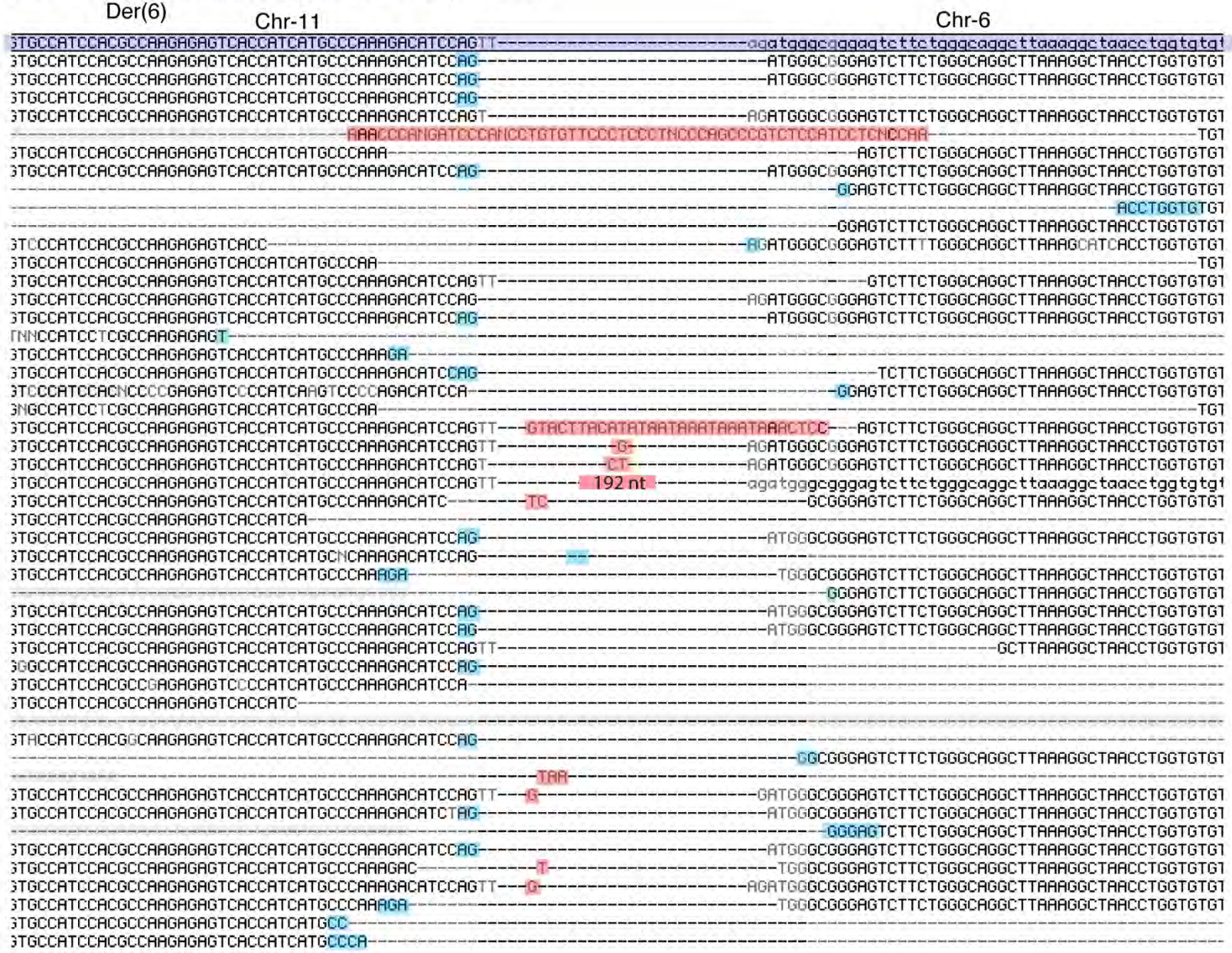

Table 2 – Translocation Junctions *Polq*$^{+/+}$ cells

Der(6)

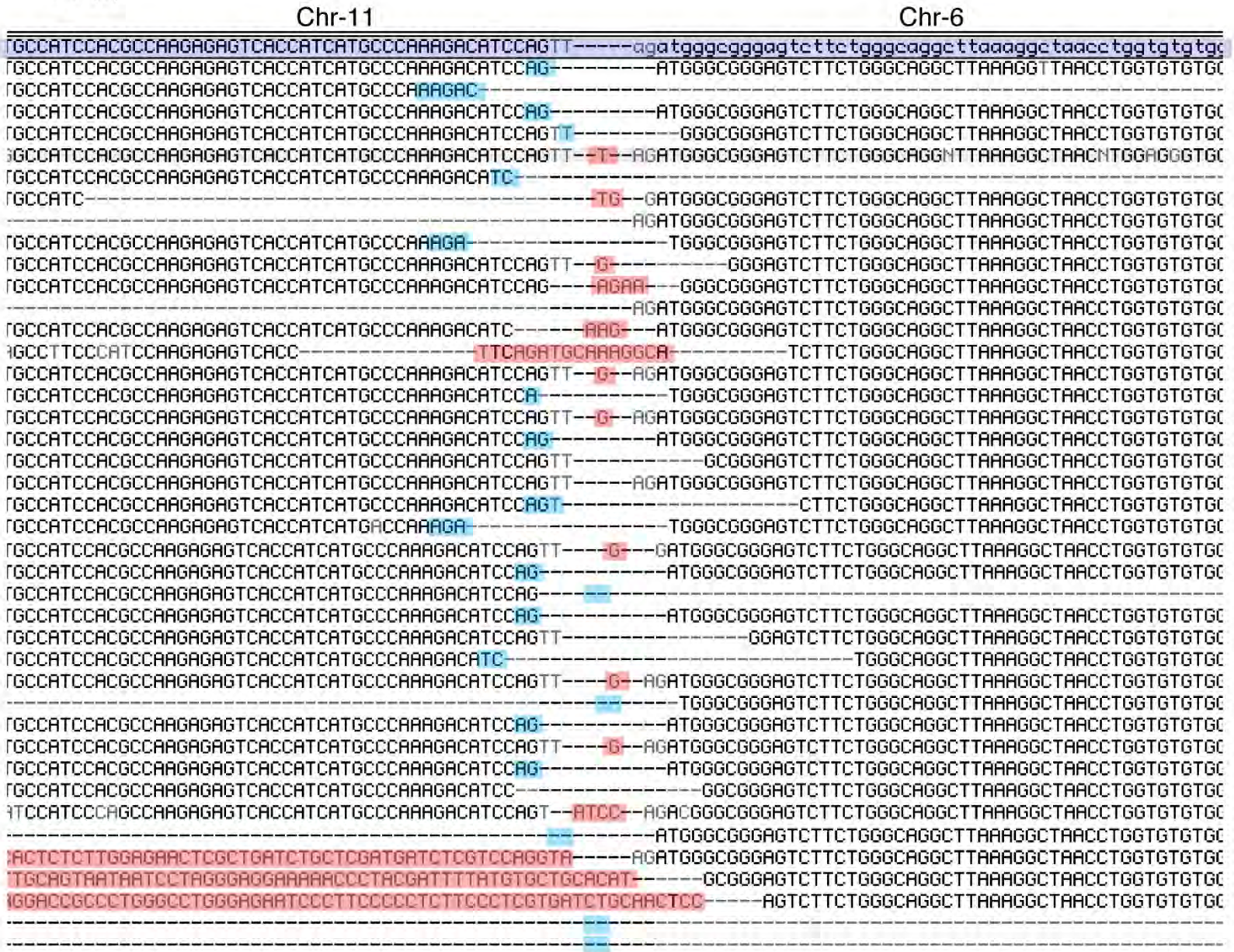

Table 3 – Translocation Junctions in *Polq*$^{+/+}$ cells

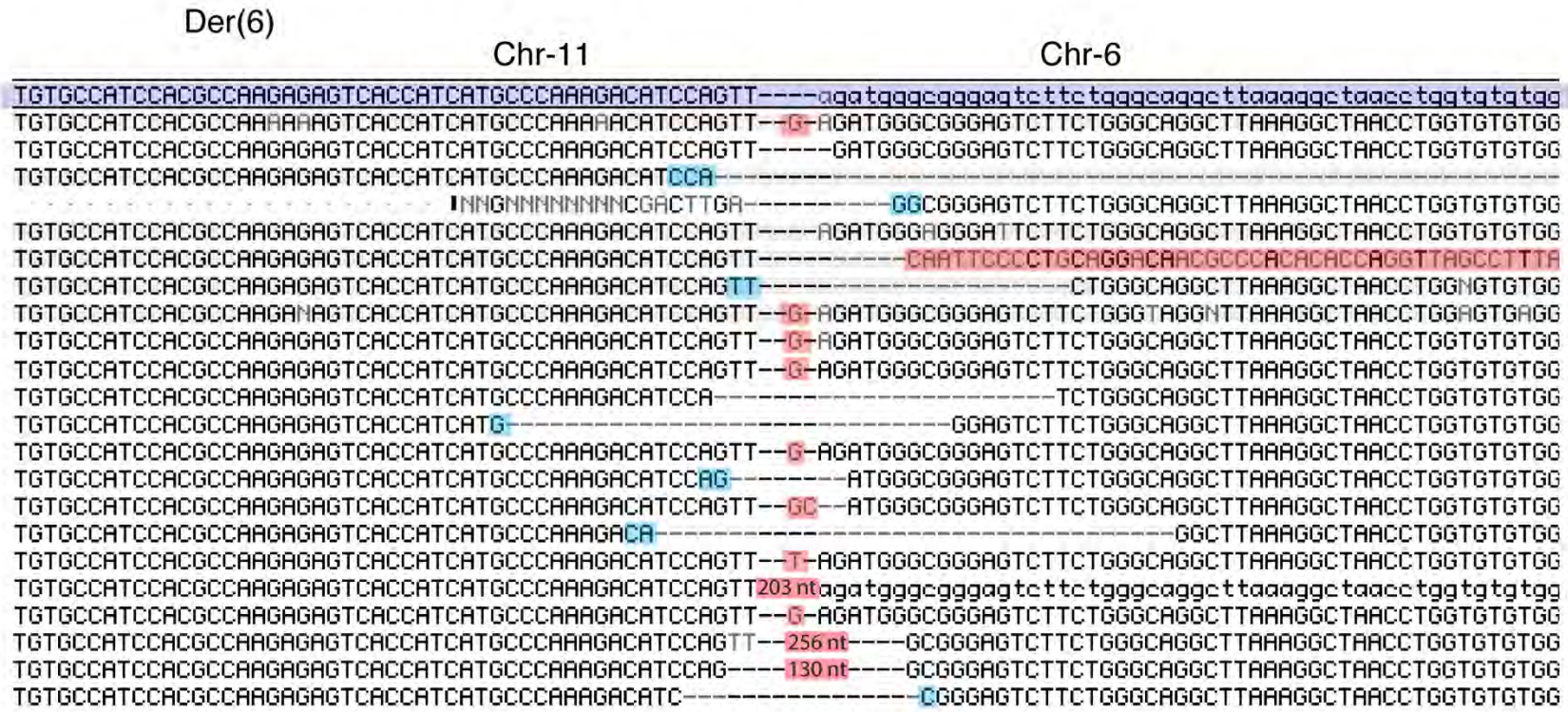

Table 4 – Translocation Junctions in *Polq*$^{\Delta Pol}$ cells

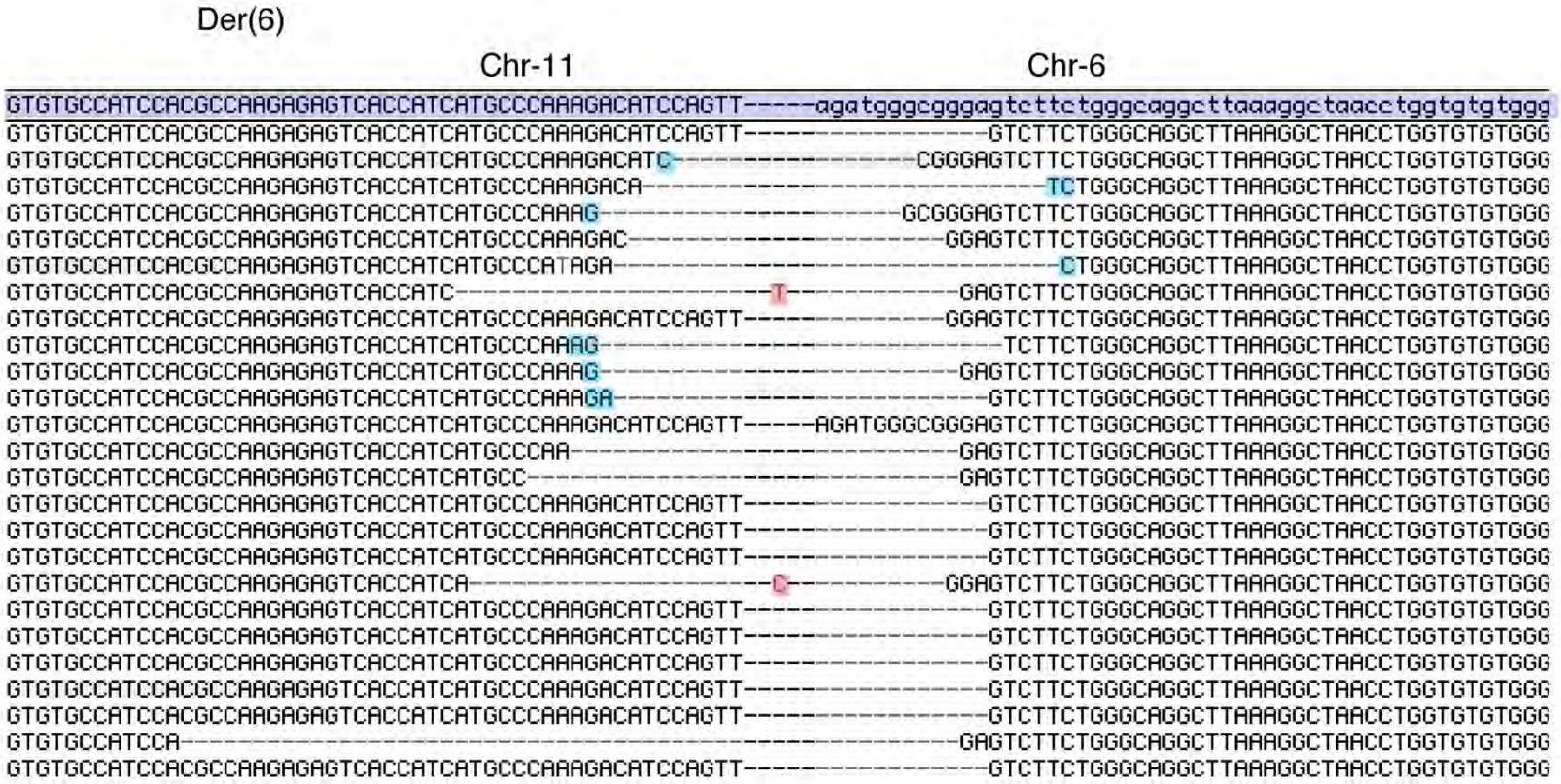

Table 5 – Translocation Junctions in *Polq*$^{\Delta Pol}$ cells

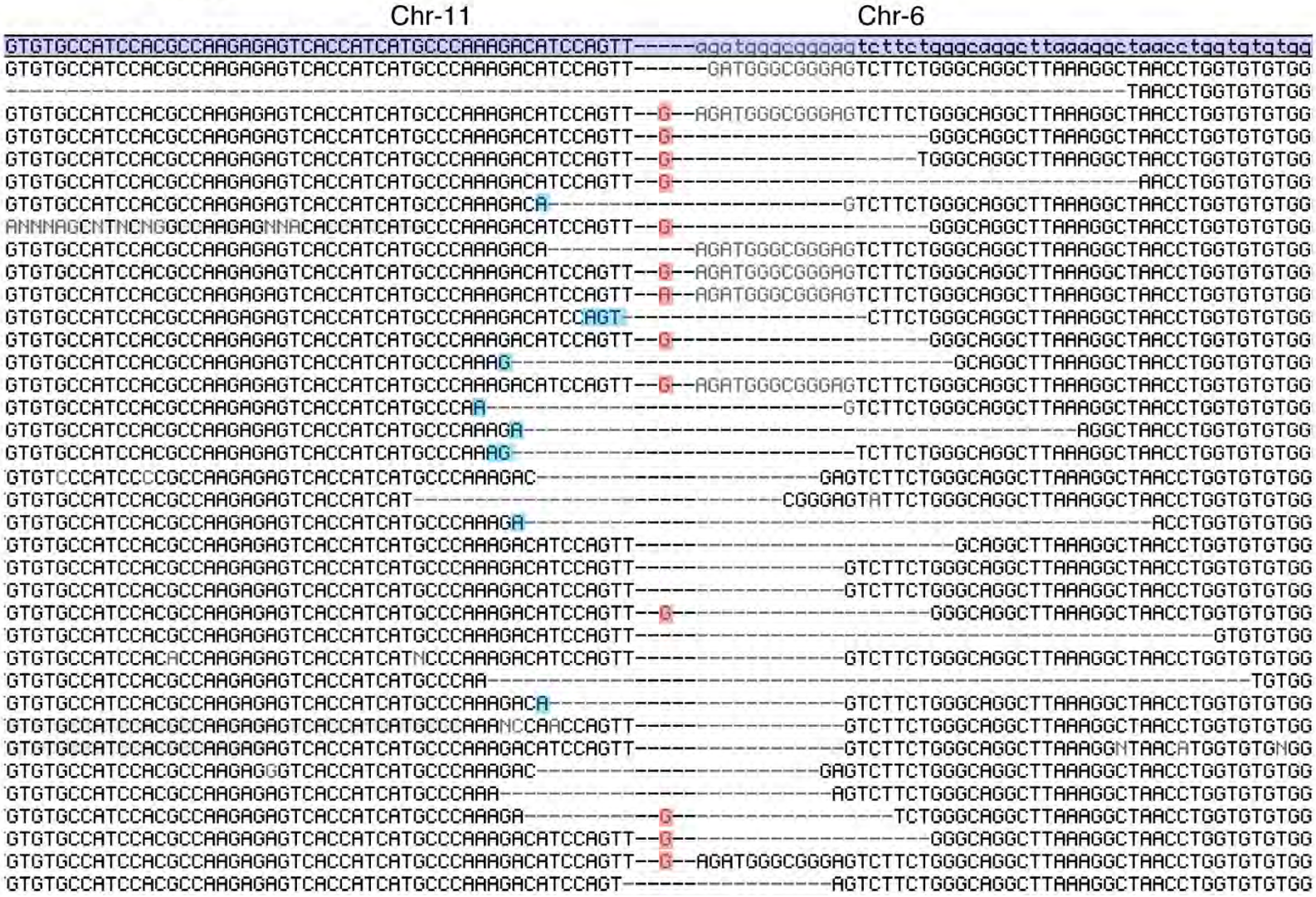

Table 6 – Translocation Junctions in *Polq*$^{\Delta Hel}$ cells

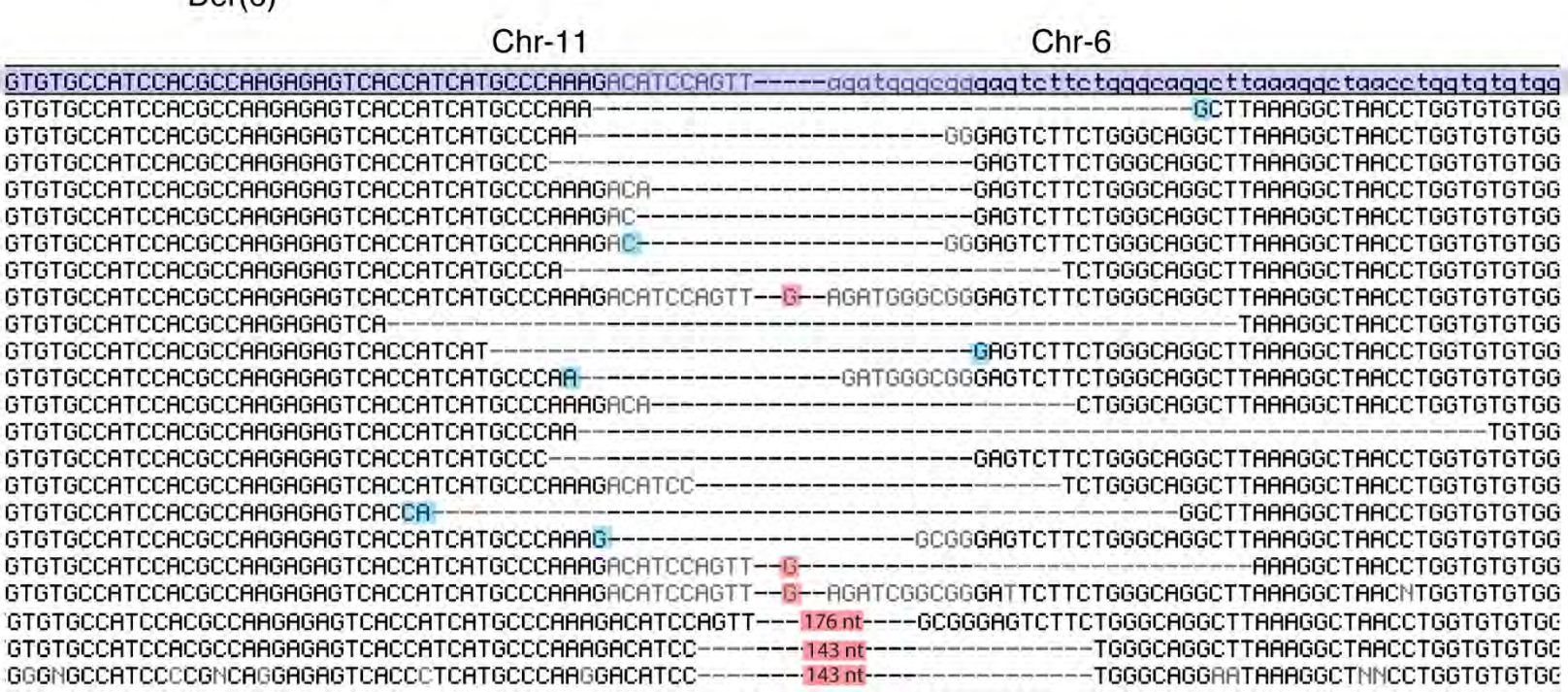

Table 7– Translocation Junctions in *Polq*$^{\Delta Hel}$ cells

Der(6)

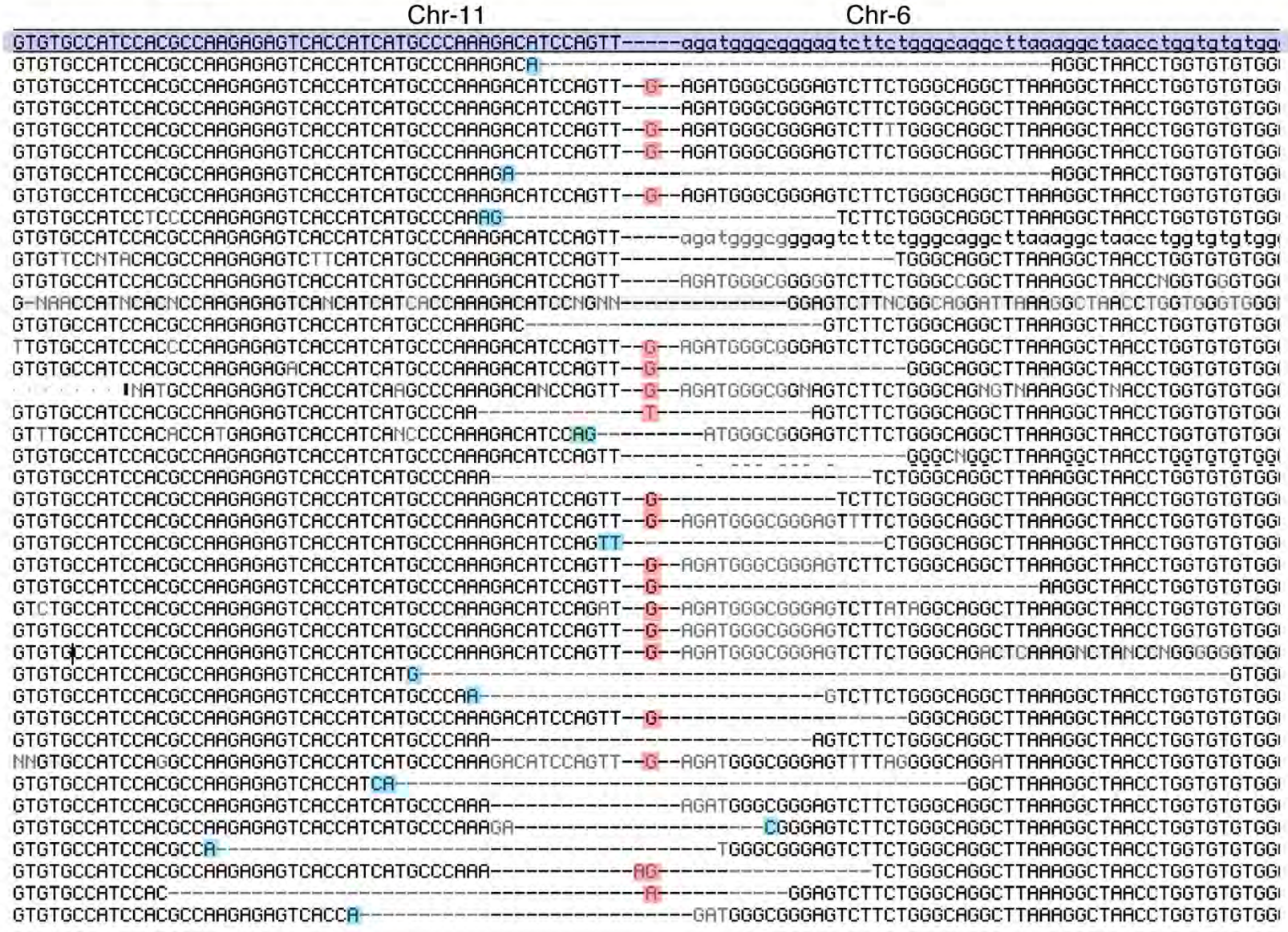

Table 8 – Translocation Junctions in *Polq*$^{\Delta Rad51}$ cells

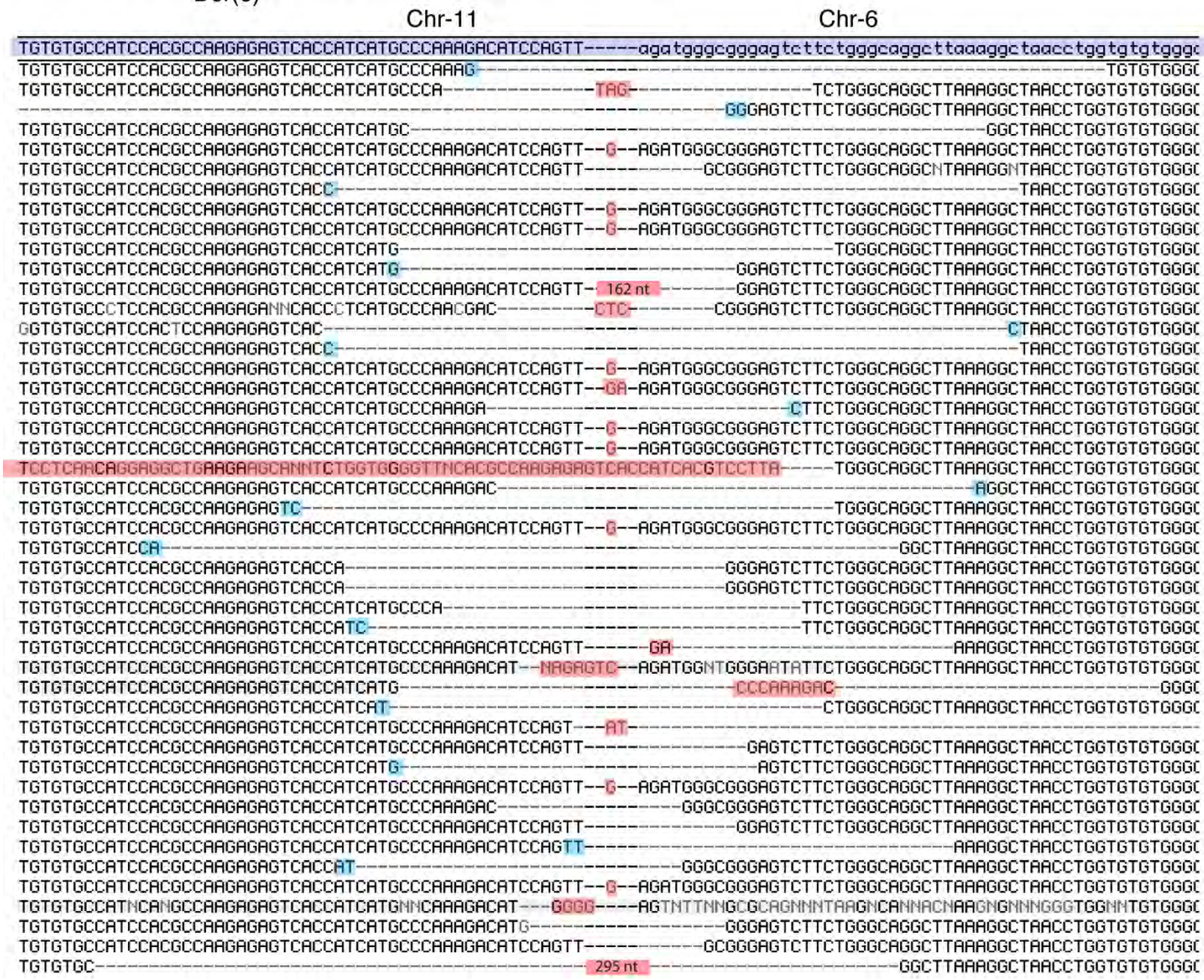

Table 9 – Translocation Junctions in *Polq*$^{\Delta Rad51}$ cells

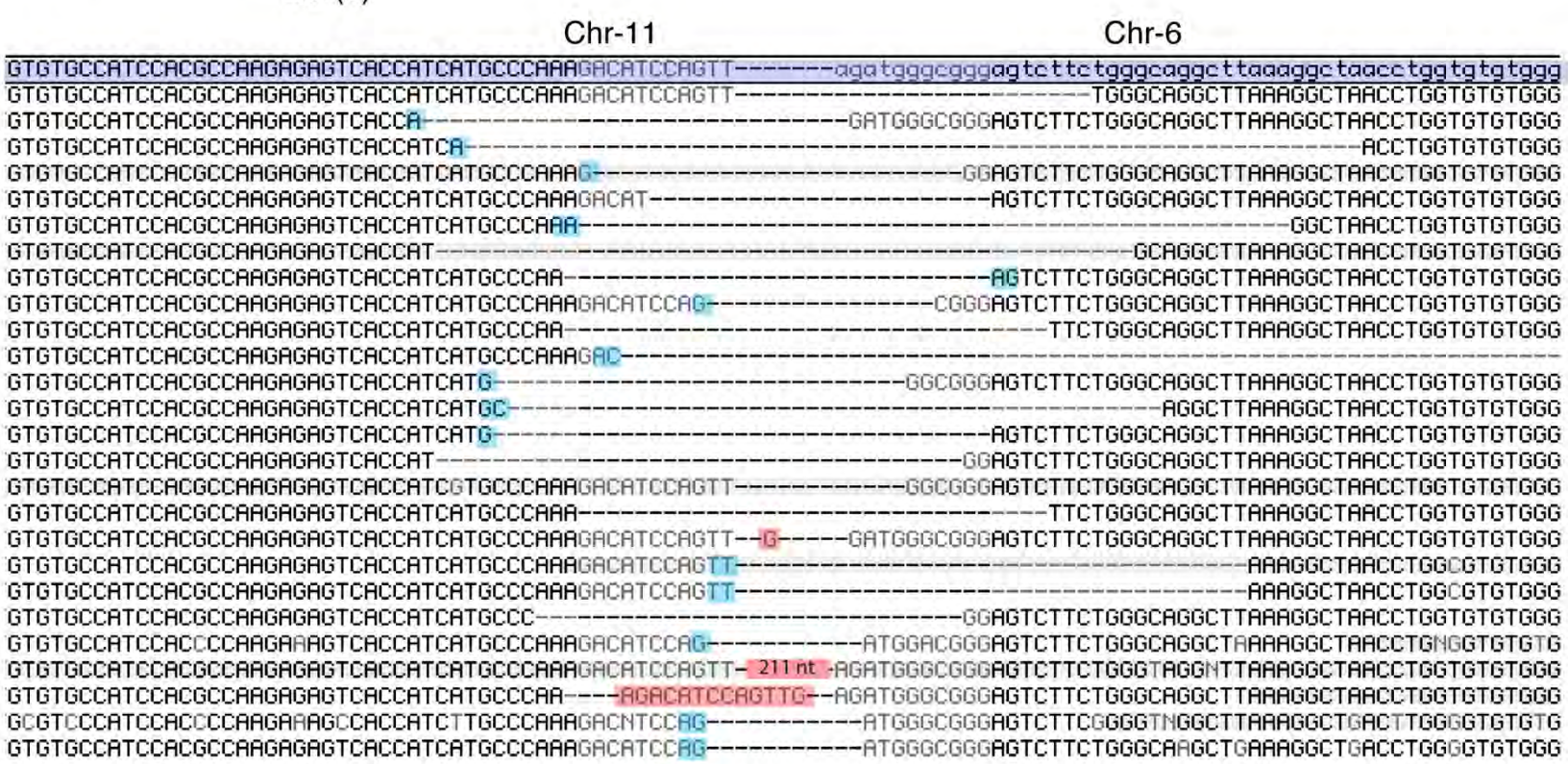

Tables 1-9: Sequences of Der (6) breakpoint junction from cells with the indicated genotype. Reference sequence is highlighted on top. Lines represent individual translocations recovered by PCR and subject to Sanger sequencing. Nucleotide insertions are marked in red. Gaps in the sequence represent nucleotide deletions. Microhomology is denoted by blue boxes.

References:

1 Sfeir, A. & de Lange, T. Removal of shelterin reveals the telomere end-protection problem. *Science* **336**, 593-597, doi:10.1126/science.1218498 (2012).

2 Robertson, E., Bradley, A., Kuehn, M. & Evans, M. Germ-line transmission of genes introduced into cultured pluripotential cells by retroviral vector. *Nature* **323**, 445-448, doi:10.1038/323445a0 (1986).

3 Cho, N. W., Dilley, R. L., Lampson, M. A. & Greenberg, R. A. Interchromosomal homology searches drive directional ALT telomere movement and synapsis. *Cell* **159**, 108-121, doi:10.1016/j.cell.2014.08.030 (2014).

4 Mateos-Gomez, P. A. *et al.* Mammalian polymerase theta promotes alternative NHEJ and suppresses recombination. *Nature* **518**, 254-257, doi:10.1038/nature14157 (2015).

5 Simsek, D. *et al.* DNA ligase III promotes alternative nonhomologous end-joining during chromosomal translocation formation. *PLoS genetics* **7**, e1002080, doi:10.1371/journal.pgen.1002080 (2011).

6 Kent, T., Chandramouly, G., McDevitt, S. M., Ozdemir, A. Y. & Pomerantz, R. T. Mechanism of microhomology-mediated end-joining promoted by human DNA polymerase theta. *Nature structural & molecular biology* **22**, 230-237, doi:10.1038/nsmb.2961 (2015).